Quantifying Primary Producer Phenology in the Canadian Arctic using Submersed Oceanographic Sensors and Satellite Remote Sensing

by

Kiran Yendamuri

A thesis submitted to the Faculty of Graduate Studies of

the University of Manitoba

in partial fulfillment of the requirements of the degree of

MASTER OF SCIENCE

Department of Environment and Geography

University of Manitoba

Winnipeg

Abstract

Arctic primary producer phenology is undergoing shifts attributed to the increased transmission of light resulting from climate change-induced declines in sea ice thickness, age, and extent. However, the investigation of phenological events, particularly near the ocean surface, is challenging due to limited time-series observations caused by logistical constraints and accessibility issues. Data collected from a subsurface oceanographic mooring deployed in Dease Strait, Nunavut, from 2017 to 2019 were used to determine primary producer biomass using the normalized difference index (NDI) chlorophyll-*a* retrieval algorithm. Sentinel-1 and RADARSAT-2 synthetic aperture radar (SAR) data and related meteorological variables were used to identify snow and sea-ice melt phase timing. The results revealed a relationship between light availability and surface primary producer timing and magnitude. Specifically, an 18-day difference in the length of ice algal blooms between 2017 and 2019 was observed, with both blooms peaking near snow melt onset and exhibiting similar daily production rates. The extended duration of the 2019 ice algal bloom was due to lower air temperatures compared to 2017, and a deeper snowpack prior to snow melt. Moreover, a 6-7 day under-ice phytoplankton bloom occurred in both years, coinciding with melt pond formation. However, the 2019 under-ice bloom exhibited a lower accumulation rate, likely due to nutrient depletion beneath the ice by the prolonged ice algal bloom. Following ice break-up in 2019, a 31-day late-summer bloom occurred via sustained wind-driven mixing, highlighting the importance of ocean-atmosphere coupling in the region following ice break-up. The findings of this thesis provide a novel approach to investigating surface primary producer phenology and suggest the potential application of this technique to support future long-term monitoring.

Acknowledgements

Above all else, I would like to express my sincere thanks and eternal gratitude to my co-supervisors, Drs. C.J. Mundy and Julienne Stroeve, for their support and guidance throughout this compelling and fun project. They took a chance on me and patiently provided their time and expertise. Witnessing how they navigated the intricacies of a scientific acumen was its own inspiring education and something that I will continue to think about and learn from in the days and years ahead.

I extend my appreciation to my committee members, Drs. Jens Ehn and Bill Williams, for their kind insights. Their ideas, shared during committee meetings and via email, provided a solid framework for advancing the project. Their perspectives also encouraged me to explore additional dimensions within the project data, which was equally enlightening.

I am grateful to all those who participated in the ICE-CAMPS 2017 field campaign and the Kitikmeot Sea Science Study mooring program, as their contributions provided the foundational project data. Special thanks to Drs. Vishnu Nandan and David Jensen for their guidance in acquiring and processing Sentinel-1 data, especially Dr. Nandan for his SAR expertise throughout the project. I would also like to acknowledge Dr. Alexander Komarov for procuring RADARSAT-2 data products through Environment and Climate Change Canada and the Canadian Space Agency. Additionally, I thank Dr. Brent Else and Christina Braybrook for providing the meteorological data and sharing their knowledge that was essential to this research.

I am grateful for the financial support received from the Natural Sciences and Engineering Research Council of Canada (NSERC) through the Discovery and Northern Research Supplement

grants awarded to Dr. C.J. Mundy, as well as the Canada 150 Research Chairs Program awarded to Dr. Julienne Stroeve.

I extend my appreciation to all my colleagues within the Department of Environment and Geography for creating an incredible atmosphere and fostering a supportive environment. A special thank you goes to the members of Dr. Mundy's lab, both past and present, whom I have had the privilege of meeting: Dr. Rémi Amiraux, Dr. Lisa Matthes, Fowzia Ahmed, Xander Bjornsson, Pascale Bouchard, Laura Dalman, Elizabeth Kitching, Jillian Reimer, and Kate Yezhova.

I want to thank of all my friends near and far for their unwavering support. Last but certainly not least, to my parents and brother, who are incredible souls, and to whom I am fortunate to call family.

Dedication

To a place, my personal retreat that changed it all: Secret Beach.

Table of Contents

List of Tables

List of Figures

List of Copyrighted Material

Contributions of Authors

The research presented in Chapter 3, titled “Surface primary producer phenology in Dease Strait, NU, Canada, examined using submersed oceanographic sensors and satellite remote sensing” involved the collective contributions of all the listed authors. As first author, I contributed to the conceptualization, design, data acquisition, analysis, interpretation, and drafting of the research. Dr. C.J. Mundy helped develop the project ideas and provided substantial guidance, logistical and financial support, and manuscript feedback. Dr. Julienne Stroeve offered valuable guidance and feedback throughout the project, provided financial support, and contributed to developing and editing the manuscript. Drs. Bill Williams and Jens Ehn assisted in project development and data interpretation. Dr. Vishnu Nandan assisted in synthetic aperture radar (SAR) data acquisition, interpretation, and support. Dr. Brent Else provided meteorological data and assistance. Dr. Alexander Komarov contributed to SAR data acquisition and support. Christina Braybrook and Mike Dempsey provided data support. All authors reviewed and revised the manuscript prior to submission to Arctic Science.

Chapter 1 | Introduction

1.1. Introduction

Due to the effects of climate change, thinning first-year ice has become the dominant sea ice in the Arctic with more of the Arctic becoming ice-free come summer (Stroeve & Notz, 2018). The reduction of sea ice thickness has increased the overall amount of light transmittance into the Arctic Ocean (Barber et al., 2015). Depending on the interaction of seasonal insolation with atmospheric and sea-surface features, the attenuated light that reaches the Arctic marine system plays a significant role in affecting the phenology of primary producers (Kirk, 2010). Ice algal colonies have been experiencing an earlier bloom cycle with increased sea ice residence time due to elevated irradiance levels from the strengthening of the positive feedback loop that increases heat input to the upper water column and enables further sea ice melt (Leu et al., 2011; Lim et al., 2022; Serreze et al., 2009). Pelagic phytoplankton production is likewise increasing in magnitude with bloom termination largely governed by nutrient availability (Lannuzel et al., 2020). Upper layer stratification from increasing ice melt has been noted to hinder nutrient supply on a regional basis due to lower levels of vertical mixing processes (Popova et al., 2010). However an increasing exposure of the Arctic Ocean has led to greater wind mixing, which counteracts stratification (Williams & Carmack, 2015). Reported seasonal features such as the prevalence of under-ice

phytoplankton blooms from thinner sea ice light transmission and autumn blooms from later freeze-up alter the framework of Arctic primary production phenology (Ardyna et al., 2020).

As the Arctic marine system continues to experience deviations away from historical norms, our understanding of light processes driving primary production remain incomplete. This gap is in part due to a lack of time series observations of the upper Arctic Ocean where a large portion of primary production occurs. The costs and difficult logistics of mounting a field campaign restrict researchers in their studies' duration, with limited possibilities to return over multiple years. Many physical and biological studies are likewise impeded by destructive sampling techniques that do not permit re-sampling of an area. Remote sensing methods have emerged to tackle these deficits. Whereas sensors aboard satellites can observe ocean colour changes as a measure of phytoplankton blooms (Craig et al., 2012; Groom et al., 2019), they cannot observe light conditions within and below the sea ice cover. Stroeve et al. (2021) attempted to remedy this by quantifying the under-ice light environment on a pan-Arctic scale using satellite-derived products, with limitations in precision being the key uncertainty. On a smaller scale, the advent of under-ice optical sensors that collect and measure the spectrum of light transmitted through ice and water represents a non-invasive technique that can be launched for extended periods to collect proxy light and primary production data (Hill et al., 2018; Legendre & Gosselin, 1991; Mundy et al., 2007). Utilizing data collected over two different years from a sub-surface taut oceanographic mooring, combined with satellite remote sensing and associated meteorological variables, my thesis will seek to improve observations and understandings of the upper Arctic Ocean light climate as it relates to timing of surface primary production.

1.2. Objectives

The goal of the thesis is to couple under-ice and satellite remote sensing methods to advance knowledge pertaining to how irradiance varies in the seasonally ice-covered Canadian Arctic and how that affects the phenology of primary producers. More precisely, my thesis objectives are the following:

1) To describe the seasonal progression of snow and sea ice melt phase timing and light in a seasonally ice-covered sea;
2) To determine characteristic seasonal features and timing of primary production;
3) To examine shifts in primary production phenology relative to physical conditions.

1.3. Structure

Including this introductory chapter, this sandwich-style thesis comprises four chapters. Chapter 2 provides an overview of pertinent physical, environmental, and biological controls of primary production development. In turn, there is a short review of the different remote sensing methods developed to approach this project. Chapter 3 is the primary scientific contribution of this thesis as a research manuscript to be submitted in a peer-reviewed journal with the following citation:

Yendamuri, K., Stroeve, J., Williams, W. J., Ehn, J., Nandan, V., Else, B. G. T., Komarov, A. S., Braybrook, C. A., Dempsey, M., and Mundy, C. J. (*In Preparation*). Surface primary producer phenology in Dease Strait, NU, Canada, examined using submersed oceanographic sensors and satellite remote sensing.

Chapter 4 ends with a summary of the key research findings and future recommendations for the application of the combined remote sensing technique.

1.4. References

Ardyna, M., Mundy, C. J., Mills, M. M., Oziel, L., Grondin, P.-L., Lacour, L., et al. (2020). Environmental drivers of under-ice phytoplankton bloom dynamics in the Arctic Ocean. *Elem Sci Anth*, *8*(1), 30. https://doi.org/10.1525/elementa.430

Barber, D. G., Hop, H., Mundy, C. J., Else, B., Dmitrenko, I. A., Tremblay, J.-E., et al. (2015). Selected physical, biological and biogeochemical implications of a rapidly changing Arctic Marginal Ice Zone. *Progress in Oceanography*, *139*, 122–150. https://doi.org/10.1016/j.pocean.2015.09.003

Craig, S. E., Jones, C. T., Li, W. K. W., Lazin, G., Horne, E., Caverhill, C., & Cullen, J. J. (2012). Deriving optical metrics of coastal phytoplankton biomass from ocean colour. *Remote Sensing of Environment*, *119*, 72–83. https://doi.org/10.1016/j.rse.2011.12.007

Groom, S., Sathyendranath, S., Ban, Y., Bernard, S., Brewin, R., Brotas, V., et al. (2019). Satellite Ocean Colour: Current Status and Future Perspective. *Frontiers in Marine Science*, *6*. https://doi.org/10.3389/fmars.2019.00485

Hill, V. J., Light, B., Steele, M., & Zimmerman, R. C. (2018). Light Availability and Phytoplankton Growth Beneath Arctic Sea Ice: Integrating Observations and Modeling. *Journal of Geophysical Research: Oceans*, *123*(5), 3651–3667. https://doi.org/10.1029/2017JC013617

Kirk, J. T. O. (2010). *Light and Photosynthesis in Aquatic Ecosystems* (3rd ed.). Cambridge: Cambridge University Press. https://doi.org/10.1017/CBO9781139168212

Lannuzel, D., Tedesco, L., van Leeuwe, M., Campbell, K., Flores, H., Delille, B., et al. (2020). The future of Arctic sea-ice biogeochemistry and ice-associated ecosystems. *Nature Climate Change*, *10*(11), 983–992. https://doi.org/10.1038/s41558-020-00940-4

Legendre, L., & Gosselin, M. (1991). In situ spectroradiometric estimation of microalgal biomass in first-year sea ice. *Polar Biology*, *11*(2). https://doi.org/10.1007/BF00234273

Leu, E., Søreide, J. E., Hessen, D. O., Falk-Petersen, S., & Berge, J. (2011). Consequences of changing sea-ice cover for primary and secondary producers in the European Arctic shelf seas: Timing, quantity, and quality. *Progress in Oceanography*, *90*(1–4), 18–32. https://doi.org/10.1016/j.pocean.2011.02.004

Lim, S. M., Payne, C. M., van Dijken, G. L., & Arrigo, K. R. (2022). Increases in Arctic sea ice algal habitat, 1985–2018. *Elementa: Science of the Anthropocene*, *10*(1), 00008. https://doi.org/10.1525/elementa.2022.00008

Mundy, C. J., Ehn, J. K., Barber, D. G., & Michel, C. (2007). Influence of snow cover and algae on the spectral dependence of transmitted irradiance through Arctic landfast first-year sea ice. *Journal of Geophysical Research*, *112*(C3), C03007. https://doi.org/10.1029/2006JC003683

Popova, E. E., Yool, A., Coward, A. C., Aksenov, Y. K., Alderson, S. G., de Cuevas, B. A., & Anderson, T. R. (2010). Control of primary production in the Arctic by nutrients and light: insights from a high resolution ocean general circulation model. *Biogeosciences*, *7*(11), 3569–3591. https://doi.org/10.5194/bg-7-3569-2010

Serreze, M. C., Barrett, A. P., Stroeve, J. C., Kindig, D. N., & Holland, M. M. (2009). The emergence of surface-based Arctic amplification. *The Cryosphere*, *3*(1), 11–19. https://doi.org/10.5194/tc-3-11-2009

Stroeve, J., & Notz, D. (2018). Changing state of Arctic sea ice across all seasons. *Environmental Research Letters*, *13*(10), 103001. https://doi.org/10.1088/1748-9326/aade56

Stroeve, J., Vancoppenolle, M., Veyssiere, G., Lebrun, M., Castellani, G., Babin, M., et al. (2021). A Multi-Sensor and Modeling Approach for Mapping Light Under Sea Ice During the Ice-Growth Season. *Frontiers in Marine Science, 7*. https://doi.org/10.3389/fmars.2020.592337

Williams, W. J., & Carmack, E. C. (2015). The 'interior' shelves of the Arctic Ocean: Physical oceanographic setting, climatology and effects of sea-ice retreat on cross-shelf exchange. *Progress in Oceanography*, *139*, 24–41. https://doi.org/10.1016/j.pocean.2015.07.008

Chapter 2 | Background

2.1. Overview

To explore the seasonal and spatial variations of the pertinent physical, environmental, and biological controls necessary for primary production to occur in Arctic first-year sea ice, this chapter examines the following aspects: a brief introduction of the optical properties and key variables associated with solar energy distribution (2.2.1); the interaction of radiation with the atmosphere and cloud cover (2.2.2.1); the principal role of snow cover in attenuating light and its melt phases (2.2.2.2); a summary of sea ice optical properties, melt phases, and its associations with primary producers (2.2.2.3); the seasonal variations in water column profiles and their associations with phytoplankton blooms (2.2.2.4); the influence of nutrient dynamics on primary producers (2.3.1); the optical properties of primary producer cells and the alterations in photosynthetic rates in response to varying levels of light (2.4.1); and, the coupled remote sensing methodology used in this research (2.5).

2.2. Physical Controls

2.2.1. Radiation Transfer Theory

The Sun emits radiation in the shortwave portion of the electromagnetic spectrum. The shortwave spectrum is divided into three categories based on their wavelength ranges: ultraviolet

(UV, 200-380 nm), visible (380-750 nm), and near-infrared (near-IR, 750-2500 nm). Photosynthetically active radiation (PAR) is restricted to 400 – 700 nm. Incident spectral shortwave radiation on a surface, or spectral irradiance ($E_{0W(\lambda)}$) is measured as the radiant flux per unit area and can be quantified as energy units (W m^{-2} nm^{-1}) or converted into photon flux ($E_{0P(\lambda)}$; µmol photons m^{-2} s^{-1} nm^{-1}).

Incident irradiance is either reflected, absorbed, or transmitted (Kirk 2010). Irradiance can be separated by its vector relative to the surface as either upwelling (E_u) or downwelling (E_d) irradiance. Based on the natural light field, measurements of reflection, attenuation, and transmission through a surface are known as apparent optical properties (AOPs). The most common AOPs in oceanography are transmittance, albedo, and the attenuation coefficient. Albedo is a unitless measurement, ranging from 0 to 1, describing the incident radiation reflected by a medium. Transmittance is the fraction of irradiance that passes through the medium, a function of the attenuation properties of a medium that can be expressed through the Beer-Lambert-Bougeur Law:

$$E_Z(z,\lambda) = (1-R)E_0(z_0,\lambda)e^{-z_0 K_d}$$

where $E_0(z_0,\lambda)$ and $E_Z(z,\lambda)$ are the incident and transmitted (to depth z(m)) spectral irradiances, respectively. Reflectance (*R*) in this formula represents the reflection off the surface. Albedo (α) is not necessarily the same as *R*, particularly over a high-scattering medium such as snow where it can be much greater, and is defined as:

$$\alpha = \frac{E_u}{E_d}$$

K_d (m^{-1}) is the downwelling attenuation coefficient and measures how light attenuates with depth. As opposed to AOPs, the properties of a medium that do not depend on the natural light field are known as inherent optical properties (IOPs). The absorption (a; m^{-1}) and scattering (b; m^{-1}) coefficients are two common IOPs used in marine optics.

2.2.2. Seasonal Progression of the Physical System

2.2.2.1. Clouds and Atmosphere

Insolation reaching the top of the atmosphere (TOA) in the Arctic is governed by seasonal and latitudinal changes in the solar zenith angle (Castellani et al., 2021). Initial seasonal insolation following polar night is marked by a large solar zenith angle, resulting in an oblique incidence angle that creates a longer path through the atmosphere (Minnett, 1999). As a result, the larger angle not only spreads the insolation over a larger area (i.e., lower irradiance), but also facilitates an increase in the number of scattering and absorption with atmospheric particles to reduce light transmission than compared to a lower solar zenith angle approaching the summer solstice (Curry et al., 1996; Eastman & Warren, 2010). Approximately 42% of incoming irradiance that reaches TOA is reflected back into space and absorbed by air molecules, aerosols, and clouds (Horvath, 1993).

Cloud presence modulates the extent of irradiance diffusivity. They are generated from low-pressure systems that force water vapour to rise, leading to water droplets and ice crystals forming around airborne particles. Cloud radiation distribution fluctuates with formation types, total cloud fraction, vertical distribution, water content and thermodynamic phase, and particle sizes (Curry et al., 1996; Eastman & Warren, 2010; Kay et al., 2008). In particular, clouds have different radiative effects depending on the time of year. In summer, clouds produce a cooling effect due to shortwave radiation scattering, whereas they act to warm the surface the rest of the

year by re-emitting radiation in the longwave spectrum (> 3-μm wavelength) (Curry et al., 1996; Eastman & Warren, 2010). Numerical modelling simulations indicate that general cloud coverages above 30% is sufficient to attenuate light (Castellani et al., 2021). However, the cloud-radiation feedback is complex and no conclusive long-term trends have been identified due to the interannual variability with seasonal sea ice concentrations. It can be reasonably inferred that cloudiness reaches peak levels in the summer due to sea ice retreat and open water periods driving released moisture into the air (Abe et al., 2015; He et al., 2019).

2.2.2.2. Snow

Snow on sea ice is considered the strongest control of light transmission to the water column. As snow grains are on the order of millimetres in size, they function as strong scatterers in a dry snowpack where scattering is the dominant IOP (Perovich, 2007). Snow scattering fraction depends on grain size, density, thickness, brine, and impurities (Warren, 1982). When snow deposits on sea ice, grains are shorn and become rounded due to gravitational settling (Iacozza & Barber, 1999; Mundy et al., 2005). Wind further reshapes snow and is treated as a vital contributor to snow layer formation (Sturm & Massom, 2017). The seasonal accumulation of snow layers, also known as the snowpack or cover, through kinetic and thermodynamic metamorphosis, contribute to increasing light attenuation. In fact, Perovich (1996) note that a snow cover as thin as 10 cm can reduce under-ice transmittance to less than 1% and creates a diffuse isotropic light environment (Fig. 1). Accordingly, a thicker snow cover will delay the start of an ice algal bloom, but prolong the bloom via added insulation from the warming atmosphere (Campbell et al., 2015; Leu et al., 2015). Highly deformed sea ice features such as ridges act as a snow trap, also increasing local snowpack thicknesses (Iacozza & Barber, 1999; Vérin et al., 2022).

Perovich & Polashenski (2012) note that the ability of snow to strongly scatter light results in a high albedo (>0.8) (Fig. 1). Snow albedo will rapidly decline through 3 melt phases to approximately 0.6 with air temperature increases. The first phase, the pendular phase, is delineated when air temperature approaches 0°C (Denoth, 1980, 1999), which leads to a rapid increase in grain size and clustering due to wet-snow metamorphism and thus a drop in albedo (Sturm & Massom, 2017). During this phase, snow grains are wet and the snowpack has less than 10% water saturation (Denoth, 1980). Above 10% saturation, the snowpack enters the funicular phase and is defined as where the pore space between snow grains is continuously saturated with water and is diverted to the snow-sea ice interface. Absorption is now the dominant IOP and creates a positive thermodynamic feedback loop promoting further snowmelt. The last phase, often referred to as slush, is the complete saturation and decay of the snowpack. This complete snow melt progression can occur from 10 days to up to a month, depending on weather conditions. (Perovich, 2007; Perovich & Polashenski, 2012; Sturm, 2002; Vérin et al., 2022).

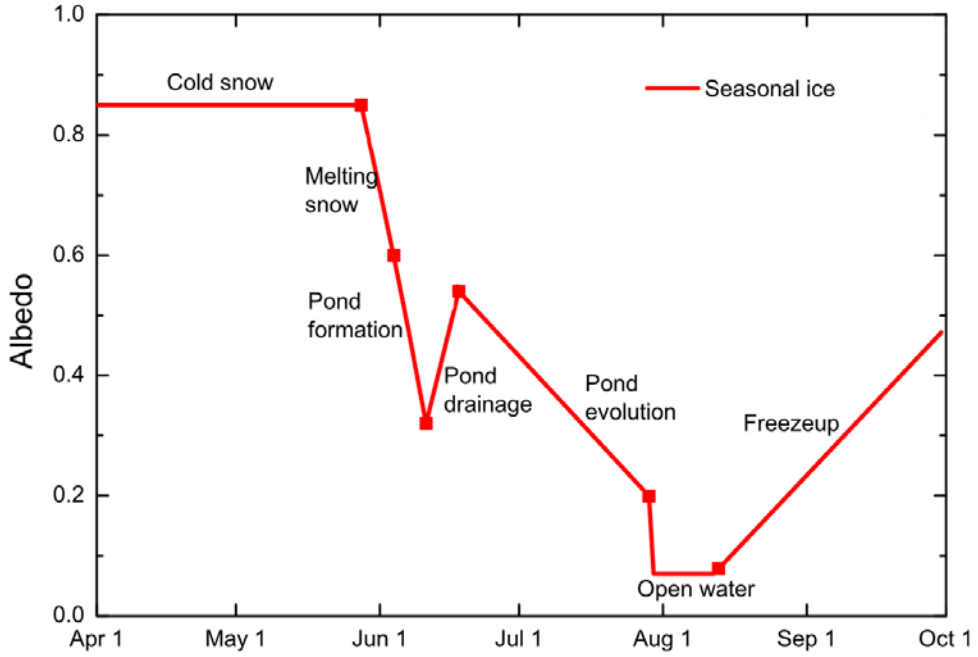

Figure 1. Key stages of seasonal albedo evolution for a first-year ice system. Modified from Perovich & Polashenski (2012). © 2023 John Wiley & Sons.

2.2.2.3. Sea Ice

The seasonal evolution of sea ice albedo is a useful measure for examining its optical properties. In summer, open seawater has an albedo (α) of ~ 0.07 (Fig. 1) (Perovich & Polashenski, 2012). Seawater has a depressed freezing point and temperature of maximum density due to its salinity (~ 32-34) (Timco & Weeks, 2010). Therefore, as seawater cools in autumn, denser water sinks, leading to surface water mixing. Frazil ice crystal formation (3-4 nm) occurs at approximately -1.8°C (i.e., freezing point is dependent on salinity), resulting in the ejection of dissolved salts and other impurities (Lund-Hansen et al., 2020; Petrich & Eicken, 2017). However, not all salts are expelled as the crystals consolidate into an ice layer and some are retained in the ice matrix, consisting mostly as brine at typical Arctic sea ice temperatures. Total brine salinity within developed sea ice is dynamic and proportional to sea ice temperature with bulk salinity following a C-shape gradient (Fig. 2) (Golden et al., 1998; Mundy & Meiners, 2021). It should be noted that ice formation will slow upon snow deposition as snow has a low thermal conductivity due to the presence of air pockets, creating an insulating layer that limits heat flow from the warmer ocean to the colder atmosphere (Sturm, 2002).

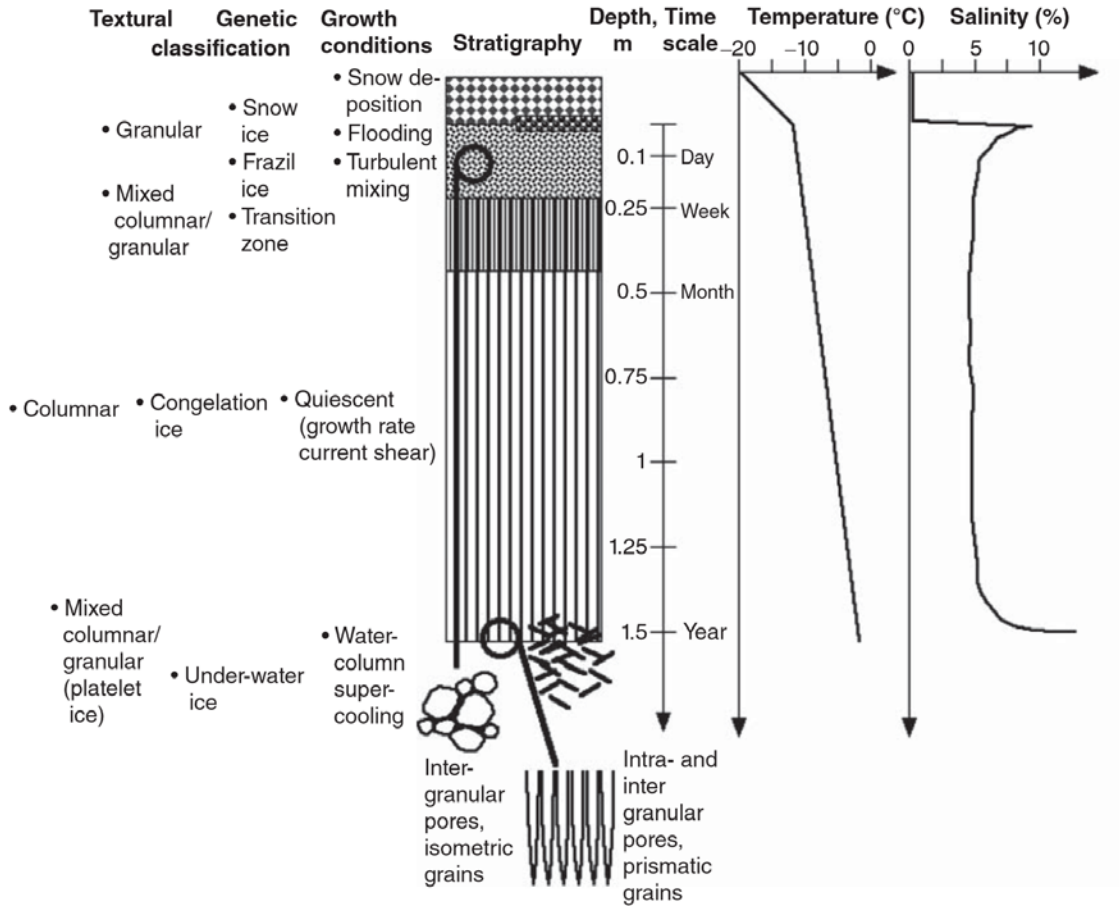

Figure 2. Classification of first-year sea ice layers in respect to their textural, growth, temperature, and salinity profiles. Figure from Petrich & Eicken (2017). © 2023 John Wiley & Sons.

Initial ice formation depends on the wave climate. In turbulent conditions, frazil ice tends to aggregate and form clusters, leading to the formation of slush and a thin grease ice layer, named after its appearance (Lund-Hansen et al., 2020; Petrich & Eicken, 2017). Grease ice has a slightly elevated albedo ($\alpha = 0.09$) due to frazil ice crystals in seawater reflecting light (Newyear & Martin, 1997). If frazil ice continues to form and accumulate in turbulent (wavy) waters, circular pancake ice floes can develop with raised edges due to collision with other pancake ice. Further consolidation will develop into an ice sheet. In contrast, under calm conditions, nilas ice forms ($\alpha = 0.16$), consisting of randomly oriented granular frazil ice crystals up to 10 cm thick (Perovich &

Polashenski, 2012; Petrich & Eicken, 2017; Weeks & Ackley, 1986). Below the granular layer, a transition layer forms, which exhibits increasing horizontal c-axis orientation of ice crystals due to geometric selection favoring faster ice growth along the crystal's a-axes (Fig. 2). At this point, the sea ice is considered young ice, with α = 0.27 and thickness ranging 10 - 30 cm (Fig. 1). Proceeding the transition layer is the columnar layer (Weeks & Hibler, 2010). Columnar sea ice contributes the bulk of sea ice thicknesses as it continues to elongate over the sea ice growth period (Weeks & Ackley, 1982). This layer is also associated with desalination mechanisms, primarily the ejection of dense brine by gravity drainage into the underlying water layer (Golden et al., 1998; Vancoppenolle et al., 2010). For sea ice thicknesses greater than 70 cm, albedo can range from 0.54-0.65 (Perovich & Polashenski, 2012; Petrich & Eicken, 2017). The bottommost layer of sea ice is the skeletal layer and is made up of lamellar protrusions that are separated by a sub-crystal structure of brine layers. The combination of these layers constitute the structure and growth processes of sea ice.

Sea ice decay begins with snow melt lowering albedo from greater than 0.8 to 0.6, as discussed in the last section, and meltwater accumulating on the sea ice surface, forming melt ponds (Eicken, 2002; Perovich & Polashenski, 2012). Despite wind-driven redistribution of snow, once snow drifts are established, they tend to remain stationary (Petrich et al., 2012b). Snow drifts are crucial in preconditioning melt pond morphology as thinner snow patches will melt earlier and more rapidly than thicker ones, resulting in a lower surface elevation for water to pool (Fig. 3) (Iacozza and Barber, 1999; Eicken et al., 2004). Initially, pond surfaces are above sea level and may temporarily freeze over from changes in atmospheric forcing (Eicken, 2002; Polashenski et al., 2012). The maximum hydraulic head (height of pond above sea level) is reached when meltwater expands horizontally, lowering albedo to a reported value of approximately 0.32 (Landy

et al., 2014; Perovich & Polashenski, 2012). Early season vertical meltwater transport occurs with draining through ice flaws, such as floe edges, cracks, or leads (Fig. 3). Pond drainage leads to the formation of a surface scattering layer (SSL), a 3-5 cm deep layer of drained ice that increases scattering, in-between melt ponds and therefore, increases average surface albedo up to ~ 0.54 (Polashenski et al., 2012; Smith et al., 2022). The SSL, known as white ice, reflects ~ 75% of incident sunlight, whereas a neighbouring melt ponded ice reflect ~ 40% of incident light (Frey et al., 2011; Light et al., 2015). Correspondingly, transmittance increases through melt ponds, which promotes the ice-albedo feedback loop: a process where radiation warms the under-ice water layer, induces basal sea ice melt to further enlarge ice flaws and enhance additional melt (Hudson et al., 2013; Itoh et al., 2011; Maykut & McPhee, 1995). Irradiance absorbed within the sea ice volume additionally contributes to ice melt and warming (Perovich et al., 1998). Vertical meltwater transport will increase as sea ice gradually connects to the sub-surface water layer until the hydraulic head is no longer present (Eicken et al., 2004). This equilibrium state occurs as sea ice ponds are level with seawater, and ponding is subject to freeboard level (Eicken et al., 2004; Landy et al., 2014). Thereafter, sea ice permeability increases and lowers albedo (α ~ 0.2) (Perovich & Polashenski, 2012), until complete structural erosion and melt occurs.

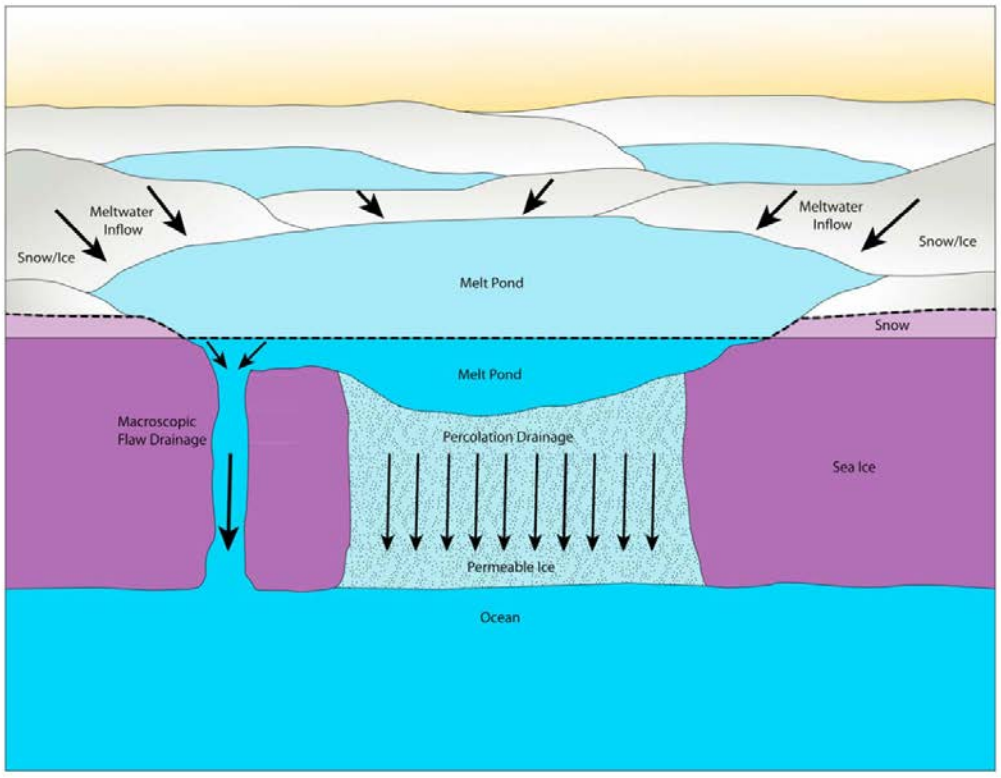

Figure 3. Schematic of ponded sea ice and the direction of meltwater transport. Figure from Polashenski et al. (2012). © 2023 John Wiley & Sons.

In terms of the two introduced inherent optical properties, the scattering and absorption coefficients of sea ice have contrasting roles. The scattering coefficient depends on sea ice microstructure: the orientation and layering of sea ice crystals (Ehn et al., 2008). Scattering is considered wavelength-independent in the visible spectrum as the refraction indices of gas, brine, and precipitated salts are weak, since the wavebands are smaller than the interacting particulates (Maykut & Light, 1995; Perovich, 2017). Incorporation of algae, sediment (Barber et al., 2021), particulate organic matter (Belzile et al., 2000), dust (Petrich et al., 2012a), and sea ice thickness itself (Palmisano & Simmons, 1987) alters spectral absorption levels. Therefore, sea ice optical properties exhibit spectral changes as a result of absorption, while changes in magnitude are attributed to scattering.

Based on water column diversity, hundreds of algal species can incorporate into sea ice actively or passively, but the number decreases over fall and winter through resource competition and adaptation to the harsh environmental conditions (Olsen et al., 2017; Poulin et al., 2011). Passive incorporation can occur when buoyant frazil ice crystals rise to the surface and collect algal cells or through selective filtering based on cell size within the granular and skeletal layer (Kauko et al., 2018; Lund-Hansen et al., 2017; Mundy & Meiners, 2021). Turbulent water conditions enhance frazil ice interaction with algal cells, thus promoting algal incorporation (Kauko et al., 2018; Weissenberger & Grossmann, 1998). The ice-water interface also influences algal colonization as rougher topography acts as a catch (Krembs et al., 2002). Active incorporation may result from algae such as diatoms, a common Arctic taxa, producing extracellular polymeric substances (EPS) that allow cells to attach to bottom sea ice (Juhl et al., 2011; Riedel et al., 2007).

Ice algal species primarily reside in the bottom 10 cm of sea ice as it has the largest habitable brine channel pore space and nutrient stores within a sea ice layer, but can be found throughout the ice volume (Leu et al., 2015). For example, flagellates tend to make up communities near the surface, diatoms dominate the bottom sea ice, and the interior has been observed to be a mixture (Van Leeuwe et al., 2018). Dalman et al. (2019) observed that strong under-ice currents can supply nutrients further up the ice matrix, expanding bottom-ice algal distribution. Ice algae are primarily expunged from sea ice due to heat influxes in spring and summer, causing brine channel flushing and the erosion and ablation of bottom sea ice (Campbell et al., 2014; Leu et al., 2015; Mundy et al., 2014; Tedesco et al., 2019).

2.2.2.4. Water Column

The progression of sea ice melt contributes to the shoaling of a fresher surface mixed layer (SML). The seasonal SML depth ranges from 5-30 m and is proportional to sea ice melt, surface

circulation, and proximity to riverine and terrestrial inputs (Peralta-Ferriz & Woodgate, 2015). Under-ice and ice-edge phytoplankton blooms that develop in the SML are constrained by nutrient supply (Ardyna et al., 2020; Janout et al., 2016; Lewis et al., 2019). Once nutrients are depleted, a less productive sub-surface chlorophyll maximum (SCM) may form in the pycnocline, the water layer underneath the SML where water density increases with depth (Fig. 4) (Palmer et al., 2013; Shiozaki et al., 2022). Mechanical stressors such as strong winds and storms enable vertical mixing between the stratified layers. Yet, the extension of open water periods in the Arctic has intensified SML heat absorption to enhance stratification further (Jackson et al., 2010).

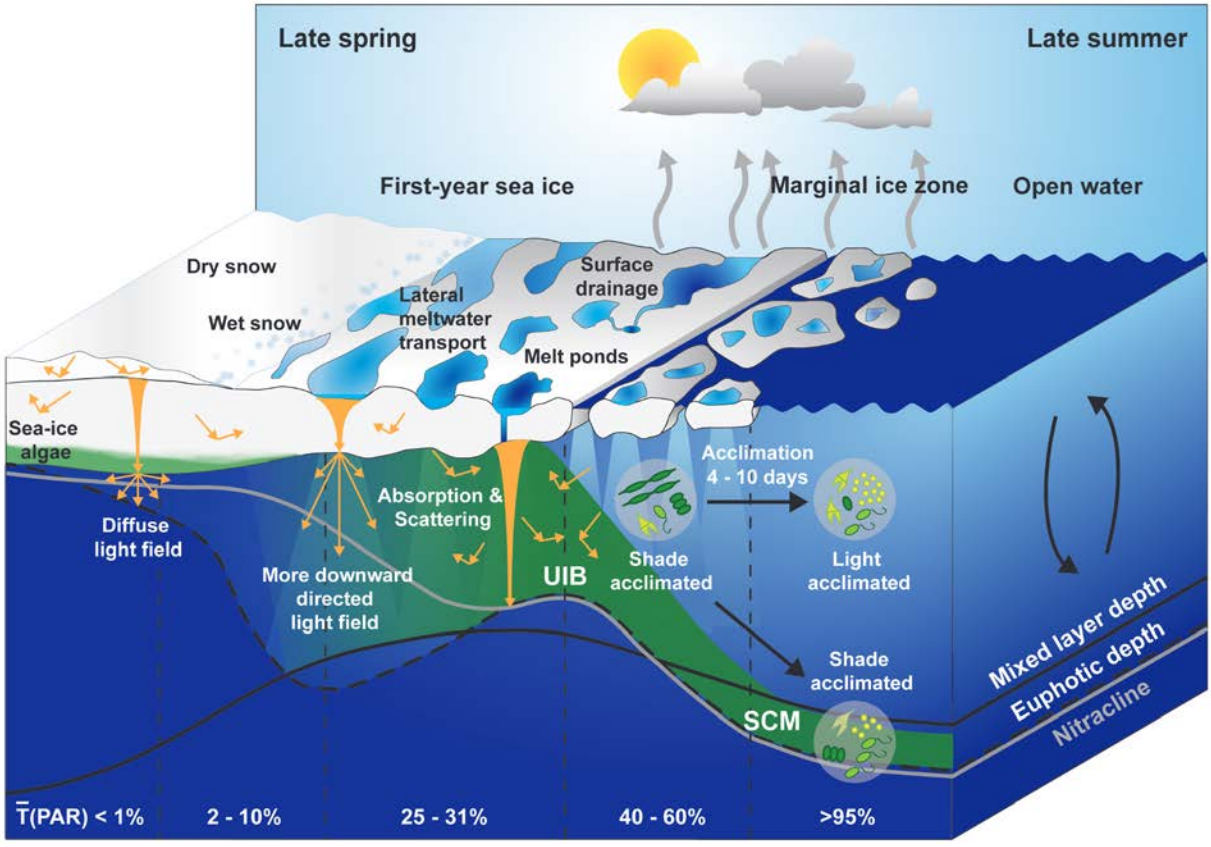

Figure 4. Seasonal progression of under-ice light transmittance (T(PAR)) in relation to biological and ocean layer constituents. Figure from Ardyna et al. (2020). © 2023 Ardyna, Mundy, Mayot, Matthes, Oziel, Horvat, Leu, Assmy, Hill, Matrai, Gale, Melnikov and Arrigo.

Light transmittance in the water column depends on snow and sea ice features such as melt ponds that can create spatial light variability at metre-length scales and shift euphotic zone depths (Fig. 4) (Frey et al., 2011; Laney et al., 2017; Perovich et al., 1998). Melt ponds alter the angular distribution of light by funnelling light downwards, producing an anisotropic light environment (Katlein et al., 2016; Matthes et al., 2019). Beneath 5-15 m, the under-ice light climate is homogenous (Matthes et al., 2020). Phytoplankton that bloom beneath the ice cover are shade-acclimated (Mundy et al., 2014). Bloom initiation has been found to occur between 4 – 10 days after ice algal bloom termination due to physical and environmental differences (Ardyna et al., 2020; Mundy et al., 2014). Assmy et al. (2017) also observed an under-ice bloom (UIB) to occur through a refrozen lead. The ability of water to scatter and absorb light is also essential in phytoplankton bloom dynamics. Scattering and absorptive constituents include sediment, coloured dissolved organic material (CDOM), living organisms and detritus (Pavlov et al., 2015).

2.3. Environmental Controls

2.3.1. Nutrient Supply

As touched upon in the last two sections, seasonal progression of radiation in the Arctic influences primary producers to assimilate differential levels of nutrients. The three essential macronutrients are dissolved forms of inorganic nitrogen, phosphorus, and silica. Although nitrogen is the primary limiting nutrient for cell growth through protein synthesis (Dugdale, 1967), phosphorus is essential for gene expression and to fix carbon to complete energy transfers during photosynthesis. Diatoms absorb silica to form their cell walls. Deviations in the cellular conservation of the Redfield ratio (106C:16N:15Si:1P) can be used to determine the health of primary producers relative to their marine environments (Daly et al., 1999; Frigstad et al., 2014; Kim et al., 2020). When considering marine environmental health, the ratio of nitrate plus nitrite

uptake relative to total inorganic nitrogen uptake (e.g., nitrate plus nitrite plus ammonium), known as the f-ratio, is used (Dugdale & Goering, 1967). A low f-ratio, or ammonium dominance, signifies a regenerated production due to the quick turnover of ammonia in the system. Regenerated production is associated with low standing stocks, smaller cells, and oligotrophic environments (Carmack & Wassmann, 2006; Li et al., 2009). Conversely, a high f-ratio indicates an ample nitrate supply, and associated primary production is commonly referred to as new production. The total supply of nutrients for primary production is the nutrient pool in the euphotic zone before bloom commencement, along with occasional injections (Tremblay & Gagnon, 2009). For example, riverine input and current transport can consist of an advective nutrient supply (Lannuzel et al., 2020). Upwelling and mixing events from winter convection processes, to shelf-break fronts, internal waves, and storm-induced mixing comprise the vertical component of nutrient delivery (Tremblay & Gagnon, 2009; Vancoppenolle et al., 2010). Vertical mixing is necessary to transport nutrients through strong summer stratification and photic zone limits (Leu et al., 2015). In certain regions, wind-driven nutrient resupply leads to fall phytoplankton blooms (Ardyna et al., 2014; Back et al., 2021; Castro de la Guardia et al., 2019). Sea ice communities receive nutrients from a convective exchange at the sea ice skeletal layer and through the remineralization of organic matter (Castellani et al., 2017; Tedesco et al., 2019).

2.4. Photosynthesis and Light Responses

Many primary producers can undergo photosynthesis in very low-light conditions. For example, ice algal communities have been found to require a minimum photon flux of 0.17 – 9 µmol photons m^{-2} s^{-1} to initiate blooms (Gosselin et al., 1986; Hancke et al., 2018; Horner & Schrader, 1982; Rysgaard et al., 2001), and a modelled 34 µmol photons m^{-2} s^{-1} for under-ice phytoplankton in a 20-m SML (Ardyna et al., 2020; Horvat et al., 2017). Light is harvested

primarily by chlorophyll-*a* pigments with a main absorption peak near 440 nm and a secondary peak near 670 nm. Accessory pigments (e.g., fucoxanthin, perodinin, chlorophyll-*b*, chlorophyll-*c*) expand spectral light absorption capabilities (Lund-Hansen et al., 2020). Pigments are found in the chloroplasts of thylakoid membranes and it is here that irradiance activates photosystem-specific electron-mediated pathways to produce energy in the form of adenosine triphosphate (ATP) and nicotinamide adenine dinucleotide phosphate (NADPH). These molecules are used to fix carbon and create products to meet the metabolic demands of regular cellular functioning and growth.

When light interacts with cell pigments, the spectral distribution of light shifts in proportion to their IOPs. The values of the chlorophyll-specific scattering coefficient (b^*_{ph}) and absorption coefficient (a^*_{ph}) are used in this regard and are governed by efficiency factors (Kirk, 2010; Morel & Bricaud, 1986). Scattering efficiency is less variable than absorption efficiency since the concentration of intracellular pigmentation affects the light path within a cell (Kirk, 2010; Morel & Bricaud, 1986; Nelson et al., 1993). Larger cells have a smaller surface area-to-volume ratio and require more light resources for regular functioning. Increases in photosynthetic pigments induce intracellular self-shading, also known as the package effect. As light travels within a cell and undergoes photosynthesis, primary producers can also re-emit a fraction of absorbed radiation as natural fluorescence. Natural fluorescence by algae emits in the 650-700 nm wavelength spectrum and is dependent on the intensity of light impinging on the cell (Lutz et al., 2001).

Primary producers acclimate to different light conditions by adjusting their pigment composition and photosynthetic machinery. In low-light situations, algae can increase photosynthetic pigments or alter electron turnover rates to increase photosynthetic efficiencies, (Cota, 1985). When irradiance increases, cells photoacclimate by elevating their maximum

photosynthetic rate and decreasing photosynthetic pigment cell content (Cota, 1985; Michel et al., 1988). Photoacclimation has been observed to take place over 48 hours (Morin et al., 2020). In the case of increasing UV radiation and high light conditions, photosystem complexes that carry chlorophyll pigments can be damaged, causing primary producers to place more energy into photoprotection strategies. Mycosporine-like amino acids for UV and carotene pigments for visible light are formed as sunscreens, but their function is a trade off with chlorophyll-absorption efficiencies (Alou-Font et al., 2013; Elliott et al., 2015; Ha et al., 2014). Another method involves quenching of excess electrons through bond-deoxygenation of xanthophyll pigments as heat (Derks & Bruce, 2018). Additionally, some diatom species within sea ice can vertically migrate away from extreme radiation conditions (Aumack et al., 2014). Phytoplankton were found to have higher photoacclimative capacities than ice algae due to their efficiency to utilize increasing levels of irradiances, whereas ice algae were nitrate-limited which reduced their photosynthetic efficiencies (Kvernvik et al., 2021). During light regime transitions, primary producers can switch from purely autotrophic strategies to heterotrophic strategies based on nutrient availability.

2.5. Remote Sensing

2.5.1. Satellite

Satellite remote sensing technology offers the ability to regularly monitor the evolution of Arctic physical and biological variables by passively or actively measuring different portions of the electromagnetic spectrum. Sensors utilizing different waveband ranges have their advantages and disadvantages. Passive visible spectrum sensors detect reflected light, restricting their application to a daytime collection and/or in the absence of clouds, but offer high levels of spatial resolution. The MODIS (Moderate Resolution Imaging Spectroradiometer) visible imaging sensor onboard NASA's Terra and Aqua satellites that launched in 1992 and 2002, respectively, remain a

popular data source due to its longevity and daily polar imaging frequency (Parera-Portell et al., 2021). Depending on the usage of its 36 channels, the spatial resolution can vary between 250 m and 1 km. MODIS imagery has been used to map sea ice thermodynamic states (Hall et al., 2004; Kang et al., 2014; Tschudi et al., 2008), cloud coverage (Ackerman et al., 2008; Kay & Gettelman, 2009), sea ice surface topography (Rösel & Kaleschke, 2012; Willmes & Heinemann, 2015), as well as phytoplankton biomass through chlorophyll-based ocean colour algorithms (Ardyna et al., 2014; Renaut et al., 2018; Shiozaki et al., 2022; Waga & Hirawake, 2020).

Unlike visible spectrum sensors, microwave wavelength sensors have received more attention to detecting Arctic surface physical properties since many microwave bands penetrate through cloud cover, can be used regardless of the time of day, and have strong contrasts in electromagnetic or dielectric properties between snow, sea ice, and water (Barber et al., 2001; Comiso, 1991). For example, the dielectric constant (ε^*) of snow is lower than ice in winter and therefore appears transparent in readings (Dierking, 2013). A medium's dielectric properties depend on its salinity, density, and temperature (Mahmud et al., 2020; Nandan et al., 2016; Yackel et al., 2001). Passive microwave satellite sensors collect natural microwave radiation readings from the Earth's surface. Due to the low amount of energy emitted at microwave frequencies, these sensors have a low spatial resolution, but the data generated continues to be invaluable for large-scale applications such as ice extent and age (Markus et al., 2009; Stroeve & Notz, 2018). Active microwave sensors are separated into two categories: imaging radar and non-imaging radar. Both forms transmit microwave signals to track surface backscatter. Non-imaging radar applications include the altimeter, which has been used to measure sea ice thickness by calculating the freeboard (Kwok, 2004). Imaging radars, specifically synthetic aperture radars (SAR), operate at swaths between 30 and 500 km and spatial resolutions between 1 and 1000 m (Dierking, 2013). The revisit

frequency enabled by satellite flight paths (at day-length time scales) make it possible to obtain high-resolution SAR time series data for physical systems (Fig. 5). Images retrieved from SAR sensors are affected by sensor parameters such as frequency, incident angle ranges, polarization types, and surface thermodynamic states (Barber & Nghiem, 1999; Livingstone et al., 1987). The most common microwave frequency used is C-band (3.75-7.5 cm, 4-8 GHz) as a compromise between ice contrast and penetration depth to enable year-round monitoring (Casey et al., 2016).

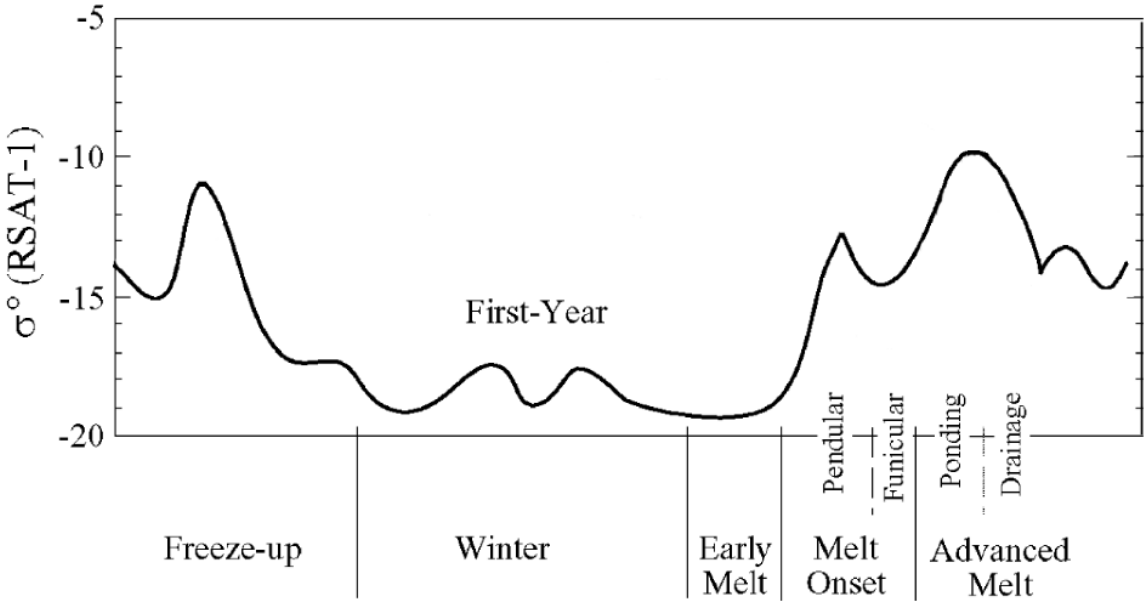

Figure 5. Summary of SAR seasonal backscatter evolution using the σ° coefficient applied to RADARSAT-1 data products. Modified from Yackel et al. (2007). © 2023 John Wiley & Sons.

2.5.2. Spectral Transmittance

Maykut and Grenfell (1975) were the first to examine that the light transmitted through sea ice results in a spectral distribution influenced by ice algae. Legendre and Gosselin (1991) took this a step further when they collected data to compute the ratio and under-ice irradiance at a wavelength pair that contrasted peak and trough absorption of chlorophyll *a*, and where

transmission through the ice was high. They found that *in situ* algal biomass estimates in first-year ice can be derived from spectral measurements of under-ice downwelling irradiance. As the method has become more widespread in recent years, different algorithms have arisen to calculate the irradiance spectra produced. Normalized difference indices (NDIs) employed by Mundy et al. (2007) have remained the most popular bio-optical method (Anhaus et al., 2021; Campbell et al., 2014; Forrest et al., 2019; Lange et al., 2016; Wongpan et al., 2018) as it explains the most data variability (Melbourne-Thomas et al., 2015). Simple ratios of spectral irradiance based on maximal absorption peaks of algal pigments have also been utilized (Fritsen et al., 2011; Honda et al., 2009). Scaled band areas, which use regression techniques to observe the strength of pigment absorption (Carrère et al., 2004), along with empirical orthogonal function analysis, which reduces the dimensionality of data to obtain dominant signals are other methods that have been considered (Katlein et al., 2015; Taylor et al., 2013). Different types of radiometer sensors, such as irradiance and radiance sensors, further enhance our understanding of light measurements. Irradiance sensors incorporate a cosine-corrected or scalar field of view to account and compensate for the angular sensitivity of the sensor and accurately measure the total incident light field. In contrast, radiance sensors are typically designed with a narrower field, allowing them to capture light from specific directions or within a limited angle (Cimoli et al., 2017). Spectral radiometers can also be categorized based on the geometric shape of their sensors. Planar light sensors have a photosensitive surface designed to capture light incident to its plane. Spherical light sensors integrate light from all directions. Spectral radiometers have been attached to L-arms (Campbell et al., 2014; Mundy et al., 2007; Wongpan et al., 2020), mounted on remotely operated vehicles (Arndt et al., 2017; Lange et al., 2016; Matthes et al., 2020), under-ice trawls (Castellani et al.,

2020; Meiners et al., 2017), and deployed via ice buoys on ice that extend a cable of sensors through a drilled ice hole (Hill et al., 2022; Hill et al., 2018).

2.6. References

Abe, M., Nozawa, T., Ogura, T., & Takata, K. (2015). Effect of retreating sea ice on Arctic cloud cover in simulated recent global warming. *Atmospheric Chemistry and Physics Discussions*, *15*(12), 17527–17552. https://doi.org/10.5194/acpd-15-17527-2015

Ackerman, S. A., Holz, R. E., Frey, R., Eloranta, E. W., Maddux, B. C., & McGill, M. (2008). Cloud Detection with MODIS. Part II: Validation. *Journal of Atmospheric and Oceanic Technology*, *25*(7), 1073–1086. https://doi.org/10.1175/2007JTECHA1053.1

Alou-Font, E., Mundy, C., Roy, S., Gosselin, M., & Agustí, S. (2013). Snow cover affects ice algal pigment composition in the coastal Arctic Ocean during spring. *Marine Ecology Progress Series*, *474*, 89–104. https://doi.org/10.3354/meps10107

Anhaus, P., Katlein, C., Nicolaus, M., Arndt, S., Jutila, A., & Haas, C. (2021). Snow Depth Retrieval on Arctic Sea Ice Using Under-Ice Hyperspectral Radiation Measurements. *Frontiers in Earth Science*, *9*. Retrieved from https://www.frontiersin.org/article/10.3389/feart.2021.711306

Ardyna, M., Babin, M., Gosselin, M., Devred, E., Rainville, L., & Tremblay, J.-É. (2014). Recent Arctic Ocean sea ice loss triggers novel fall phytoplankton blooms. *Geophysical Research Letters*, *41*(17), 6207–6212. https://doi.org/10.1002/2014GL061047

Ardyna, M., Mundy, C. J., Mayot, N., Matthes, L. C., Oziel, L., Horvat, C., et al. (2020). Under-Ice Phytoplankton Blooms: Shedding Light on the "Invisible" Part of Arctic Primary Production. *Frontiers in Marine Science*, *7*, 608032. https://doi.org/10.3389/fmars.2020.608032

Arndt, S., Meiners, K. M., Ricker, R., Krumpen, T., Katlein, C., & Nicolaus, M. (2017). Influence of snow depth and surface flooding on light transmission through Antarctic pack ice. *Journal of Geophysical Research: Oceans*, *122*(3), 2108–2119. https://doi.org/10.1002/2016JC012325

Assmy, P., Fernández-Méndez, M., Duarte, P., Meyer, A., Randelhoff, A., Mundy, C. J., et al. (2017). Leads in Arctic pack ice enable early phytoplankton blooms below snow-covered sea ice. *Scientific Reports*, *7*(1), 40850. https://doi.org/10.1038/srep40850

Aumack, C. F., Juhl, A. R., & Krembs, C. (2014). Diatom vertical migration within land-fast Arctic sea ice. *Journal of Marine Systems*, *139*, 496–504. https://doi.org/10.1016/j.jmarsys.2014.08.013

Back, D.-Y., Ha, S.-Y., Else, B., Hanson, M., Jones, S. F., Shin, K.-H., et al. (2021). On the impact of wastewater effluent on phytoplankton in the Arctic coastal zone: A case study in the Kitikmeot Sea of the Canadian Arctic. *Science of The Total Environment*, *764*, 143861. https://doi.org/10.1016/j.scitotenv.2020.143861

Barber, D. G., Yackel, J. J., & Hanesiak, J. M. (2001). Sea Ice, RADARSAT-1 and Arctic Climate Processes: A Review and Update. *Canadian Journal of Remote Sensing*, *27*(1), 51–61. https://doi.org/10.1080/07038992.2001.10854919

Barber, D. G., Harasyn, M. L., Babb, D. G., Capelle, D., McCullough, G., Dalman, L. A., et al. (2021). Sediment-laden sea ice in southern Hudson Bay: Entrainment, transport, and biogeochemical implications. *Elem Sci Anth*, *9*(1), 00108.

Barber, David G., & Nghiem, S. V. (1999). The role of snow on the thermal dependence of microwave backscatter over sea ice. *Journal of Geophysical Research: Oceans*, *104*(C11), 25789–25803. https://doi.org/10.1029/1999JC900181

Belzile, C., Johannessen, S. C., Gosselin, M., Demers, S., & Miller, W. L. (2000). Ultraviolet attenuation by dissolved and particulate constituents of first-year ice during late spring in an Arctic polynya. *Limnology and Oceanography*, *45*(6), 1265–1273. https://doi.org/10.4319/lo.2000.45.6.1265

Campbell, K., Mundy, C. J., Barber, D. G., & Gosselin, M. (2015). Characterizing the sea ice algae chlorophyll a –snow depth relationship over Arctic spring melt using transmitted irradiance. *Journal of Marine Systems*, *147*, 76–84. https://doi.org/10.1016/j.jmarsys.2014.01.008

Campbell, Karley, Mundy, C. J., Barber, D. G., & Gosselin, M. (2014). Remote Estimates of Ice Algae Biomass and Their Response to Environmental Conditions during Spring Melt. *ARCTIC*, *67*(3), 375. https://doi.org/10.14430/arctic4409

Carmack, E., & Wassmann, P. (2006). Food webs and physical–biological coupling on pan-Arctic shelves: Unifying concepts and comprehensive perspectives. *Progress in Oceanography*, *71*(2), 446–477. https://doi.org/10.1016/j.pocean.2006.10.004

Carrère, V., Spilmont, N., & Davoult, D. (2004). Comparison of simple techniques for estimating chlorophyll a concentration in the intertidal zone using high spectral-resolution field-spectrometer data. *Marine Ecology Progress Series*, *274*, 31–40. https://doi.org/10.3354/meps274031

Casey, J. A., Howell, S. E. L., Tivy, A., & Haas, C. (2016). Separability of sea ice types from wide swath C- and L-band synthetic aperture radar imagery acquired during the melt season. *Remote Sensing of Environment*, *174*, 314–328. https://doi.org/10.1016/j.rse.2015.12.021

Castellani, G., Losch, M., Lange, B. A., & Flores, H. (2017). Modeling Arctic sea-ice algae: Physical drivers of spatial distribution and algae phenology. *Journal of Geophysical Research: Oceans*, *122*(9), 7466–7487. https://doi.org/10.1002/2017JC012828

Castellani, G., Schaafsma, F. L., Arndt, S., Lange, B. A., Peeken, I., Ehrlich, J., et al. (2020). Large-Scale Variability of Physical and Biological Sea-Ice Properties in Polar Oceans. *Frontiers in Marine Science*, *7*. https://doi.org/10.3389/fmars.2020.00536

Castellani, G., Veyssière, G., Karcher, M., Stroeve, J., Banas, S. N., Bouman, A. H., et al. (2021). Shine a light: Under-ice light and its ecological implications in a changing Arctic Ocean. *Ambio*. https://doi.org/10.1007/s13280-021-01662-3

Castro de la Guardia, L., Garcia-Quintana, Y., Claret, M., Hu, X., Galbraith, E. D., & Myers, P. G. (2019). Assessing the Role of High-Frequency Winds and Sea Ice Loss on Arctic Phytoplankton Blooms in an Ice-Ocean-Biogeochemical Model. *Journal of Geophysical Research: Biogeosciences*, *124*(9), 2728–2750. https://doi.org/10.1029/2018JG004869

Cimoli, E., Meiners, K. M., Lund-Hansen, L. C., & Lucieer, V. (2017). Spatial variability in sea-ice algal biomass: an under-ice remote sensing perspective. *Advances in Polar Science*, *28*(4), 30. https://doi.org/10.13679/j.advps.2017.4.00268

Comiso, J. C. (1991). Satellite remote sensing of the Polar Oceans. *Journal of Marine Systems*, *2*(3–4), 395–434. https://doi.org/10.1016/0924-7963(91)90044-U

Cota, G. F. (1985). Photoadaptation of high Arctic ice algae. *Nature*, *315*(6016), 219–222. https://doi.org/10.1038/315219a0

Curry, J. A., Schramm, J. L., Rossow, W. B., & Randall, D. (1996). Overview of Arctic Cloud and Radiation Characteristics. *Journal of Climate*, *9*(8), 1731–1764. https://doi.org/10.1175/1520-0442(1996)009<1731:OOACAR>2.0.CO;2

Dalman, L. A., Else, B. G. T., Barber, D., Carmack, E., Williams, W. J., Campbell, K., et al. (2019). Enhanced bottom-ice algal biomass across a tidal strait in the Kitikmeot Sea of the Canadian Arctic. *Elem Sci Anth*, *7*(1), 22. https://doi.org/10.1525/elementa.361

Daly, K. L., Wallace, D. W. R., Smith Jr., W. O., Skoog, A., Lara, R., Gosselin, M., et al. (1999). Non-Redfield carbon and nitrogen cycling in the Arctic: Effects of ecosystem structure and dynamics. *Journal of Geophysical Research: Oceans*, *104*(C2), 3185–3199. https://doi.org/10.1029/1998JC900071

Denoth, A. (1980). The Pendular-Funicular Liquid Transition in Snow. *Journal of Glaciology*, *25*(91), 93–98. https://doi.org/10.3189/S0022143000010315

Denoth, A. (1999). Wet snow pendular regime: the amount of water in ring-shaped configurations. *Cold Regions Science and Technology*, *30*(1), 13–18. https://doi.org/10.1016/S0165-232X(99)00007-5

Derks, A. K., & Bruce, D. (2018). Rapid regulation of excitation energy in two pennate diatoms from contrasting light climates. *Photosynthesis Research*, *138*(2), 149–165. https://doi.org/10.1007/s11120-018-0558-0

Dierking, W. (2013). Sea Ice Monitoring by Synthetic Aperture Radar. *Oceanography*, *26*(2). https://doi.org/10.5670/oceanog.2013.33

Dugdale, R. C. (1967). Nutrient Limitation in the Sea: Dynamics, Identification, and Significance1. *Limnology and Oceanography*, *12*(4), 685–695. https://doi.org/10.4319/lo.1967.12.4.0685

Dugdale, R. C., & Goering, J. J. (1967). Uptake of New and Regenerated Forms of Nitrogen in Primary Productivity1. *Limnology and Oceanography*, *12*(2), 196–206. https://doi.org/10.4319/lo.1967.12.2.0196

Eastman, R., & Warren, S. G. (2010). Interannual Variations of Arctic Cloud Types in Relation to Sea Ice. *Journal of Climate*, *23*(15), 4216–4232. https://doi.org/10.1175/2010JCLI3492.1

Ehn, J. K., Papakyriakou, T. N., & Barber, D. G. (2008). Inference of optical properties from radiation profiles within melting landfast sea ice. *Journal of Geophysical Research*, *113*(C9), C09024. https://doi.org/10.1029/2007JC004656

Eicken, H. (2002). Tracer studies of pathways and rates of meltwater transport through Arctic summer sea ice. *Journal of Geophysical Research*, *107*(C10), 8046. https://doi.org/10.1029/2000JC000583

Eicken, H., Grenfell, T. C., Perovich, D. K., Richter-Menge, J. A., & Frey, K. (2004). Hydraulic controls of summer Arctic pack ice albedo. *Journal of Geophysical Research: Oceans*, *109*(C8), C08007. https://doi.org/10.1029/2003JC001989

Elliott, A., Mundy, C., Gosselin, M., Poulin, M., Campbell, K., & Wang, F. (2015). Spring production of mycosporine-like amino acids and other UV-absorbing compounds in sea ice-associated algae communities in the Canadian Arctic. *Marine Ecology Progress Series*, *541*, 91–104. https://doi.org/10.3354/meps11540

Forrest, A. L., Lund-Hansen, L. C., Sorrell, B. K., Bowden-Floyd, I., Lucieer, V., Cossu, R., et al. (2019). Exploring Spatial Heterogeneity of Antarctic Sea Ice Algae Using an Autonomous

Underwater Vehicle Mounted Irradiance Sensor. *Frontiers in Earth Science*, *0*. https://doi.org/10.3389/feart.2019.00169

Frey, K. E., Perovich, D. K., & Light, B. (2011). The spatial distribution of solar radiation under a melting Arctic sea ice cover. *Geophysical Research Letters*, *38*(22), 6. https://doi.org/10.1029/2011GL049421

Frigstad, H., Andersen, T., Bellerby, R., Silyakova, A., & Hessen, D. (2014). Variation in the seston C:N ratio of the Arctic Ocean and pan-Arctic shelves. *Journal of Marine Systems*, *129*, 214–223. https://doi.org/10.1016/j.jmarsys.2013.06.004

Fritsen, C. H., Wirthlin, E. D., Momberg, D. K., Lewis, M. J., & Ackley, S. F. (2011). Bio-optical properties of Antarctic pack ice in the early austral spring. *Deep Sea Research Part II: Topical Studies in Oceanography*, *58*(9), 1052–1061. https://doi.org/10.1016/j.dsr2.2010.10.028

Golden, K. M., Ackley, S. F., & Lytle, V. I. (1998). The Percolation Phase Transition in Sea Ice. *Science*, *282*(5397), 2238–2241. https://doi.org/10.1126/science.282.5397.2238

Gosselin, M., Legendre, L., Therriault, J.-C., Demers, S., & Rochet, M. (1986). Physical control of the horizontal patchiness of sea-ice microalgae. *Marine Ecology Progress Series*, *29*, 289–298. https://doi.org/10.3354/meps029289

Ha, S.-Y., Min, J.-O., Joo, H. M., Chung, K. H., Shin, K.-H., Yang, E., & Kang, S.-H. (2014). Production rate estimation of mycosporine-like amino acids in two Arctic melt ponds by stable isotope probing with NAH ^{13} CO $_{3}$. *Journal of Phycology*, *50*(5), 901–907. https://doi.org/10.1111/jpy.12221

Hall, D. K., Key, J. R., Casey, K. A., Riggs, G. A., & Cavalieri, D. J. (2004). Sea ice surface temperature product from MODIS. *IEEE Transactions on Geoscience and Remote Sensing*, *42*(5), 1076–1087. https://doi.org/10.1109/TGRS.2004.825587

Hancke, K., Lund-Hansen, L. C., Lamare, M. L., Højlund Pedersen, S., King, M. D., Andersen, P., & Sorrell, B. K. (2018). Extreme Low Light Requirement for Algae Growth Underneath Sea Ice: A Case Study From Station Nord, NE Greenland: MINIMUM LIGHT REQUIREMENT FOR ICE ALGAE. *Journal of Geophysical Research: Oceans*, *123*(2), 985–1000. https://doi.org/10.1002/2017JC013263

He, M., Hu, Y., Chen, N., Wang, D., Huang, J., & Stamnes, K. (2019). High cloud coverage over melted areas dominates the impact of clouds on the albedo feedback in the Arctic. *Scientific Reports*, *9*(1), 9529. https://doi.org/10.1038/s41598-019-44155-w

Hill, V., Light, B., Steele, M., & Sybrandy, A. L. (2022). Contrasting Sea-Ice Algae Blooms in a Changing Arctic Documented by Autonomous Drifting Buoys. *Journal of Geophysical Research: Oceans*, *127*(7). https://doi.org/10.1029/2021JC017848

Hill, V. J., Light, B., Steele, M., & Zimmerman, R. C. (2018). Light Availability and Phytoplankton Growth Beneath Arctic Sea Ice: Integrating Observations and Modeling. *Journal of Geophysical Research: Oceans*, *123*(5), 3651–3667. https://doi.org/10.1029/2017JC013617

Honda, M. C., Sasaoka, K., Kawakami, H., Matsumoto, K., Watanabe, S., & Dickey, T. (2009). Application of underwater optical data to estimation of primary productivity. *Deep Sea Research Part I: Oceanographic Research Papers*, *56*(12), 2281–2292. https://doi.org/10.1016/j.dsr.2009.08.009

Horner, R., & Schrader, G. C. (1982). Relative Contributions of Ice Algae, Phytoplankton, and Benthic Microalgae to Primary Production in Nearshore Regions of the Beaufort Sea. *ARCTIC*, *35*(4), 485–503. https://doi.org/10.14430/arctic2356

Horvat, C., Jones, D. R., Iams, S., Schroeder, D., Flocco, D., & Feltham, D. (2017). The frequency and extent of sub-ice phytoplankton blooms in the Arctic Ocean. *Science Advances*, *3*(3), e1601191. https://doi.org/10.1126/sciadv.1601191

Horvath, H. (1993). Atmospheric light absorption—A review. *Atmospheric Environment. Part A. General Topics*, *27*(3), 293–317. https://doi.org/10.1016/0960-1686(93)90104-7

Hudson, S. R., Granskog, M. A., Sundfjord, A., Randelhoff, A., Renner, A. H. H., & Divine, D. V. (2013). Energy budget of first-year Arctic sea ice in advanced stages of melt. *Geophysical Research Letters*, *40*(11), 2679–2683. https://doi.org/10.1002/grl.50517

Iacozza, J., & Barber, D. G. (1999). An examination of the distribution of snow on sea-ice. *Atmosphere-Ocean*, *37*(1), 21–51. https://doi.org/10.1080/07055900.1999.9649620

Itoh, M., Inoue, J., Shimada, K., Zimmermann, S., Kikuchi, T., Hutchings, J., et al. (2011). Acceleration of sea-ice melting due to transmission of solar radiation through ponded ice area in the Arctic Ocean: results of in situ observations from icebreakers in 2006 and 2007. *Annals of Glaciology*, *52*(57), 249–260. https://doi.org/10.3189/172756411795931471

Jackson, J. M., Carmack, E. C., McLaughlin, F. A., Allen, S. E., & Ingram, R. G. (2010). Identification, characterization, and change of the near-surface temperature maximum in the Canada Basin, 1993–2008. *Journal of Geophysical Research*, *115*(C5), C05021. https://doi.org/10.1029/2009JC005265

Janout, M. A., Hölemann, J., Waite, A. M., Krumpen, T., von Appen, W.-J., & Martynov, F. (2016). Sea-ice retreat controls timing of summer plankton blooms in the Eastern Arctic Ocean. *Geophysical Research Letters*, *43*(24), 12,493-12,501. https://doi.org/10.1002/2016GL071232

Juhl, A., Krembs, C., & Meiners, K. (2011). Seasonal development and differential retention of ice algae and other organic fractions in first-year Arctic sea ice. *Marine Ecology Progress Series*, *436*, 1–16. https://doi.org/10.3354/meps09277

Kang, D., Im, J., Lee, M.-I., & Quackenbush, L. J. (2014). The MODIS ice surface temperature product as an indicator of sea ice minimum over the Arctic Ocean. *Remote Sensing of Environment*, *152*, 99–108. https://doi.org/10.1016/j.rse.2014.05.012

Katlein, C., Arndt, S., Nicolaus, M., Perovich, D. K., Jakuba, M. V., Suman, S., et al. (2015). Influence of ice thickness and surface properties on light transmission through A rctic sea ice. *Journal of Geophysical Research: Oceans*, *120*(9), 5932–5944. https://doi.org/10.1002/2015JC010914

Katlein, C., Perovich, D. K., & Nicolaus, M. (2016). Geometric Effects of an Inhomogeneous Sea Ice Cover on the under Ice Light Field. *Frontiers in Earth Science*, *4*. https://doi.org/10.3389/feart.2016.00006

Kauko, H. M., Olsen, L. M., Duarte, P., Peeken, I., Granskog, M. A., Johnsen, G., et al. (2018). Algal Colonization of Young Arctic Sea Ice in Spring. *Frontiers in Marine Science*, *5*. Retrieved from https://www.frontiersin.org/articles/10.3389/fmars.2018.00199

Kay, J. E., & Gettelman, A. (2009). Cloud influence on and response to seasonal Arctic sea ice loss. *Journal of Geophysical Research: Atmospheres*, *114*(D18). https://doi.org/10.1029/2009JD011773

Kay, J. E., L'Ecuyer, T., Gettelman, A., Stephens, G., & O'Dell, C. (2008). The contribution of cloud and radiation anomalies to the 2007 Arctic sea ice extent minimum. *Geophysical Research Letters*, *35*(8), L08503. https://doi.org/10.1029/2008GL033451

Kim, K., Ha, S.-Y., Kim, B. K., Mundy, C. J., Gough, K. M., Pogorzelec, N. M., & Lee, S. H. (2020). Carbon and nitrogen uptake rates and macromolecular compositions of bottom-ice

algae and phytoplankton at Cambridge Bay in Dease Strait, Canada. *Annals of Glaciology*, 1–11. https://doi.org/10.1017/aog.2020.17

Kirk, J. T. O. (2010). *Light and Photosynthesis in Aquatic Ecosystems* (3rd ed.). Cambridge: Cambridge University Press. https://doi.org/10.1017/CBO9781139168212

Krembs, C., Tuschling, K., & v. Juterzenka, K. (2002). The topography of the ice-water interface – its influence on the colonization of sea ice by algae. *Polar Biology*, *25*(2), 106–117. https://doi.org/10.1007/s003000100318

Kvernvik, A., Hoppe, C., Greenacre, M., Verbiest, S., Wiktor, J., Gabrielsen, T., et al. (2021). Arctic sea ice algae differ markedly from phytoplankton in their ecophysiological characteristics. *Marine Ecology Progress Series*, *666*, 31–55. https://doi.org/10.3354/meps13675

Kwok, R. (2004). Annual cycles of multiyear sea ice coverage of the Arctic Ocean: 1999–2003. *Journal of Geophysical Research: Oceans*, *109*(C11). https://doi.org/10.1029/2003JC002238

Landy, J., Ehn, J., Shields, M., & Barber, D. (2014). Surface and melt pond evolution on landfast first-year sea ice in the Canadian Arctic Archipelago. *Journal of Geophysical Research: Oceans*, *119*(5), 3054–3075. https://doi.org/10.1002/2013JC009617

Laney, S. R., Krishfield, R. A., & Toole, John. M. (2017). The euphotic zone under Arctic Ocean sea ice: Vertical extents and seasonal trends: The euphotic zone under Arctic sea ice. *Limnology and Oceanography*, *62*(5), 1910–1934. https://doi.org/10.1002/lno.10543

Lange, B. A., Katlein, C., Nicolaus, M., Peeken, I., & Flores, H. (2016). Sea ice algae chlorophyll a concentrations derived from under-ice spectral radiation profiling platforms. *Journal of Geophysical Research: Oceans*, *121*(12), 8511–8534. https://doi.org/10.1002/2016JC011991

Lannuzel, D., Tedesco, L., van Leeuwe, M., Campbell, K., Flores, H., Delille, B., et al. (2020). The future of Arctic sea-ice biogeochemistry and ice-associated ecosystems. *Nature Climate Change*, *10*(11), 983–992. https://doi.org/10.1038/s41558-020-00940-4

Legendre, L., & Gosselin, M. (1991). In situ spectroradiometric estimation of microalgal biomass in first-year sea ice. *Polar Biology*, *11*(2). https://doi.org/10.1007/BF00234273

Leu, E., Mundy, C. J., Assmy, P., Campbell, K., Gabrielsen, T. M., Gosselin, M., et al. (2015). Arctic spring awakening – Steering principles behind the phenology of vernal ice algal blooms. *Progress in Oceanography*, *139*, 151–170. https://doi.org/10.1016/j.pocean.2015.07.012

Lewis, K. M., Arntsen, A. E., Coupel, P., Joy-Warren, H., Lowry, K. E., Matsuoka, A., et al. (2019). Photoacclimation of Arctic Ocean phytoplankton to shifting light and nutrient limitation: Photoacclimation to shifting light and nutrients. *Limnology and Oceanography*, *64*(1), 284–301. https://doi.org/10.1002/lno.11039

Li, W. K. W., McLaughlin, F. A., Lovejoy, C., & Carmack, E. C. (2009). Smallest Algae Thrive As the Arctic Ocean Freshens. *Science*, *326*(5952), 539–539. https://doi.org/10.1126/science.1179798

Light, B., Perovich, D. K., Webster, M. A., Polashenski, C., & Dadic, R. (2015). Optical properties of melting first-year Arctic sea ice. *Journal of Geophysical Research: Oceans*, *120*(11), 7657–7675. https://doi.org/10.1002/2015JC011163

Livingstone, C. E., Singh, K. P., & Gray, A. L. (1987). Seasonal and Regional Variations of Active/Passive Microwave Signatures of Sea Ice. *IEEE Transactions on Geoscience and Remote Sensing*, *GE-25*(2), 159–173. https://doi.org/10.1109/TGRS.1987.289815

Lund-Hansen, L. C., Hawes, I., Nielsen, M. H., & Sorrell, B. K. (2017). Is colonization of sea ice by diatoms facilitated by increased surface roughness in growing ice crystals? *Polar Biology*, *40*(3), 593–602. https://doi.org/10.1007/s00300-016-1981-3

Lund-Hansen, L. C., Søgaard, D. H., Sorrell, B. K., Gradinger, R., & Meiners, K. M. (2020). *Arctic Sea Ice Ecology: Seasonal Dynamics in Algal and Bacterial Productivity*. Cham: Springer International Publishing. https://doi.org/10.1007/978-3-030-37472-3

Lutz, V. A., Sathyendaranath, S., Head, E. J. H., & Li, W. K. W. (2001). Changes in the In Vivo Absorption and Fluorescence Excitation Spectra with Growth Irradiance in Three Species of Phytoplankton. *Journal of Plankton Research*, *23*(6), 555–569. https://doi.org/10.1093/plankt/23.6.555

Mahmud, M. S., Nandan, V., Howell, S. E. L., Geldsetzer, T., & Yackel, J. (2020). Seasonal evolution of L-band SAR backscatter over landfast Arctic sea ice. *Remote Sensing of Environment*, *251*, 112049. https://doi.org/10.1016/j.rse.2020.112049

Markus, T., Stroeve, J. C., & Miller, J. (2009). Recent changes in Arctic sea ice melt onset, freezeup, and melt season length. *Journal of Geophysical Research: Oceans*, *114*(C12). https://doi.org/10.1029/2009JC005436

Matthes, L. C., Ehn, J. K., L.-Girard, S., Pogorzelec, N. M., Babin, M., & Mundy, C. J. (2019). Average cosine coefficient and spectral distribution of the light field under sea ice: Implications for primary production. *Elementa: Science of the Anthropocene*, *7*, 25. https://doi.org/10.1525/elementa.363

Matthes, Lisa C., Mundy, C. J., L.-Girard, S., Babin, M., Verin, G., & Ehn, J. K. (2020). Spatial Heterogeneity as a Key Variable Influencing Spring-Summer Progression in UVR and PAR Transmission Through Arctic Sea Ice. *Frontiers in Marine Science*, *7*, 183. https://doi.org/10.3389/fmars.2020.00183

Maykut, G. A., & Light, B. (1995). Refractive-index measurements in freezing sea-ice and sodium chloride brines. *Applied Optics*, *34*(6), 950–961. https://doi.org/10.1364/AO.34.000950

Maykut, G. A., & McPhee, M. G. (1995). Solar heating of the Arctic mixed layer. *Journal of Geophysical Research*, *100*(C12), 24691. https://doi.org/10.1029/95JC02554

Maykut, Gary A., & Grenfell, T. C. (1975). The spectral distribution of light beneath first-year sea ice in the Arctic Ocean1: Light beneath sea ice. *Limnology and Oceanography*, *20*(4), 554–563. https://doi.org/10.4319/lo.1975.20.4.0554

Meiners, K. M., Arndt, S., Bestley, S., Krumpen, T., Ricker, R., Milnes, M., et al. (2017). Antarctic pack ice algal distribution: Floe-scale spatial variability and predictability from physical parameters. *Geophysical Research Letters*, *44*(14), 7382–7390. https://doi.org/10.1002/2017GL074346

Melbourne-Thomas, J., Meiners, K., Mundy, C., Schallenberg, C., Tattersall, K., & Dieckmann, G. (2015). Algorithms to estimate Antarctic sea ice algal biomass from under-ice irradiance spectra at regional scales. *Marine Ecology Progress Series*, *536*, 107–121. https://doi.org/10.3354/meps11396

Michel, C., Legendre, L., Demers, S., & Therriault, J.-C. (1988). Photoadaptation of sea-ice microalgae in springtime: photosynthesis and carboxylating enzymes. *Marine Ecology Progress Series*, *50*(1/2), 177–185.

Minnett, P. J. (1999). The Influence of Solar Zenith Angle and Cloud Type on Cloud Radiative Forcing at the Surface in the Arctic. *Journal of Climate*, *12*(1), 147–158. https://doi.org/10.1175/1520-0442(1999)012<0147:TIOSZA>2.0.CO;2

Morel, A., & Bricaud, A. (1986). Inherent optical properties of algal cells including picoplankton: Theoretical and experimental results. *Can. Bull. Fish. Aquat. Sci.*, *214*, 521–559.

Morin, P., Lacour, T., Grondin, P., Bruyant, F., Ferland, J., Forget, M., et al. (2020). Response of the sea-ice diatom Fragilariopsis cylindrus to simulated polar night darkness and return to light. *Limnology and Oceanography*, *65*(5), 1041–1060. https://doi.org/10.1002/lno.11368

Mundy, C., Gosselin, M., Gratton, Y., Brown, K., Galindo, V., Campbell, K., et al. (2014). Role of environmental factors on phytoplankton bloom initiation under landfast sea ice in Resolute Passage, Canada. *Marine Ecology Progress Series*, *497*, 39–49. https://doi.org/10.3354/meps10587

Mundy, C. J., & Meiners, K. M. (2021). Ecology of Arctic Sea Ice. In *Arctic Ecology* (pp. 261–288). John Wiley & Sons, Ltd. https://doi.org/10.1002/9781118846582.ch10

Mundy, C. J., Barber, D. G., & Michel, C. (2005). Variability of snow and ice thermal, physical and optical properties pertinent to sea ice algae biomass during spring. *Journal of Marine Systems*, *58*(3–4), 107–120. https://doi.org/10.1016/j.jmarsys.2005.07.003

Mundy, C. J., Ehn, J. K., Barber, D. G., & Michel, C. (2007). Influence of snow cover and algae on the spectral dependence of transmitted irradiance through Arctic landfast first-year sea ice. *Journal of Geophysical Research*, *112*(C3), C03007. https://doi.org/10.1029/2006JC003683

Nandan, V., Geldsetzer, T., Islam, T., Yackel, John. J., Gill, J. P. S., Fuller, Mark. C., et al. (2016). Ku-, X- and C-band measured and modeled microwave backscatter from a highly saline snow cover on first-year sea ice. *Remote Sensing of Environment*, *187*, 62–75. https://doi.org/10.1016/j.rse.2016.10.004

Nelson, N., Prezelin, B., & Bidigare, R. (1993). Phytoplankton light absorption and the package effect in California coastal waters. *Marine Ecology Progress Series*, *94*, 217–227. https://doi.org/10.3354/meps094217

Newyear, K., & Martin, S. (1997). A comparison of theory and laboratory measurements of wave propagation and attenuation in grease ice. *Journal of Geophysical Research: Oceans*, *102*(C11), 25091–25099. https://doi.org/10.1029/97JC02091

Olsen, L. M., Laney, S. R., Duarte, P., Kauko, H. M., Fernández-Méndez, M., Mundy, C. J., et al. (2017). The seeding of ice algal blooms in Arctic pack ice: The multiyear ice seed repository hypothesis: Seeding of Ice Algae in Arctic Pack Ice. *Journal of Geophysical Research: Biogeosciences*, *122*(7), 1529–1548. https://doi.org/10.1002/2016JG003668

Palmer, M. A., van Dijken, G. L., Mitchell, B. G., Seegers, B. J., Lowry, K. E., Mills, M. M., & Arrigo, K. R. (2013). Light and nutrient control of photosynthesis in natural phytoplankton populations from the Chukchi and Beaufort seas, Arctic Ocean. *Limnology and Oceanography*, *58*(6), 2185–2205. https://doi.org/10.4319/lo.2013.58.6.2185

Palmisano, A. C., & Simmons, G. M. (1987). Spectral downwelling irradiance in an Antarctic lake. *Polar Biology*, *7*(3), 145–151. https://doi.org/10.1007/BF00259202

Parera-Portell, J. A., Ubach, R., & Gignac, C. (2021). An improved sea ice detection algorithm using MODIS: application as a new European sea ice extent indicator. *The Cryosphere*, *15*(6), 2803–2818. https://doi.org/10.5194/tc-15-2803-2021

Pavlov, A. K., Granskog, M. A., Stedmon, C. A., Ivanov, B. V., Hudson, S. R., & Falk-Petersen, S. (2015). Contrasting optical properties of surface waters across the Fram Strait and its potential biological implications. *Journal of Marine Systems*, *143*, 62–72. https://doi.org/10.1016/j.jmarsys.2014.11.001

Peralta-Ferriz, C., & Woodgate, R. A. (2015). Seasonal and interannual variability of pan-Arctic surface mixed layer properties from 1979 to 2012 from hydrographic data, and the dominance of stratification for multiyear mixed layer depth shoaling. *Progress in Oceanography*, *134*, 19–53. https://doi.org/10.1016/j.pocean.2014.12.005

Perovich, D. K. (1996). *The optical properties of sea ice*. Hanover, N.H.: US Army Corps of Engineers, Cold Regions Research & Engineering Laboratory ; [Springfield, Va. : Available from National Technical Information Service.

Perovich, D. K. (2007). Light reflection and transmission by a temperate snow cover. *Journal of Glaciology*, *53*(181), 201–210. https://doi.org/10.3189/172756507782202919

Perovich, D. K. (2017). Sea ice and sunlight. In *Sea Ice* (pp. 110–137). John Wiley & Sons, Ltd. https://doi.org/10.1002/9781118778371.ch4

Perovich, D. K., & Polashenski, C. (2012). Albedo evolution of seasonal Arctic sea ice. *Geophysical Research Letters*, *39*(8), 6. https://doi.org/10.1029/2012GL051432

Perovich, D. K., Roesler, C. S., & Pegau, W. S. (1998). Variability in Arctic sea ice optical properties. *Journal of Geophysical Research: Oceans*, *103*(C1), 1193–1208. https://doi.org/10.1029/97JC01614

Petrich, C., & Eicken, H. (2017). Overview of sea ice growth and properties. In *Sea Ice* (pp. 1–41). John Wiley & Sons, Ltd. https://doi.org/10.1002/9781118778371.ch1

Petrich, C., Nicolaus, M., & Gradinger, R. (2012). Sensitivity of the light field under sea ice to spatially inhomogeneous optical properties and incident light assessed with three-dimensional Monte Carlo radiative transfer simulations. *Cold Regions Science and Technology*, *73*, 1–11. https://doi.org/10.1016/j.coldregions.2011.12.004

Petrich, C., Eicken, H., Polashenski, C. M., Sturm, M., Harbeck, J. P., Perovich, D. K., & Finnegan, D. C. (2012). Snow dunes: A controlling factor of melt pond distribution on Arctic sea ice. *Journal of Geophysical Research: Oceans*, *117*(C9). https://doi.org/10.1029/2012JC008192

Polashenski, C., Perovich, D., & Courville, Z. (2012). The mechanisms of sea ice melt pond formation and evolution. *Journal of Geophysical Research: Oceans*, *117*(C1). https://doi.org/10.1029/2011JC007231

Poulin, M., Daugbjerg, N., Gradinger, R., Ilyash, L., Ratkova, T., & von Quillfeldt, C. (2011). The pan-Arctic biodiversity of marine pelagic and sea-ice unicellular eukaryotes: a first-attempt assessment. *Marine Biodiversity*, *41*(1), 13–28. https://doi.org/10.1007/s12526-010-0058-8

Renaut, S., Devred, E., & Babin, M. (2018). Northward Expansion and Intensification of Phytoplankton Growth During the Early Ice-Free Season in Arctic. *Geophysical Research Letters*, *45*(19), 10,590-10,598. https://doi.org/10.1029/2018GL078995

Riedel, A., Michel, C., Gosselin, M., & LeBlanc, B. (2007). Enrichment of nutrients, exopolymeric substances and microorganisms in newly formed sea ice on the Mackenzie shelf. *Marine Ecology Progress Series*, *342*, 55–67. https://doi.org/10.3354/meps342055

Rösel, A., & Kaleschke, L. (2012). Exceptional melt pond occurrence in the years 2007 and 2011 on the Arctic sea ice revealed from MODIS satellite data: MELT PONDS ON ARCTIC SEA ICE. *Journal of Geophysical Research: Oceans*, *117*(C5), n/a-n/a. https://doi.org/10.1029/2011JC007869

Rysgaard, S., Kühl, M., Glud, R. N., & Hansen, J. W. (2001). Biomass, production and horizontal patchiness of sea ice algae in a high-Arctic fjord (Young Sound, NE Greenland). *Marine Ecology Progress Series*, *223*, 15–26.

Shiozaki, T., Fujiwara, A., Sugie, K., Nishino, S., Makabe, A., & Harada, N. (2022). Bottom-associated phytoplankton bloom and its expansion in the Arctic Ocean. *Global Change Biology*, *28*(24), 7286–7295. https://doi.org/10.1111/gcb.16421

Smith, M. M., Light, B., Macfarlane, A. R., Perovich, D. K., Holland, M. M., & Shupe, M. D. (2022). Sensitivity of the Arctic Sea Ice Cover to the Summer Surface Scattering Layer. *Geophysical Research Letters*, *49*(9), e2022GL098349. https://doi.org/10.1029/2022GL098349

Stroeve, J., & Notz, D. (2018). Changing state of Arctic sea ice across all seasons. *Environmental Research Letters*, *13*(10), 103001. https://doi.org/10.1088/1748-9326/aade56

Sturm, M. (2002). Winter snow cover on the sea ice of the Arctic Ocean at the Surface Heat Budget of the Arctic Ocean (SHEBA): Temporal evolution and spatial variability. *Journal of Geophysical Research*, *107*(C10), 8047. https://doi.org/10.1029/2000JC000400

Sturm, M., & Massom, R. A. (2017). Snow in the sea ice system: friend or foe? In *Sea Ice* (pp. 65–109). John Wiley & Sons, Ltd. https://doi.org/10.1002/9781118778371.ch3

Taylor, B. B., Taylor, M. H., Dinter, T., & Bracher, A. (2013). Estimation of relative phycoerythrin concentrations from hyperspectral underwater radiance measurements—A statistical approach. *Journal of Geophysical Research: Oceans*, *118*(6), 2948–2960. https://doi.org/10.1002/jgrc.20201

Tedesco, L., Vichi, M., & Scoccimarro, E. (2019). Sea-ice algal phenology in a warmer Arctic. *Science Advances*, *5*(5), eaav4830. https://doi.org/10.1126/sciadv.aav4830

Timco, G. W., & Weeks, W. F. (2010). A review of the engineering properties of sea ice. *Cold Regions Science and Technology*, *60*(2), 107–129. https://doi.org/10.1016/j.coldregions.2009.10.003

Tremblay, J.-É., & Gagnon, J. (2009). The effects of irradiance and nutrient supply on the productivity of Arctic waters: a perspective on climate change. In J. C. J. Nihoul & A. G. Kostianoy (Eds.), *Influence of Climate Change on the Changing Arctic and Sub-Arctic Conditions* (pp. 73–93). Dordrecht: Springer Netherlands. https://doi.org/10.1007/978-1-4020-9460-6_7

Tschudi, M. A., Maslanik, J. A., & Perovich, D. K. (2008). Derivation of melt pond coverage on Arctic sea ice using MODIS observations. *Remote Sensing of Environment*, *112*(5), 2605–2614. https://doi.org/10.1016/j.rse.2007.12.009

Van Leeuwe, M., Tedesco, L., Arrigo, K. R., Assmy, P., Campbell, K., Meiners, K. M., et al. (2018). Microalgal community structure and primary production in Arctic and Antarctic sea ice: A synthesis. *Elem Sci Anth*, *6*(1), 4. https://doi.org/10.1525/elementa.267

Vancoppenolle, M., Goosse, H., de Montety, A., Fichefet, T., Tremblay, B., & Tison, J.-L. (2010). Modeling brine and nutrient dynamics in Antarctic sea ice: The case of dissolved silica. *Journal of Geophysical Research: Oceans*, *115*(C2). https://doi.org/10.1029/2009JC005369

Vérin, G., Domine, F., Babin, M., Picard, G., & Arnaud, L. (2022). Metamorphism of snow on Arctic sea ice during the melt season: impact on spectral albedo and radiative fluxes through snow. *The Cryosphere*, *16*(9), 3431–3449. https://doi.org/10.5194/tc-16-3431-2022

Waga, H., & Hirawake, T. (2020). Changing Occurrences of Fall Blooms Associated With Variations in Phytoplankton Size Structure in the Pacific Arctic. *Frontiers in Marine Science*, *7*. Retrieved from https://www.frontiersin.org/articles/10.3389/fmars.2020.00209

Warren, S. G. (1982). Optical properties of snow. *Reviews of Geophysics*, *20*(1), 67–89. https://doi.org/10.1029/RG020i001p00067

Weeks, W., & Hibler, W. D. (2010). *On Sea Ice*. Fairbanks: University of Alaska Press.

Weeks, W. F., & Ackley, S. F. (1982). The Growth, Structure, and Properties of Sea Ice. In N. Untersteiner (Ed.), *The Geophysics of Sea Ice* (pp. 9–164). Boston, MA: Springer US. https://doi.org/10.1007/978-1-4899-5352-0_2

Weissenberger, J., & Grossmann, S. (1998). Experimental formation of sea ice: importance of water circulation and wave action for incorporation of phytoplankton and bacteria. *Polar Biology*, *20*(3), 178–188. https://doi.org/10.1007/s003000050294

Willmes, S., & Heinemann, G. (2015). Pan-Arctic lead detection from MODIS thermal infrared imagery. *Annals of Glaciology*, *56*(69), 29–37. https://doi.org/10.3189/2015AoG69A615

Wongpan, P, Meiners, K. M., Langhorne, P. J., Heil, P., Smith, I. J., Leonard, G. H., et al. (2018). Estimation of Antarctic Land-Fast Sea Ice Algal Biomass and Snow Thickness From Under-Ice Radiance Spectra in Two Contrasting Areas. *Journal of Geophysical Research, 123*, 1907–1923. https://doi.org/10.1002/2017JC013711

Wongpan, Pat, Nomura, D., Toyota, T., Tanikawa, T., Meiners, K. M., Ishino, T., et al. (2020). Using under-ice hyperspectral transmittance to determine land-fast sea-ice algal biomass in Saroma-ko Lagoon, Hokkaido, Japan. *Annals of Glaciology*, 1–10. https://doi.org/10.1017/aog.2020.69

Yackel, J. J., Barber, D. G., & Papakyriakou, T. N. (2001). On the estimation of spring melt in the North Water polynya using RADARSAT-1. *Atmosphere-Ocean*, *39*(3), 195–208. https://doi.org/10.1080/07055900.2001.9649676

Yackel, J. J., Barber, D. G., Papakyriakou, T. N., & Breneman, C. (2007). First-year sea ice spring melt transitions in the Canadian Arctic Archipelago from time-series synthetic aperture radar data, 1992–2002. *Hydrological Processes*, *21*(2), 253–265. https://doi.org/10.1002/hyp.6240

Chapter 3 | Surface primary producer phenology in Dease Strait, NU, Canada, examined using submersed oceanographic sensors and satellite remote sensing

Yendamuri, K., Stroeve, J., Williams, W. J., Ehn, J., Nandan, V., Else, B. G. T., Komarov, A. S., Braybrook, C. A., Dempsey, M., and Mundy, C. J. (*In Preparation*).

Abstract

The transition to a thinner, seasonal Arctic sea-ice cover has affected the timing of primary producer (PP) phenology, resulting in earlier ice algal bloom termination and protracted phytoplankton blooms, primarily due to increased light availability. However, due to logistic constraints, few studies capture the complete seasonal evolution of PPs and their physical drivers. Here, we combine transmitted spectral irradiance data derived from subsurface oceanographic moorings with synthetic aperture radar (SAR) products, and related meteorological variables to study light availability in Dease Strait and how it relates to timing and magnitude of surface (<8.5 m depth) PPs for 2017 and 2019. We observed ice algal blooms in 2017 and 2019, lasting 66 and 84 days, respectively, peaking within 2 days of snow melt onset. In 2019, lower temperatures and a deeper snowpack before early snow melt extended the bloom. Melt pond formation exponentially increased light transmission, enabling a short, 6-7 day under-ice phytoplankton bloom in both years, likely influenced by regional nutrient-limitation, although the 2019 bloom was less productive, possibly due to the longer ice algal boom depleting surface nutrients. After ice break-up in 2019, a 31-day surface late-summer bloom occurred via sustained wind-driven mixing. Our findings suggest that the combined remote sensing technique has novel applicability

in other settings and provides valuable insights on the changing state of PP phenology, highlighting the vital need of accumulating long-term Arctic observations in discerning climate change effects on the region.

3.1. Introduction

Arctic sea ice extent (Stroeve & Notz, 2018), thickness (Kwok, 2018), and age (Comiso, 2012) are rapidly declining, caused by the strengthening ice-albedo feedback and associated polar amplification mechanisms (Rantanen et al., 2022). This decline is a significant driver of change in ice algal and phytoplankton production due to impacts on sea ice habitat and an increasing availability of light for photosynthesis (Barber et al., 2015). Superimposed on this change is interannual variability in processes that impact regional down to local primary producer bloom lengths and magnitudes (Hill et al., 2022; Nielsen et al., 2023; Oziel et al., 2019). Bloom phenology offsets are an important area of biogeochemical investigation as they alter the balance of organic matter transfer through marine food webs and carbon cycling efficiencies (Else et al., 2019; Søreide et al., 2010; Tremblay et al., 2015).

Ice algal bloom initiation occurs after polar night when sufficient photosynthetically active radiation (PAR; 400-700 nm) transmits through snow and sea ice to the ice algal community that primarily inhabits the bottommost 10 cm of sea ice (Horner et al., 1992). A snow layer attenuates approximately 10 times more PAR than sea ice (Perovich, 1996, 2007), making its thickness a primary control for ice algal bloom initiation. In addition to PAR availability, nutrient supply from the underlying water column can co-limit ice algal production (Campbell et al., 2016; Cota et al., 1987). Termination of the ice algal bloom occurs as temperatures increase in late spring (Horner & Schrader, 1982; Mundy et al., 2014; Selz et al., 2018). Snow and sea ice melt shift the spectral quality of the under-ice light field to an increase and deepening of light at peak chlorophyll-

absorption wavelengths initiating an under-ice phytoplankton bloom (UIB) (Horvat et al., 2017; Mundy et al., 2014). Historically, phytoplankton blooms were typically considered to initiate during ice-edge retreats; however, UIBs are now considered an ubiquitous occurrence throughout the Arctic (Ardyna et al., 2020a; Arrigo et al., 2012; Assmy et al., 2017; Kauko et al., 2019; Mundy et al., 2014; Payne et al., 2021; Randelhoff et al., 2020; Vérin et al., 2022). The extent of UIB magnitude is proportional to regional nutrient supply, water column structure, light availability, and grazing pressure (Ardyna et al., 2020b). With the delay in ice freeze-up dates throughout the Arctic, fall phytoplankton blooms are documented to become more prevalent (Ardyna et al., 2014). The mode of nutrient replenishment is likely the source of fall bloom origins, which may emerge from wind-driven or storm-induced mixing of the water column (Castro de la Guardia et al., 2019; Waga & Hirawake, 2020).

In polar regions, satellite sensors have proven incredibly useful to observe sea ice and the surface ocean. For example, active microwave imagers in the form of synthetic aperture radar (SAR) can provide a record of snow and sea ice thermodynamic melt phase timing based on associated changes in electrical conductivity relative to SAR emissions (Livingstone et al., 1987; Barber et al., 2001; Yackel et al., 2007; Gill et al., 2015; Casey et al., 2016; Mahmud et al., 2020). During the open water period, optical satellite sensors such as the Moderate-Resolution Imaging Spectrometer (MODIS) instrument aboard the Aqua satellite can detect ice-edge phytoplankton bloom timing and biomass based on ocean colour chlorophyll-*a* (chl-*a*) algorithms (Arrigo & van Dijken, 2011; Janout et al., 2016; Kahru et al., 2016). However, satellite observations of primary production from optical sensors are limited by cloud cover, depth of the bloom peak, and in the case of ice algal and under-ice blooms, sea-ice presence.

To quantify primary producer biomass from an under-ice remote sensing approach, chlorophyll *a* (chl-*a*) concentration retrieval algorithms have emerged based on the relationship between transmitted under-ice spectra using a spectral radiometer during bloom periods and corresponding ice algal chl-*a* concentration samples. Legendre & Gosselin (1991) were the first to examine this relationship. Later, Mundy et al. (2007) developed and applied a chlorophyll retrieval algorithm using a normalized difference index (NDI), which has grown in popularity among other reported algorithms due to its relative simplicity and robustness (Campbell et al., 2014; Forrest et al., 2019; Lange et al., 2016; Melbourne-Thomas et al., 2015; Veyssière et al., 2022; Wongpan et al., 2020). The method has been used in Arctic and Antarctic contexts (Fritsen et al., 2011; Meiners et al., 2017), with radiometers attached to L-arms (Campbell et al., 2014; Wongpan et al., 2018; Wongpan et al., 2020), fastened to a sled (Nicolaus & Katlein, 2013), fixed to AUVs and ROVs (Arndt et al., 2017; Anhaus et al., 2021; Lange et al., 2016), and using a buoy attached to drift ice (Hill et al., 2018; Hill et al., 2022).

In order to progress our understanding and resolve knowledge gaps of Arctic primary producer phenology, this study aims to combine satellite and underwater remote sensing techniques to quantify how changes in snow and sea ice melt progression simultaneously facilitate light transmission and bloom timing in a landfast sea ice environment of Dease Strait, Nunavut, Canada. Dease Strait is a seasonally ice-covered narrow channel within the Kitikmeot Sea of the Canadian Arctic Archipelago. The region is distinct for its strong stratification in the summer due to substantial riverine inputs relative to dense Pacific-origin waters that form a two-layer estuarine like system (Williams et al., 2019).

Following Howell et al. (2019), we acquired SAR products from both Sentinel-1 and RADATSAT-2 satellite arrays, air temperature data from a meteorological station close to our study

site, and collected optical MODIS imagery to identify snow and sea ice thermodynamic melt phases. Using sensors aboard a subsurface oceanographic mooring deployed during the 2017 and 2019 bloom periods, we derived light characteristics and proxy chl-*a* concentration metrics. We end with a discussion on how the synthesis of these methods facilitates our comprehension of biophysical processes in the Arctic marine system and discuss its potential for future applications.

3.2. Methods

3.2.1. Study Area

The study was located within Dease Strait, NU, Canada, situated near the Finlayson Islands (Fig. 1a). It was part of the 2017 Ice Covered Ecosystem-Cambridge Bay Process Study (ICE-CAMPS) and Kitikmeot Sea Science Study (K_3S) field campaigns and mooring deployments. The study site has an annual landfast first-year sea ice cover, with local primary production strongly nitrogen limited (Back et al., 2021; Bluhm et al., 2022; Campbell et al., 2016), largely due to substantial riverine input and associated stratification (Williams et a., 2019).

3.2.2. Data Collection

3.2.2.1. SAR Products

C-band SAR products (centre frequency = 5.405 GHz) were obtained from both Sentinel-1 (S1) satellites, Sentinel-1A and Sentinel-1B, in Interferometric Wide (IW) and Extra Wide (EW) mode, and from RADARSAT-2 (R2) in ScanSAR Wide mode (SCWA) over the mooring coordinates (69.017ºN, 105.733ºW) for each deployment period (*see 2.2.3.*) (Table 1). Quad and dual-polarized S1A and S1B products are freely available from Alaska Satellite Facility's online database, Vertex. Dual polarized RSAT2 products were made available under the context of a Joint Project with Environment and Climate Change Canada and subsequently approved by the

Canadian Space Agency. Only co-polarized HH products were used in this study as per Howell et al. (2019).

Table 1. SAR imaging mode descriptions between satellite arrays.

Product	Swath width (km)	Imaging resolution (m)	Incidence angle range
S1-IW	250	5 x 20	29.1° - 46.0°
S1-EW	410	20 x 40	18.9° - 47.0°
R2-SCWA	500	100 x 100	20.0° - 49.0°

3.2.2.2. MODIS-Derived Products

True-color daily Level 1B MODIS (Aqua) optical imagery over the mooring location were obtained from MODIS Science Team (2017). Level 1B MODIS data contain geolocated and calibrated top-of-the atmosphere reflectances corrected for Rayleigh scattering to generate natural-coloured images from MODIS bands 1, 3 and 4 (250 to 500 m spatial resolution).

Level-3 ocean color products were used to retrieve near-surface chl-*a* concentrations (mg m^{-3}) (NASA Ocean Biology Processing Group, 2022), at a data product resolution of 4 km. Products were generated based on an algorithm developed by Hu et al. (2019) that derives the relationship between satellite-based reflectance ($R_{rs}(\lambda)$) for blue and green visible spectral wavelengths within MODIS bands 8-16, and *in situ* chl-*a* measurements.

3.2.2.3. Mooring Deployment

From 8 August 2016 to 12 August 2017, and 18 August 2018 to 18 September 2019, a subsurface oceanographic mooring was deployed from the *R/V Martin Bergmann* in Dease Strait, close to the Finlayson Islands (Fig. 1; 29 km from Cambridge Bay, Nunavut). The mooring was anchored at a depth of 82 m, with its topmost package sitting 8.5 m from the surface. The package held a surface-facing hyperspectral radiometer (HyperOCR, Satlantic), which has a spectral range

of 350 to 800 nm at a 3.4-nm resolution, with integrated wiper that recorded downwelling spectral irradiance every two hours. An ECO-Triplet fluorometer (Wetlabs) with integrated wiper was positioned at the same depth to measure *in vivo* chl-*a* fluorescence recording measurements at half-hour intervals.

3.2.2.4. Meteorological Variables

Weather data for 2017 and 2019 were obtained from a meteorological tower on Qikirtaarjuk Island, 5.5 km southwest of the mooring's location (Fig. 1; Butterworth & Else, 2018). The tower was power-intensive and solar-powered, and therefore, data were available for roughly four months each year which coincided with sufficient seasonal insolation levels. In 2017, the data collection period ranged from 4 May to 12 August 2017 and 10 April to 30 July 2019. The sensors installed on the tower and used in this study included an air temperature sensor (Campbell Scientific) mounted at 5 m above ground level and a net radiometer (Kipp & Zonen) at 2.8 m above ground level that monitored downwelling and upwelling shortwave irradiance. The tower base was roughly 3 m above sea level. Downwelling shortwave irradiance was converted to PAR photon flux ($E_{0(PAR)}$) using a factor of 4.15 as described by Halverson & Pawlowicz (2013). To extend the meteorological coverage over the mooring deployment period, daily wind speed (m s^{-1}) was gathered from Cambridge Bay's airport weather station (NAV Canada).

3.2.2.5. Field Sampling

Every three days from 26 April to 9 May 2017, transmitted spectral irradiance and corresponding ice cores were collected from four sites along a 5.4-km long transect near the Finlayson Islands chain (Fig. 1: Sites 1-4). Additionally, on 12 May, another set of measurements were collected from nine sites, encompassing 4 km^2 with samples collected from under thin (L: < 10 cm) and thick (H: >10 cm) snow covers at each site (Fig. 1: Sites A-I). Transmitted spectral

irradiance (cosine corrected) measurements were first collected at each sample location via lowering a HyperOCR through a 25-cm auger hole and positioning 1.5 m south of the hole using a mechanical arm. At least 5 measurements of transmitted irradiance were measured at each sample location. Then, two to four ice cores were collected at the irradiance measurement site using a 9-cm Mark II Kovacs ice corer. The bottom 10 cm of each ice core was sectioned into three segments: bottom (0-2 cm), middle (2-5 cm), and top (5-10 cm). The ice core samples were melted in the dark overnight in filtered seawater (FSW, filtered through a GF/F, Whatman, glass fiber filter) at a dilution of 3 FSW:1 ice melt. Melted samples were filtered through GF/F filters for fluorometric analysis to determine chl-*a* concentration (Parsons et al., 1984). Additional sampling details can be found elsewhere (Kim et al. 2020; Pogorzelec et al. 2022).

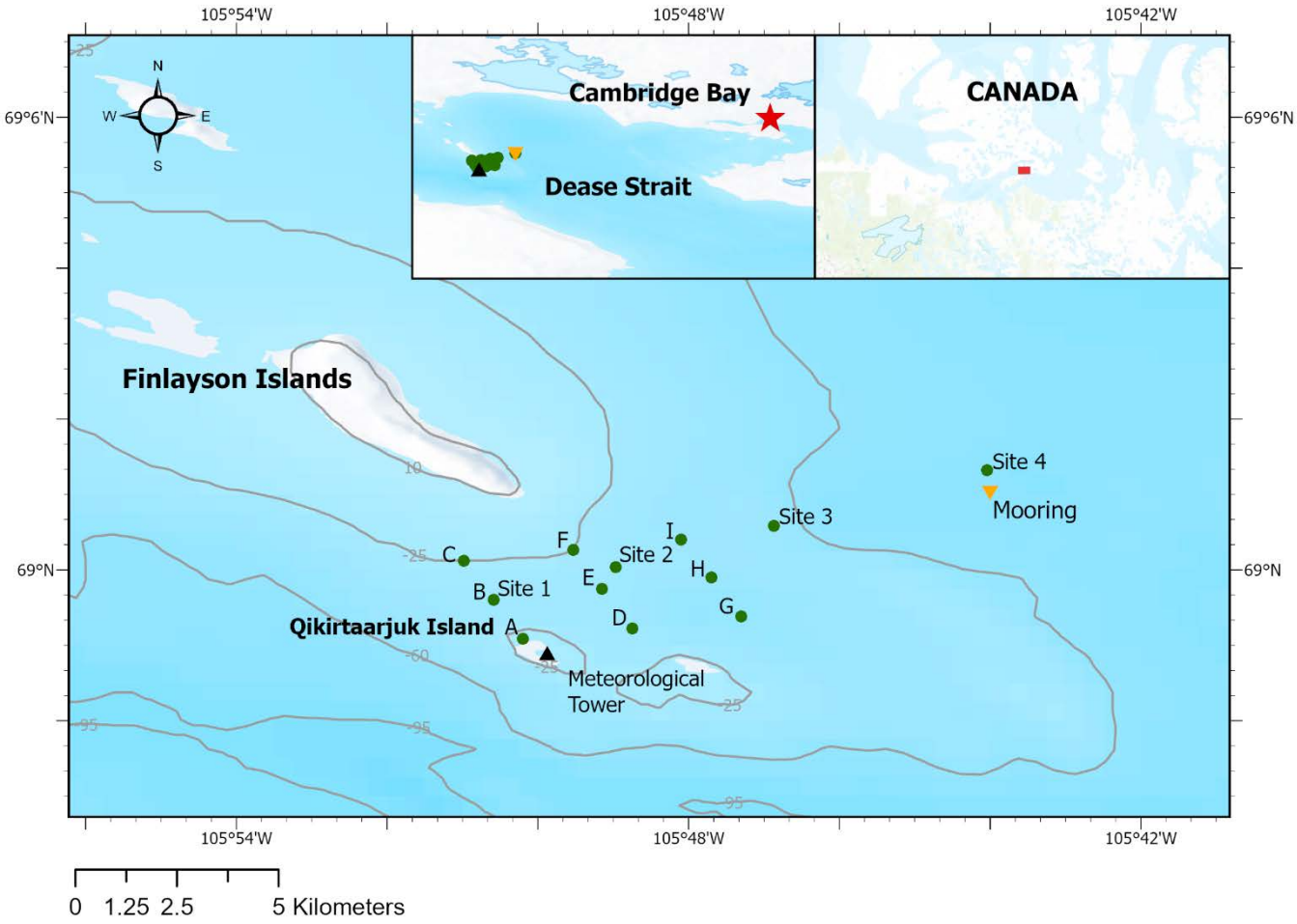

Figure 1. Map of the study site in Dease Strait with the mooring location (orange triangle), the 2017 ICE-CAMPS sample locations (green circles), the seasonal meteorological station (black triangle) and nearby Cambridge Bay, Nunavut (image subset).

3.2.3. Data Analysis

3.2.3.1. SAR Processing and Physical Event Retrieval

Sentinel-1 (S1) SAR products with incidence angles that deviated more than five degrees were removed from the analysis to avoid incidence angle dependent backscatter differences; this accounted for less than 5% of the total data between years. HH dual-polarized products from S1 were used to increase the available temporal resolution between S1 and R2, and reduce noise levels. Standardized SAR processing took place in SNAP (version 8.0), which included the chain of applying an orbit file, radiometric calibration, speckle noise filtering, geometric range-doppler

terrain correction, and conversion to decibels. All products were radiometrically calibrated to gamma naught (γ^0_{HH}) to further reduce the sensitivity of incidence angle differences (Howell et al., 2019; Small, 2011). To ensure consistency with the radiometer footprint (15 m) and variations in the smallest pixel size between S1 and RSAT2, an average pixel mask of 18x50 m was applied to all products.

The five thermodynamic melt regimes (Winter, Early Melt, Melt Onset, Pond Onset, Open Water) were characterized from cross-examining backscatter values with air temperature data, and verified using Level 1B MODIS optical imagery. Winter was considered as the period prior to Early Melt (EM). The latter was defined as commencing when the averaged daily air temperature increased above -5°C and the presence of a γ^0_{HH} inflection point due to changes in the basal snow layer and ice surface scattering (Barber et al., 2001; Livingstone et al., 1987; Yackel et al., 2007). Melt Onset (MO) was delineated by the timing of when daily averaged air temperature increases above 0°C and γ^0_{HH} peaks due to volume scattering from snow grains wetted with brine (Howell et al., 2019). Pond Onset (PO) was confirmed via: visual inspection of a true-color composite MODIS image that clearly showed the presence of water (blue colour) on the ice surface; a second peak in γ^0_{HH} from surface scattering at the air-water interface of melt ponds (Casey et al., 2016); and an exponential increase in transmitted light observed at the mooring. Open Water (OW) timing was identified through the simultaneous occurrence of wind-induced backscatter increase and distinct drop in MODIS reflectance corresponding to seawater presence.

3.2.3.2. Transmitted Irradiance

Transmitted downwelling spectral irradiance in μW cm^{-2} nm^{-1} ($E_{zW(\lambda)}$) data were interpolated from 3.4 to 1 nm intervals and then converted to spectral photon flux in μmol photons m^{-2} s^{-1} nm^{-1} ($E_{zP(\lambda)}$) using:

$$E_{zP(\lambda)} = \frac{E_{zW(\lambda)}\,\lambda\,10^{-5}}{hcN_A}$$

where λ is the wavelength (nm), h is Planck's constant (6.626 x 10^{-34} J s), c is the speed of light (2.998 x 10^{8} m s^{-1}), N_A is Avogadro's number (6.022 x 10^{23} mol^{-1}), and 10^{-5} is a conversion factor between units. The transmitted spectral photon flux was also integrated over the wavelength range of 400-700 nm to determine transmitted PAR at mooring radiometer-level ($E_{z(PAR)}$). Finally, transmitted photosynthetically usable radiation ($E_{z(PUR)}$) was calculated as the product between a representative algal absorption spectra obtained from Ehn & Mundy (2013) and $E_{zP(\lambda)}$, and then integrated over PAR (Morel, 1978).

3.2.3.3. Normalized Difference Index (NDI)

Following Mundy et al. (2007), normalized difference indices (NDI) were calculated across all PAR wavelength pairs:

$$NDI = \left[\frac{E_{zP(\lambda_1)} - E_{zP(\lambda_2)}}{E_{zP(\lambda_1)} + E_{zP(\lambda_2)}}\right]$$

To select the optimal wavelength pairs, NDI values were correlated against chl-*a* concentration samples using R (version 4.1.2). Optimal NDI wavelength pair selection consisted of 1) a large Pearson correlation coefficient, 2) within the range of peak chl-*a* absorption and minimal snow and water influence (400 – 550 nm), 3) outside the HyperOCR spectral resolution (i.e., 3.4 nm), and 4) yielded the greatest R^2 from the linear regression of chl-*a* versus NDI. The optimal NDI was then applied to the two years of transmitted spectral irradiance from the mooring. The linear equation from the associated regression was used to covert NDI values into chl-*a* concentration (mg m^{-2}). Daily median values were used to avoid low solar angle effects and a 10% local weighted scatter-plot smoothing (LOESS) fit was applied.

3.2.3.4. Bloom Timing

Building upon Mieruch et al. (2010) and Adams et al. (2022), the search interval of each ice algal bloom period was restricted to the first day of diurnal insolation variability in the system until the peak of the bloom noted by the LOESS fitted data. The ice algal bloom start date was chosen as the first positive value delineated in the first-order derivative time series that aligned with a strong decline in daily variability in chl-*a* concentration NDI estimates and prior to the seasonal increase in chl-*a* concentration. Similarly, timing of the phytoplankton bloom periods was determined by identifying the first positive value in the first-order derivative time series that led to a substantial increase and peak in the smoothed chl-*a* concentration time series and was verified through *in vivo* chl-*a* fluorescence measurements. Once ice algal and phytoplankton bloom timing was established for both years, using a C:chl-*a* ratio of 50 (Harris, 1986), a carbon net accumulation estimate was produced for each bloom following that described in Mundy et al. (2014). Retrieved Level 3 MODIS data products were converted from volumetric (mg m^{-3}) to areal (mg m^{-2}) chl-*a* concentration above the mooring via multiplying by 8.5 m.

3.3. Results

3.3.1. Physical Conditions and Melt Phase Identification

S1 and RSAT2 SAR products were processed for each annual period, beginning from the first insolation day (11 January) and ending when the mooring was retrieved in 2017 (12 August) and 2019 (18 September). Co-polarized gamma naught (γ°_{HH}) backscatter across the winter periods features low oscillations when air temperatures were below -5°C (Fig. 2e, f), inferring the presence of a cold and dry snowpack. 2017 was warmer than 2019, leading to earlier classifications for all melt phases. Early melt commenced on 17 May 2017 and 26 May 2019. In both years, 0.2% of incident PAR was transmitted through snow-covered sea ice to the 8.5-m depth of the mooring

irradiance sensor as early melt commenced (Fig. 2g, h). Thereafter, air temperature increased and reached the 0°C daily-averaged temperature threshold and backscatter peak for melt onset delineation (Fig. 2c, d). Melt onset occurred on 19 May 2017 and 1 June 2019.

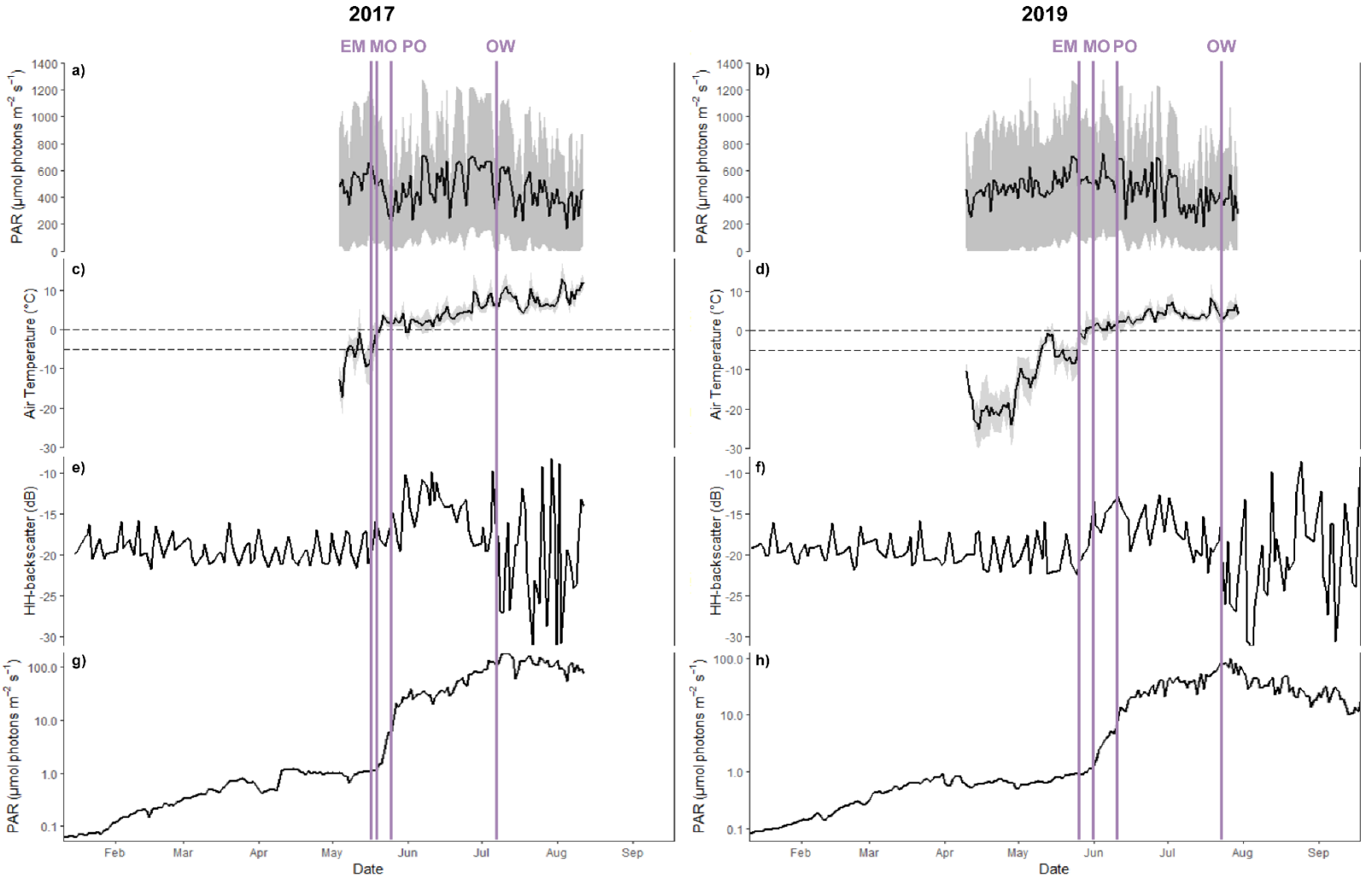

Figure 2. Time series of daily averaged incident PAR ($E_{0(PAR)}$) and air temperature (± SD in grey shade) retrieved from the Qikirtaarjuk Island meteorological tower, SAR γ°_{HH}, and transmitted daily-averaged PAR ($E_{z(PAR)}$) on the mooring for 2017 (a, c, e and g) and 2019 (b, d, f, and h), respectively. Air temperatures of -5 and 0°C are highlighted as horizontal dashed lines in c and d, while vertical purple lines identify early melt (EM), melt onset (MO), pond onset (PO), and the first date of open water (OW) above the mooring location.

MODIS imagery visually confirmed the validity of the pond onset threshold and corresponding γ°_{HH} peak used for both years. Pond onset occurred 6 days after melt onset in 2017 (26 May), and 10 days after melt onset in 2019 (11 June), leading to a 16-day difference in the

timing of pond onset between the two years. The average air temperature during the transition from melt to pond onset for 2017 and 2019 was 1.54°C and 1.12°C, respectively. During this snow melt phase in 2019, air temperature occasionally dipped below 0°C, whereas in 2017 it remained above 0°C. In comparison to early melt, there was 2% light transmittance at pond onset. During the pond onset phase, $E_{z(PAR)}$ levels increased at a higher rate than during the melt onset transition.

For both years, the period from pond onset to open water took place over 42 days. Ice break-up occurred on 7 July 2017 and 23 July 2019. In 2017, ice cover over the mooring location broke up and cleared away from the mooring location within a day. However, the ice cover in 2019 detached from the northern coast of the Dease Strait on 17 July, resulting in a large floe that drifted southeast over the mooring and did not fully break-up until 23 July. After break-up, wind-induced surface roughening created large γ°_{HH} oscillations. The seasonal peak in $E_{z(PAR)}$ with an average of ~40% PAR transmittance to 8.5 m occurred shortly after ice break-up on 12 July and 27 July in 2017 and 2019, respectively.

3.3.2. NDI Calibration

Figure 3a presents the Pearson correlation matrix of chl-*a* concentration measured during the 2017 field campaign versus the NDI wavelength combinations from under-ice arm measurements. The wavelength ranges of 440 to 490 nm and 675 to 690 nm that correspond to peak chl-*a* absorption were noted to have greater correlation coefficients. Following the selection criteria of Mundy et al. (2007), the NDI (480:473) was within the waveband of minimal snow and water absorption influence (400 to 550 nm), greater than the 3.4 nm spectral resolution, and had a large Pearson correlation coefficient ($r = 0.842$, $p < 0.01$). Linear regression of NDI (480:473) versus chl-*a* concentration was significant ($p < 0.001$) with an R^2 of 0.71 (Figure 3b). The resultant

relationship, chl-*a* = (NDI (480:473) – 0.017)/0.0013, was used to estimate chl-*a* concentration (mg m^{-2}) for the mooring-based hyperspectral data.

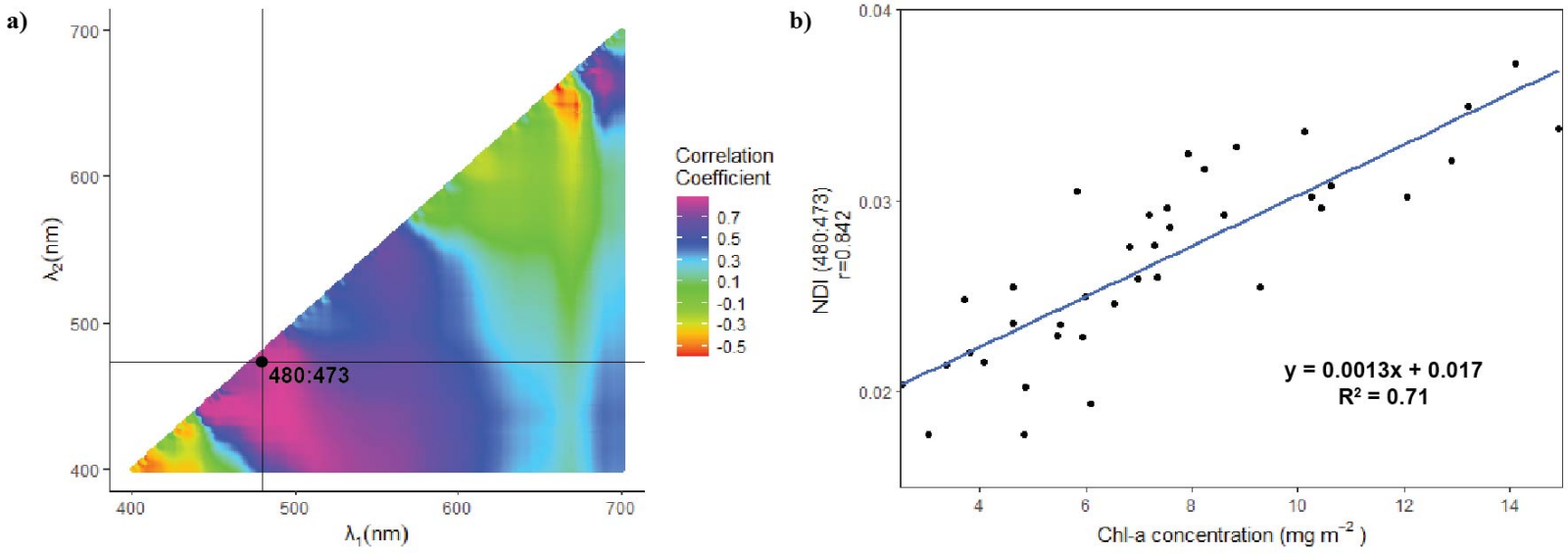

Figure 3. Pearson correlation matrix computed for all PAR NDI wavelength combination from the ICE-CAMPS field samples (a) and linear regression plot for NDI (480:473) and chl-*a* concentration samples (b).

3.3.3. Primary Producer Phenology

Daily median LOESS smoothed and calibrated chl-*a* concentration for the ice algal search interval period and associated daily upper and lower quartiles are plotted in Figures S1a and b. The range between quartiles was high before 1 March, when daily-averaged transmitted PAR was <0.34 μmol photons m^{-2} s^{-1}. The first-order derivative highlights inflection points in the smoothed chl-*a* concentration time series used to determine events of the blooms (onset, end; Figures S1c and d). The ice algal bloom onset did not differ significantly between years, occurring on 16 March 2017 and 11 March 2019. Assuming bloom onset was the start of any algal accumulation in the sea ice and upper water column, the chl-*a* concentration time series was zeroed to this value, which was 3.7 mg m^{-2} and 5.1 mg m^{-2} in 2017 and 2019, respectively (Fig. 4a, b). Thereafter, ice algal bloom end dates occurred on 21 May 2017 (66-day ice algal bloom) and 3 June 2019 (84-day ice

algal bloom). Both blooms peaked near melt onset. The 2019 ice algal bloom had a greater peak magnitude at 14.9 mg m^{-2} than in 2017 at 11.4 mg m^{-2}. In each year, chl-*a* concentration accumulation was consistent, yet at a slow rate. It is interesting to note that the first-order derivative time series showed small oscillations during this slow accumulation of chl-*a* concentration in the sea ice that appeared to match the lunar cycle. In terms of productivity, the net accumulation rates were similar between 2017 (12.28 mg C m^{-2} d^{-1}) and 2019 (10.34 mg C m^{-2} d^{-1}) (Table 2). Furthermore, the PUR:PAR ratio reached a maximum of ~0.64 at bloom onset in early to mid March and was similar between 2017 and 2019 (~0.63), slowly decreasing as the ice algal bloom accumulated chl-*a* concentration (Fig. 5).

Table 2. Bloom-specific daily net accumulation rates and corresponding statistical parameters.

Bloom		**Sample Size (n)**	**R^2**	**P-value**	**Daily Net Accumulation Rates (mg C m^{-2} d^{-1})**
2017	ice algae	66	0.91	$p < 0.001$	12.28
	under-ice bloom	7	0.84	$p < 0.001$	71.70
2019	ice algae	84	0.93	$p < 0.001$	10.34
	under-ice bloom	6	0.93	$p < 0.001$	27.38
	late-summer bloom	31	0.75	$p < 0.001$	23.30

The decline of ice algal chl-*a* concentration was associated with an increase in transmitted PAR that was accentuated with onset of surface melt pond formation (Fig. 2g, h & 5a, b). The increase in PAR halted as a short under-ice phytoplankton bloom (UIB) occurred in both 2017 and

2019 from 1 to 8 June (7-day UIB) and 16 to 22 June (6-day UIB), respectively. Fluorometric *in-vivo* chl-*a* estimates on the 2017 mooring verified the UIB where the bloom peak matched between datasets (Fig. 4a-c). As the NDI chl-*a* concentration estimates were calibrated to ice algae, the values presented for the UIB cannot be directly interpreted as absolute values. However, daily accumulation rates were still estimated where the UIB in 2017 was observed to be more productive (71.70 mg C m^{-2} d^{-1}) than in 2019 (27.38 mg C m^{-2} d^{-1}).

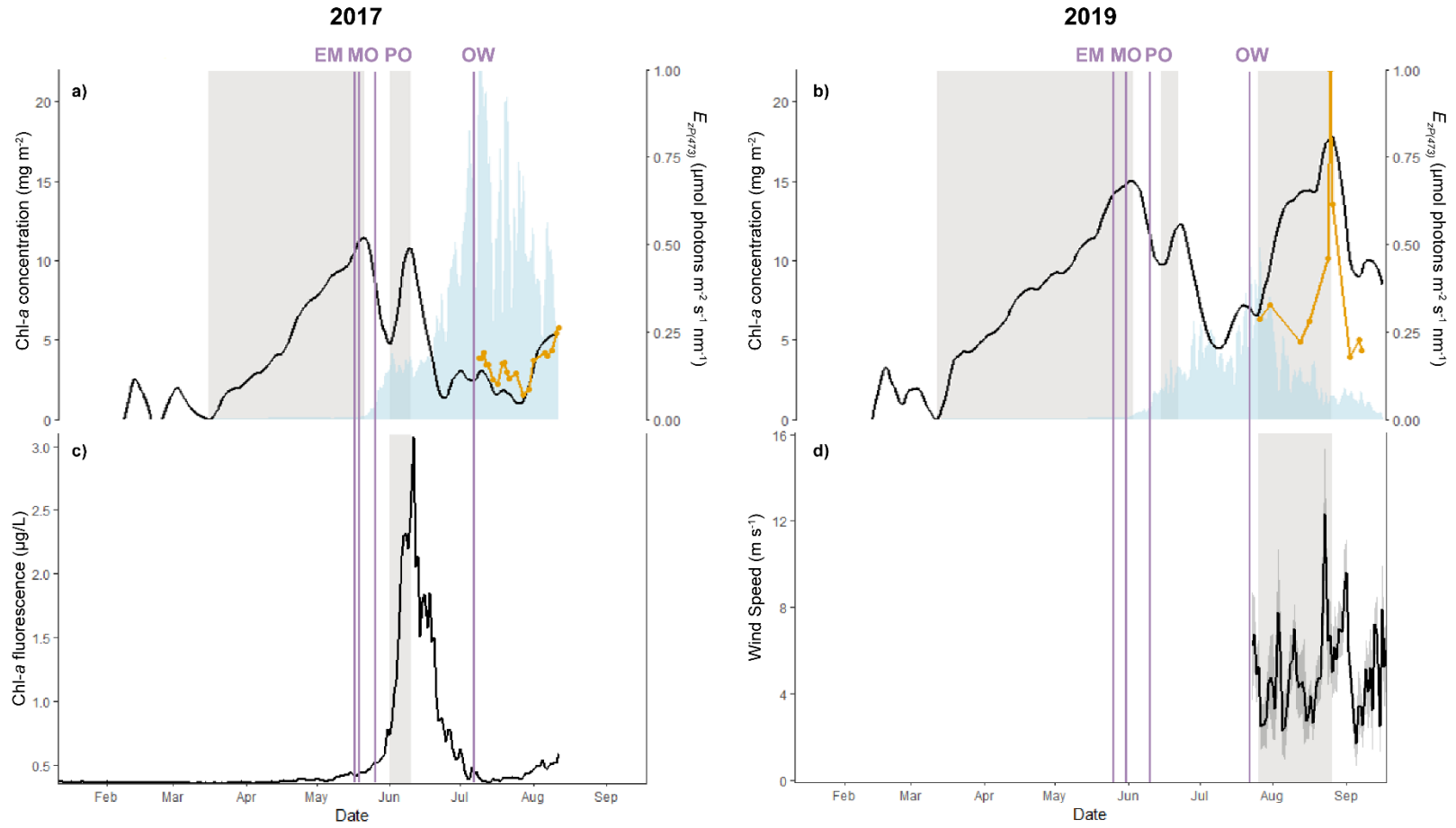

Figure 4. Time series of daily ice algal and phytoplankton phenology for 2017 (a) and 2019 (b), *in vivo* chl-*a* fluorescence at 8.5 m (c), and wind speed (d) retrieved from the Cambridge Bay airport weather station. The black line represents the radiometer LOESS-fitted median chl-*a* concentration. The gray-shaded areas are identified bloom periods and blue shading plots transmitted light at 473 nm ($E_{zP(473)}$), one of the calibrated NDI wavelengths used. The orange line is MODIS-retrieved chl-*a* concentration. Vertical purple lines identify early melt (EM), melt onset (MO), pond onset (PO), and the first date of open water (OW) above the mooring location.

Termination of the UIB led to an increase in transmitted PAR at 8.5 m depth in both years (Fig. 2g, h). The increase continued through ice break-up and corresponded to a similar increase in the PUR:PAR ratio up to 0.63 in 2017 and 0.62 in 2019 (Fig. 5). However, the PUR:PAR ratio never reached the value it was in late March, i.e., during the commencement of the ice algal bloom.

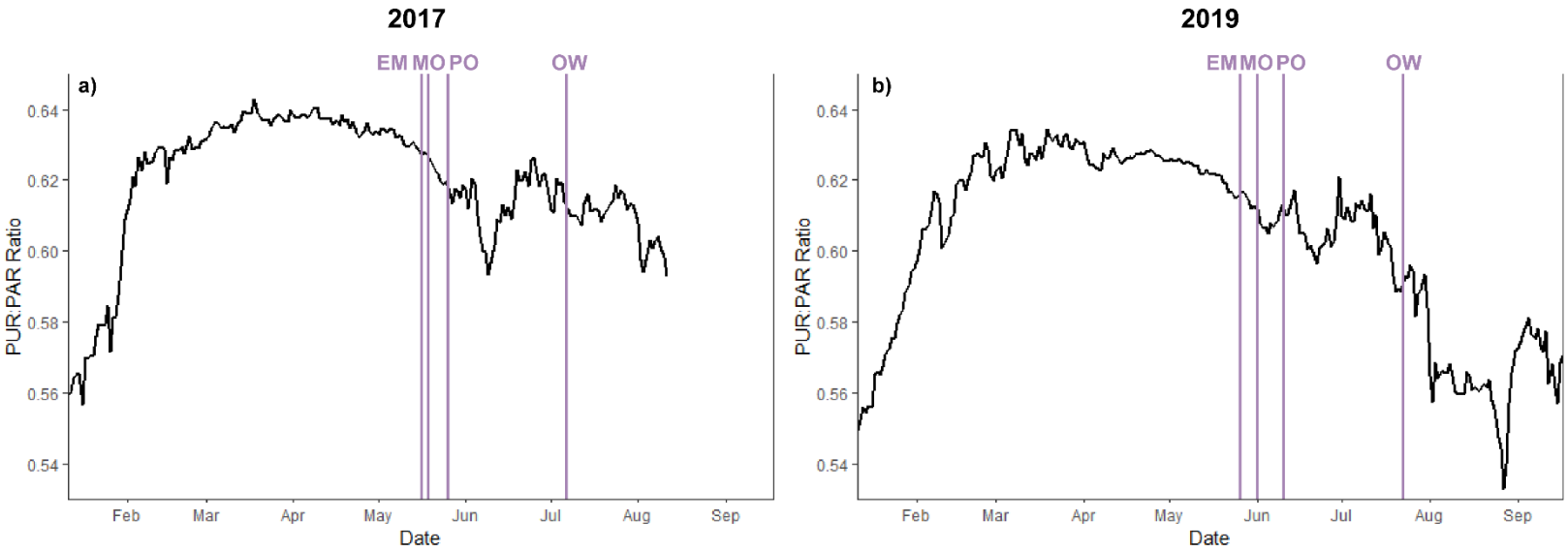

Figure 5. PUR:PAR ratios for 2017 (a) and 2019 (b). Vertical lines identify early melt (EM), melt onset (MO), pond onset (PO), and the first date of open water (OW) above the mooring location.

Towards the end of July in both years, there was evidence of phytoplankton activity at the surface, observed via an increase in chl-*a* concentration and decrease in the PUR:PAR ratio (Fig. 4a, b and 5a, b). In 2017, the increase in chl-*a* concentration continued until the end of the mooring time series on 12 August; however, it did not meet our classification criteria of a true late-summer phytoplankton bloom. The extended time series in 2019 (mooring retrieval date of 18 September) revealed that a substantial increase in chl-*a* concentration (surpassing the value of the ice algal bloom) and corresponding decrease in the PUR:PAR ratio that lasted from 26 July to 26 August (31 days). The 2019 late-summer bloom had a similar accumulation rate to that of the under-ice bloom (Table 2). Retrieved Level 3 MODIS ocean colour chlorophyll concentration product (Fig. 4b) closely matched that estimated from the mooring NDI chl-*a* time series. Spearman rank

correlation analysis for the NDI-based and MODIS-derived chl-*a* concentration estimates resulted in r_s = 0.86 in 2017 (n=20), and r_s = 0.56 for 2019 (n=10). It is important to note that there were more overcast days in 2019 during the late-summer bloom period, resulting in fewer clean MODIS images. Daily averaged wind data retrieved from the airport in Cambridge Bay for the 2019 OW period (Fig. 4d) showed strong wind speeds at >8 m s^{-1} during the late-summer bloom period. Wind-induced waves were also evidenced by greater SAR backscatter in the second half of August (Fig. 2f).

3.4. Discussion

3.4.1. Melt Phases and Their Impact on PAR Transmittance

Our method to characterize the melt phases was heavily reliant on air temperature thresholds, MODIS optical imagery, known FYI seasonal backscatter cycling, and the corresponding under-ice light climate. Transmitted PAR at an 8.5-m depth ($E_{z(PAR)}$) followed a similar trend with melt progression in both years. The winter increase in $E_{z(PAR)}$ prior to March was proportional to elevating insolation levels after polar night and corresponded to the PUR:PAR ratio reaching its highest values in winter, suggesting minimal algal absorption in the upper ocean during this period. The influence of snow on limiting light transmittance dominates this period (Matthes et al., 2020; Maykut & Grenfell, 1975; Nicolaus et al., 2013).

As air temperature rises above -5°C, the snowpack warms and undergoes physical and thermodynamic transformations. Upon early snow melt, snow grains experience slight kinetic growth and rounding (Colbeck, 1982), along with minor water inclusions (Barber et al., 1995; Casey et al., 2016). However, the metamorphosis occurring during this stage likely had minimal influence on $E_{z(PAR)}$ relative to the seasonal increase in insolation. It is only as melt onset is

approached that wet metamorphism starts to dominate, causing a rapid growth in snow grains (Vérin et al., 2022), leading to a decrease in surface albedo (Mundy et al., 2014; Perovich, 2007), and an exponential increase in light transmission that continues through the transition from melt to pond onset. Water increasingly replaces air within the interstices of the snowpack (Denoth, 1980), shifting the snowpack from a scattering-dominant to an absorption-dominant state. This transition facilitates further melt, resulting in snowpack depth decline and enhancing light transmission. Additionally, ice algae attenuate PAR through sea ice during the transition from winter to early melt to melt onset (Hill et al., 2022; Mundy et al., 2014; Welch & Bergmann, 1989), noted through a leveling off in $E_{z(PAR)}$ and a decrease in the PUR:PAR ratio during the accumulation phase of the bloom. Accordingly, the loss of the ice algal layer after melt onset likely contributed to increased light transmission into the upper water column.

Calculations of the rate of change (exponential slope) during transitions between melt phases, including the pond onset to open water transition, indicate that the greatest increase in light transmission occurred during melt to pond onset. The rate of change from melt to pond onset in 2017 (0.114 μmol photons m^{-2} s^{-1} d^{-1}) was steeper compared to 2019 (0.042 μmol photons m^{-2} s^{-1} d^{-1}), with the transition extended by 4 additional days in 2019. The difference can be attributed in part to the air temperature variations between 2017 and 2019, as 2019 experienced lower temperatures on average during this transition period and occasional drops below 0°C, likely resulting in the refreezing of layers within the melting snowpack (Granskog et al., 2006). Additionally, proxy snow depth data retrieved from Cambridge Bay suggested that the snowpack was potentially deeper in 2019 than that in 2017 by up to 10 cm prior to early melt (Environment Canada, 2022). As deeper snow covers can slow the melt process (Iacozza & Barber, 1999), it is suggested the longer 2019 pond onset transition was also a function of the deeper snow cover. It

is noted that the 6-10 days for melt to pond onset transition observed in our study align with previous time series observations that reported 8-10 days (Casey et al., 2016; Mundy et al., 2014).

The development of melt ponds during the pond onset to open water transition resulted in a further increase in transmitted PAR to the under-ice environment. The initial rapid increase continued from the previous transition toward pond onset was likely a function of a continued decrease in surface albedo as the relatively smooth and impermeable FYI sea ice surface initially floods (Eicken, 2002; Polashenski et al., 2012). This increase was followed by a slower, steady rise in transmitted PAR as ponds likely developed, becoming deeper and more transparent (Fetterer & Untersteiner, 1998; Landy et al., 2014; Matthes et al. 2020), while snow cover between ponds transitioned to a drained surface ice scattering layer with a slightly lower albedo (Light et al., 2022; Matthes et al., 2020). The UIB in both years attenuated PAR reaching the under-ice water column early in the ponding phase and corresponded to a decrease in PUR:PAR ratio values, indicating a reduction in photosynthetic light quality in the surface waters. Following the UIB end, the PUR:PAR rapidly rebounded to pre-UIB values, implying little algal matter was present in the surface ocean. The peak of seasonal PAR transmittance occurred in the days after ice break-up in July, well after the June solstice due to the sea ice cover, showing light limitation still influences bloom timing in the local system during this period. That is, the impact of an earlier melt with a warming climate (Stroeve & Notz, 2018) will lead to increased PAR reaching the water column.

3.4.2. Surface Bloom Phenology

This study provides the first complete quantification of interannual primary producer bloom timing for a landfast seasonal sea ice Arctic marine system. Previous observations of ice algal bloom phenology for landfast sites were reviewed in Leu et al. (2015). They compiled regional data for different time spans (years to decades), averaged data per region, and statistically

fitted curves to bottom chl-*a* concentration time series. Using these fits, bloom start and end dates were extracted following the approach used here of positive ice algal accumulation to its bloom peak. For comparison, the 2-year averaged ice algal bloom period for Dease Strait was 75 (± 9 SD) days. This value fell in the mid-range of bloom periods from Leu et al. (2015), with Resolute Passage, Nunavut exhibiting the shortest duration (54 days) and Utqiagvik, Alaska having the longest duration (92 days). It is noted that ice algal bloom onset could be slightly earlier than determined in our study due to limitations of our measurements. For example, there is a dependence of our NDI chl-*a* determination on the sensitivity of the hyperspectral irradiance sensor, where early season measurements were impacted by low solar angles and the attenuation of available light through the snow, sea ice and water column to an 8.5-m depth. However, the start dates reported here in mid-March fall in the expected range of bloom onsets given other field-based and modelling estimates (Leu et al., 2015; Lim et al., 2022).

Although the bloom reached greater chl-*a* concentrations in 2019, the 2017 ice algal accumulation rate was similar. This indicates that the deeper snow cover in 2019 extended the algal bloom period due to insulation of the ice bottom from a warming atmosphere (Leu et al. 2015). Therefore, our data suggest the net impact of a deeper snow cover is positive (greater biomass build up) on ice algae in this particular area of the Arctic. Campbell et al. (2016) provided evidence of light and nutrient co-limitation during the spring ice algal bloom in Dease Strait, a surmised function of low light supply at night and nutrient limitation during the day. Indeed, Kim et al. (2020) note that carbon accumulation rates in Dease Strait were lower than found elsewhere in the Canadian Arctic Archipelago (Michel et al., 2002; Nozais et al., 2001; Smith et al., 1988; Smith & Herman, 1991), owing to strong regional nutrient-limitation (Campbell et al., 2016; Back et al. 2021). A slower growth rate and extended bloom period could thus allow for greater nutrient

supply, permitting a greater biomass build-up in the ice. The decline in ice algal concentration thereafter is likely tied to bottom-ice sloughing with a warming ice cover and associated ice bottom melt erosion and brine drainage (Apollonio, 1965; Fortier et al., 2002; Mundy et al., 2014; Selz et al., 2018).

An interesting aspect of the ice algal bloom was oscillations in the first-derivative chl-*a* concentration time series that had a similar periodicity to the fortnightly lunar cycle with troughs mostly matching the full/new moon (spring tide under a M2-dominated tidal cycle; Rotermund et al., 2021). Mechanical erosion of the ice algal layer combined with enhanced nutrient re-supply to the ice bottom during spring tides can promote periodicity in ice algal biomass, physiology, and production (Cota et al., 1987; Gosselin et al., 1985). Accordingly, the troughs in our dataset matched with spring tides and therefore, peaks in accumulation occurred with the switch towards neap tide as the algae likely exhausted the tidal re-supply of nutrients to the ice algal habitat during the spring tide.

A short UIB occurred within 10-12 days after the peak of the ice algal bloom in both years. The UIB commenced 6 days after pond onset in 2017 and 5 days after in 2019. Prior reports indicate that UIBs are often associated with pond formation due to increased light transmittance to the upper water column (Arrigo et al., 2014; Matthes et al., 2020; Mundy et al., 2014; Oziel et al., 2019). It is noted that the increase of *in vivo* chl-*a* fluorescence occurred before the NDI-determined initiation of the UIB. This discrepancy presents a limitation of the NDI-method due to the radiometer integrating all light above the sensor, consequently masking the UIB start with the end of the ice algal bloom. In total, the UIB lasted 7 days in 2017 and 6 days in 2019, with the former exhibiting a larger daily accumulation rate. Since ice algae expend nutrients from the sub-surface waters (Cota et al., 1987), the larger ice algal bloom in 2019 could have limited the

magnitude of the UIB, given that Dease Strait is already a nitrogen-deplete system (Back et al., 2021; Campbell et al., 2016; Kim et al., 2020; Williams et al., 2019). Indeed, Back et al. (2021) observed a short-lived and relatively minor surface UIB prior to ice break-up in 2018 as well.

It is important to note that the NDI-technique was calibrated to ice algae and not phytoplankton, suggesting caution should be taken when interpreting the magnitude of the UIB. Unfortunately, data did not exist to accomplish the calibration. However, the relatively close match in peak magnitude with satellite derived chl-*a* concentration during the open water period provided some confidence in the estimate. In productive waters, UIB biomass are typically orders of magnitude greater than that of ice algal blooms and constitute a significant proportion of annual primary production (Arrigo et al., 2012; Oziel et al., 2019; Payne et al., 2021). A common occurrence in the Arctic, particularly in oligotrophic regions where surface nutrients are rapidly exhausted during the spring bloom, is a sub-surface chl-*a* maximum (SCM) layer that forms along the pycnocline and nitracline (Ardyna & Arrigo, 2020; Martin et al., 2010). This note highlights another limitation on the interpretation of our bloom phenology dataset in that it is limited to the sea ice cover and upper 8.5-m water column. Although driven by wastewater discharge in Cambridge Bay, the spring-summer open water bloom documented in Back et al. (2021) was largely concentrated along the pycnocline between 20 to 30 m with little chl-*a* concentration observed above 10 m. Therefore, it is plausible that our observations missed the main open water bloom for the area. Immediately after ice break-up, the euphotic zone extended well-below 8.5 m with 35.1% PAR transmittance reaching this depth in 2017 and 44.4% in 2019. Applying a surface reflectance of 5% (Singh et al., 2022) with Beer-Bouguer-Lambert's law (Wei & Lee, 2013) using $E_{0(PAR)}$ from the meteorological tower and $E_{z(PAR)}$ at 8.5 m provided an estimated PAR attenuation coefficient of 0.117 and 0.089 m^{-1}, respectively, for 2017 and 2019. From this, a rough estimate of

the euphotic zone, using a 1% surface transmittance definition, was estimated to be 39 m in 2017 and 51 m in 2019, which was similar to that estimated in Back et al. (2021) during the open water period. This estimated euphotic zone supports the likely potential for greater primary production occurring below 8.5 m.

The presence of a late-summer bloom in the region, such as that observed here in 2019, was previously documented (Back et al. 2021). Back et al. (2021) showed that open water primary production was largely restricted to an SCM. Furthermore, they showed an increase in surface production during fall in 2018, occurring during a period of greater winds and mixing of nutrients from below the mixed layer to the surface. Similarly, the 2019 late-summer surface bloom occurred as winds increased with maximum speeds exceeding 10 $m\ s^{-1}$ in our study. Dease Strait stratification is weak in winter, whereas the influx of terrestrial runoff and sea ice melt during spring produces strong stratification, impeding vertical mixing during the spring-summer transition (Rotermund et al., 2021; Williams et al., 2019). This strong stratification greatly limits surface primary production during spring and summer (Back et al. 2021; this study). Although, the fall bloom's production in Back et al. (2021) was minor in comparison to the main summer bloom, primary production was concentrated in the upper 10-m water column during fall. In 2019, the late-summer surface chl-*a* accumulation was of similar magnitude as that of the under-ice bloom, yet occurring over five times the duration. It is likely that the sustained winds enhanced nutrient supply from below the mixed layer to promote an extended bloom observed here, supporting the importance of wind-mixing on primary production in the local system.

The normalized MODIS chl-*a* concentration products verified the late summer surface bloom event with its peak values being similar to the NDI-derived chl-*a* concentration. The fact that the hyperspectral radiometer was based on transmitted light and the MODIS sensor is based

on reflectance at the water surface, indicates that the radiometer could likely detect the bloom lower in the water column prior to the satellite sensor. However, cloud cover was also a limitation on the optical satellite sensor time series as well as the 4-km data product resolution. Regardless, the earlier increase in the NDI-derived time series suggests that the bloom was influenced not only by mixing nutrients, but by the presence of an SCM. This suggestion provides further insight on how wind-induced blooms can develop in polar seas. Observations and projections of sea ice retreat and consequent lengthening of open water periods suggest increased atmospheric-ocean coupling (Barber et al., 2015; Crawford et al., 2021; Mioduszewski et al., 2018; Stroeve & Notz, 2018; Williams & Carmack, 2015), potentially leading to an intensification of wind-induced blooms. Accordingly, it is concluded that the application of *in situ* transmitted spectral irradiance data provides strong promise to enhance surface observations of the Arctic Ocean and can be used in conjunction with other remote sensing techniques to support studies on bloom phenology.

3.5. Supplementary Material

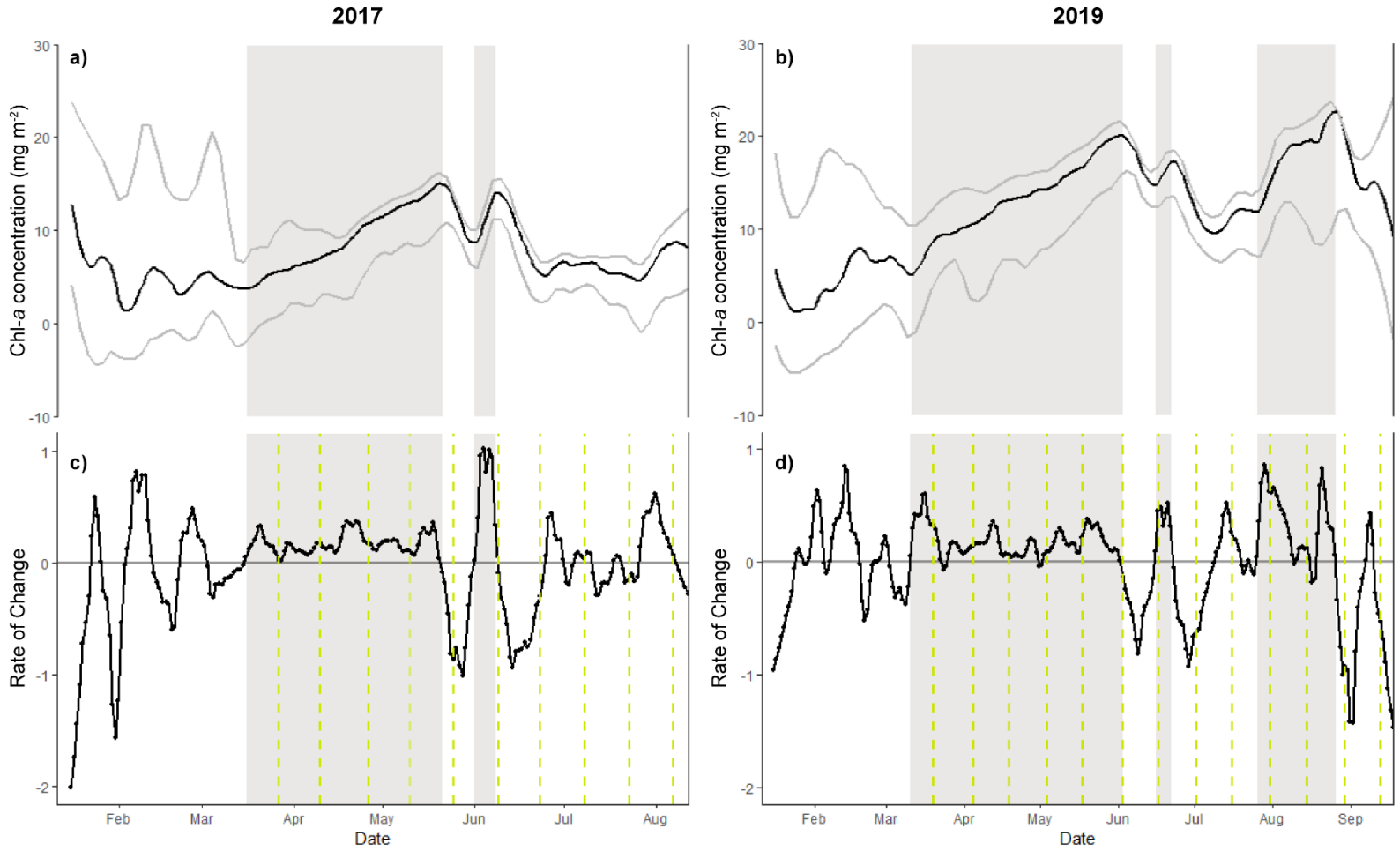

Figure S1. Time series of bloom search intervals for LOESS fitted median chl-*a* concentration and their upper and lower quartiles for 2017 (a) and 2019 (b), with associated first-derivatives of chl-*a* concentration (c, d). Gray-shaded areas are identified bloom period. Horizontal gray line is the threshold for positive growth rate. Dashed green lines are dates of full/new moon phases.

3.6. References

Adams, H., Ye, J., Persaud, B. D., Slowinski, S., Kheyrollah Pour, H., & Van Cappellen, P. (2022). Rates and timing of chlorophyll-*a* increases and related environmental variables in global temperate and cold-temperate lakes. *Earth System Science Data*, *14*(11), 5139–5156. https://doi.org/10.5194/essd-14-5139-2022

Anhaus, P., Katlein, C., Nicolaus, M., Arndt, S., Jutila, A., & Haas, C. (2021). Snow Depth Retrieval on Arctic Sea Ice Using Under-Ice Hyperspectral Radiation Measurements. *Frontiers in Earth Science*, *9*. Retrieved from https://www.frontiersin.org/article/10.3389/feart.2021.711306

Apollonio, S. (1965). Chlorophyll in Arctic Sea Ice. *ARCTIC*, *18*(2), 118–122. https://doi.org/10.14430/arctic3457

Ardyna, M., & Arrigo, K. R. (2020). Phytoplankton dynamics in a changing Arctic Ocean. *Nature Climate Change*, *10*(10), 892–903. https://doi.org/10.1038/s41558-020-0905-y

Ardyna, M., Babin, M., Gosselin, M., Devred, E., Rainville, L., & Tremblay, J.-É. (2014). Recent Arctic Ocean sea ice loss triggers novel fall phytoplankton blooms. *Geophysical Research Letters*, *41*(17), 6207–6212. https://doi.org/10.1002/2014GL061047

Ardyna, M., Mundy, C. J., Mayot, N., Matthes, L. C., Oziel, L., Horvat, C., et al. (2020a). Under-Ice Phytoplankton Blooms: Shedding Light on the "Invisible" Part of Arctic Primary Production. *Frontiers in Marine Science*, *7*, 608032. https://doi.org/10.3389/fmars.2020.608032

Ardyna, M., Mundy, C. J., Mills, M. M., Oziel, L., Grondin, P.-L., Lacour, L., et al. (2020b). Environmental drivers of under-ice phytoplankton bloom dynamics in the Arctic Ocean. *Elem Sci Anth*, *8*(1), 30. https://doi.org/10.1525/elementa.430

Arndt, S., Meiners, K. M., Ricker, R., Krumpen, T., Katlein, C., & Nicolaus, M. (2017). Influence of snow depth and surface flooding on light transmission through Antarctic pack ice. *Journal of Geophysical Research: Oceans*, *122*(3), 2108–2119. https://doi.org/10.1002/2016JC012325

Arrigo, K. R., & van Dijken, G. L. (2011). Secular trends in Arctic Ocean net primary production. *Journal of Geophysical Research: Oceans*, *116*(C9). https://doi.org/10.1029/2011JC007151

Arrigo, K. R., Perovich, D. K., Pickart, R. S., Brown, Z. W., van Dijken, G. L., Lowry, K. E., et al. (2012). Massive Phytoplankton Blooms Under Arctic Sea Ice. *Science*, *336*(6087), 1408–1408. https://doi.org/10.1126/science.1215065

Arrigo, K. R., Brown, Z. W., & Mills, M. M. (2014). Sea ice algal biomass and physiology in the Amundsen Sea, Antarctica. *Elementa: Science of the Anthropocene*, *2*, 000028. https://doi.org/10.12952/journal.elementa.000028

Assmy, P., Fernández-Méndez, M., Duarte, P., Meyer, A., Randelhoff, A., Mundy, C. J., et al. (2017). Leads in Arctic pack ice enable early phytoplankton blooms below snow-covered sea ice. *Scientific Reports*, *7*(1), 40850. https://doi.org/10.1038/srep40850

Back, D.-Y., Ha, S.-Y., Else, B., Hanson, M., Jones, S. F., Shin, K.-H., et al. (2021). On the impact of wastewater effluent on phytoplankton in the Arctic coastal zone: A case study in the Kitikmeot Sea of the Canadian Arctic. *Science of The Total Environment*, *764*, 143861. https://doi.org/10.1016/j.scitotenv.2020.143861

Barber, D. G., Papakyriakou, T. N., Ledrew, E. F., & Shokr, M. E. (1995). An examination of the relation between the spring period evolution of the scattering coefficient (σ) and radiative

fluxes over Jandfast sea-ice. *International Journal of Remote Sensing*, *16*(17), 3343–3363. https://doi.org/10.1080/01431169508954634

Barber, D. G., Yackel, J. J., & Hanesiak, J. M. (2001). Sea Ice, RADARSAT-1 and Arctic Climate Processes: A Review and Update. *Canadian Journal of Remote Sensing*, *27*(1), 51–61. https://doi.org/10.1080/07038992.2001.10854919

Barber, David G., Hop, H., Mundy, C. J., Else, B., Dmitrenko, I. A., Tremblay, J.-E., et al. (2015). Selected physical, biological and biogeochemical implications of a rapidly changing Arctic Marginal Ice Zone. *Progress in Oceanography*, *139*, 122–150. https://doi.org/10.1016/j.pocean.2015.09.003

Bluhm, B. A., Brown, K., Rotermund, L., Williams, W., Danielsen, S., & Carmack, E. C. (2022). New distribution records of kelp in the Kitikmeot Region, Northwest Passage, Canada, fill a pan-Arctic gap. *Polar Biology*, *45*(4), 719–736. https://doi.org/10.1007/s00300-022-03007-6

Butterworth, B. J., & Else, B. G. T. (2018). Dried, closed-path eddy covariance method for measuring carbon dioxide flux over sea ice. *Atmospheric Measurement Techniques*, *11*(11), 6075–6090. https://doi.org/10.5194/amt-11-6075-2018

Campbell, K., Mundy, C. J., Landy, J. C., Delaforge, A., Michel, C., & Rysgaard, S. (2016). Community dynamics of bottom-ice algae in Dease Strait of the Canadian Arctic. *Progress in Oceanography*, *149*, 27–39. https://doi.org/10.1016/j.pocean.2016.10.005

Campbell, Karley, Mundy, C. J., Barber, D. G., & Gosselin, M. (2014). Remote Estimates of Ice Algae Biomass and Their Response to Environmental Conditions during Spring Melt. *ARCTIC*, *67*(3), 375. https://doi.org/10.14430/arctic4409

Casey, J. A., Howell, S. E. L., Tivy, A., & Haas, C. (2016). Separability of sea ice types from wide swath C- and L-band synthetic aperture radar imagery acquired during the melt season. *Remote Sensing of Environment*, *174*, 314–328. https://doi.org/10.1016/j.rse.2015.12.021

Castro de la Guardia, L., Garcia-Quintana, Y., Claret, M., Hu, X., Galbraith, E. D., & Myers, P. G. (2019). Assessing the Role of High-Frequency Winds and Sea Ice Loss on Arctic Phytoplankton Blooms in an Ice-Ocean-Biogeochemical Model. *Journal of Geophysical Research: Biogeosciences*, *124*(9), 2728–2750. https://doi.org/10.1029/2018JG004869

Colbeck, S. C. (1982). An overview of seasonal snow metamorphism. *Reviews of Geophysics*, *20*(1), 45–61. https://doi.org/10.1029/RG020i001p00045

Comiso, J. C. (2012). Large Decadal Decline of the Arctic Multiyear Ice Cover. *Journal of Climate*, *25*(4), 1176–1193. https://doi.org/10.1175/JCLI-D-11-00113.1

Cota, G. F., Prinsenberg, S. J., Bennett, E. B., Loder, J. W., Lewis, M. R., Anning, J. L., et al. (1987). Nutrient fluxes during extended blooms of Arctic ice algae. *Journal of Geophysical Research*, *92*(C2), 1951. https://doi.org/10.1029/JC092iC02p01951

Crawford, A., Stroeve, J., Smith, A., & Jahn, A. (2021). Arctic open-water periods are projected to lengthen dramatically by 2100. *Communications Earth & Environment*, *2*(1), 1–10. https://doi.org/10.1038/s43247-021-00183-x

Denoth, A. (1980). The Pendular-Funicular Liquid Transition in Snow. *Journal of Glaciology*, *25*(91), 93–98. https://doi.org/10.3189/S0022143000010315

Ehn, J. K., & Mundy, C. J. (2013). Assessment of light absorption within highly scattering bottom sea ice from under-ice light measurements: Implications for Arctic ice algae primary production. *Limnology and Oceanography*, *58*(3), 893–902. https://doi.org/10.4319/lo.2013.58.3.0893

Eicken, H. (2002). Tracer studies of pathways and rates of meltwater transport through Arctic summer sea ice. *Journal of Geophysical Research*, *107*(C10), 8046. https://doi.org/10.1029/2000JC000583

Else, B. G. T., Whitehead, J. J., Galindo, V., Ferland, J., Mundy, C. J., Gonski, S. F., et al. (2019). Response of the Arctic Marine Inorganic Carbon System to Ice Algae and Under-Ice Phytoplankton Blooms: A Case Study Along the Fast-Ice Edge of Baffin Bay. *Journal of Geophysical Research: Oceans*, *124*(2), 1277–1293. https://doi.org/10.1029/2018JC013899

Environment Canada. (2022). Available at.https://climate.weather.gc.ca/climate_data/daily_data_e.html?StationID=53512. Accessed May 2, 2022.

Fetterer, F., & Untersteiner, N. (1998). Observations of melt ponds on Arctic sea ice. *Journal of Geophysical Research: Oceans*, *103*(C11), 24821–24835. https://doi.org/10.1029/98JC02034

Forrest, A. L., Lund-Hansen, L. C., Sorrell, B. K., Bowden-Floyd, I., Lucieer, V., Cossu, R., et al. (2019). Exploring Spatial Heterogeneity of Antarctic Sea Ice Algae Using an Autonomous Underwater Vehicle Mounted Irradiance Sensor. *Frontiers in Earth Science*, *0*. https://doi.org/10.3389/feart.2019.00169

Fortier, M., Fortier, L., Michel, C., & Legendre, L. (2002). Climatic and biological forcing of the vertical flux of biogenic particles under seasonal Arctic sea ice. *Marine Ecology Progress Series*, *225*, 1–16. https://doi.org/10.3354/meps225001

Fritsen, C. H., Wirthlin, E. D., Momberg, D. K., Lewis, M. J., & Ackley, S. F. (2011). Bio-optical properties of Antarctic pack ice in the early austral spring. *Deep Sea Research Part II: Topical Studies in Oceanography*, *58*(9), 1052–1061. https://doi.org/10.1016/j.dsr2.2010.10.028

Gill, J. P. S., Yackel, J. J., Geldsetzer, T., & Fuller, M. C. (2015). Sensitivity of C-band synthetic aperture radar polarimetric parameters to snow thickness over landfast smooth first-year sea ice. *Remote Sensing of Environment*, *166*, 34–49. https://doi.org/10.1016/j.rse.2015.06.005

Gosselin, M., Legendre, L., Demers, S., & Ingram, R. G. (1985). Responses of Sea-Ice Microalgae to Climatic and Fortnightly Tidal Energy Inputs (Manitounuk Sound, Hudson Bay). *Canadian Journal of Fisheries and Aquatic Sciences*, *42*(5), 999–1006. https://doi.org/10.1139/f85-125

Granskog, M. A., Vihma, T., Pirazzini, R., & Cheng, B. (2006). Superimposed ice formation and surface energy fluxes on sea ice during the spring melt–freeze period in the Baltic Sea. *Journal of Glaciology*, *52*(176), 119–127. https://doi.org/10.3189/172756506781828971

Halverson, M. J., & Pawlowicz, R. (2013). High-resolution observations of chlorophyll-a biomass from an instrumented ferry: Influence of the Fraser River plume from 2003 to 2006. *Continental Shelf Research*, *59*, 52–64. https://doi.org/10.1016/j.csr.2013.04.010

Harris, G. P. (1986). *Phytoplankton ecology: structure, function, and fluctuation*. London ; Chapman and Hall.

Hill, V., Light, B., Steele, M., & Sybrandy, A. L. (2022). Contrasting Sea-Ice Algae Blooms in a Changing Arctic Documented by Autonomous Drifting Buoys. *Journal of Geophysical Research: Oceans*, *127*(7). https://doi.org/10.1029/2021JC017848

Hill, V. J., Light, B., Steele, M., & Zimmerman, R. C. (2018). Light Availability and Phytoplankton Growth Beneath Arctic Sea Ice: Integrating Observations and Modeling. *Journal of*

Geophysical Research: Oceans, *123*(5), 3651–3667. https://doi.org/10.1029/2017JC013617

Horner, R., & Schrader, G. C. (1982). Relative Contributions of Ice Algae, Phytoplankton, and Benthic Microalgae to Primary Production in Nearshore Regions of the Beaufort Sea. *ARCTIC*, *35*(4), 485–503. https://doi.org/10.14430/arctic2356

Horner, R., Ackley, StephenF., Dieckmann, GerhardS., Gulliksen, B., Hoshiai, T., Legendre, L., et al. (1992). Ecology of sea ice biota: 1. Habitat, terminology, and methodology. *Polar Biology*, *12*(3–4). https://doi.org/10.1007/BF00243113

Horvat, C., Jones, D. R., Iams, S., Schroeder, D., Flocco, D., & Feltham, D. (2017). The frequency and extent of sub-ice phytoplankton blooms in the Arctic Ocean. *Science Advances*, *3*(3), e1601191. https://doi.org/10.1126/sciadv.1601191

Howell, S. E. L., Small, D., Rohner, C., Mahmud, M. S., Yackel, J. J., & Brady, M. (2019). Estimating melt onset over Arctic sea ice from time series multi-sensor Sentinel-1 and RADARSAT-2 backscatter. *Remote Sensing of Environment*, *229*, 48–59. https://doi.org/10.1016/j.rse.2019.04.031

Hu, C., Feng, L., Lee, Z., Franz, B. A., Bailey, S. W., Werdell, P. J., & Proctor, C. W. (2019). Improving Satellite Global Chlorophyll a Data Products Through Algorithm Refinement and Data Recovery. *Journal of Geophysical Research: Oceans*, *124*(3), 1524–1543. https://doi.org/10.1029/2019JC014941

Iacozza, J., & Barber, D. G. (1999). An examination of the distribution of snow on sea-ice. *Atmosphere-Ocean*, *37*(1), 21–51. https://doi.org/10.1080/07055900.1999.9649620

Janout, M. A., Hölemann, J., Waite, A. M., Krumpen, T., von Appen, W.-J., & Martynov, F. (2016). Sea-ice retreat controls timing of summer plankton blooms in the Eastern Arctic Ocean. *Geophysical Research Letters*, *43*(24), 12,493-12,501. https://doi.org/10.1002/2016GL071232

Ji, R., Jin, M., & Varpe, Ø. (2013). Sea ice phenology and timing of primary production pulses in the Arctic Ocean. *Global Change Biology*, *19*(3), 734–741. https://doi.org/10.1111/gcb.12074

Kahru, M., Lee, Z., Mitchell, B. G., & Nevison, C. D. (2016). Effects of sea ice cover on satellite-detected primary production in the Arctic Ocean. *Biology Letters*, *12*(11), 20160223. https://doi.org/10.1098/rsbl.2016.0223

Kauko, H. M., Pavlov, A. K., Johnsen, G., Granskog, M. A., Peeken, I., & Assmy, P. (2019). Photoacclimation State of an Arctic Underice Phytoplankton Bloom. *Journal of Geophysical Research: Oceans*, *124*(3), 1750–1762. https://doi.org/10.1029/2018JC014777

Kim, K., Ha, S.-Y., Kim, B. K., Mundy, C. J., Gough, K. M., Pogorzelec, N. M., & Lee, S. H. (2020). Carbon and nitrogen uptake rates and macromolecular compositions of bottom-ice algae and phytoplankton at Cambridge Bay in Dease Strait, Canada. *Annals of Glaciology*, 1–11. https://doi.org/10.1017/aog.2020.17

Kwok, R. (2018). Arctic sea ice thickness, volume, and multiyear ice coverage: losses and coupled variability (1958–2018). *Environmental Research Letters*, *13*(10), 105005. https://doi.org/10.1088/1748-9326/aae3ec

Landy, J., Ehn, J., Shields, M., & Barber, D. (2014). Surface and melt pond evolution on landfast first-year sea ice in the Canadian Arctic Archipelago. *Journal of Geophysical Research: Oceans*, *119*(5), 3054–3075. https://doi.org/10.1002/2013JC009617

Lange, B. A., Katlein, C., Nicolaus, M., Peeken, I., & Flores, H. (2016). Sea ice algae chlorophyll a concentrations derived from under-ice spectral radiation profiling platforms. *Journal of Geophysical Research: Oceans*, *121*(12), 8511–8534. https://doi.org/10.1002/2016JC011991

Legendre, L., & Gosselin, M. (1991). In situ spectroradiometric estimation of microalgal biomass in first-year sea ice. *Polar Biology*, *11*(2). https://doi.org/10.1007/BF00234273

Leu, E., Mundy, C. J., Assmy, P., Campbell, K., Gabrielsen, T. M., Gosselin, M., et al. (2015). Arctic spring awakening – Steering principles behind the phenology of vernal ice algal blooms. *Progress in Oceanography*, *139*, 151–170. https://doi.org/10.1016/j.pocean.2015.07.012

Light, B., Smith, M. M., Perovich, D. K., Webster, M. A., Holland, M. M., Linhardt, F., et al. (2022). Arctic sea ice albedo: Spectral composition, spatial heterogeneity, and temporal evolution observed during the MOSAiC drift. *Elementa: Science of the Anthropocene*, *10*(1), 000103. https://doi.org/10.1525/elementa.2021.000103

Lim, S. M., Payne, C. M., van Dijken, G. L., & Arrigo, K. R. (2022). Increases in Arctic sea ice algal habitat, 1985–2018. *Elementa: Science of the Anthropocene*, *10*(1), 00008. https://doi.org/10.1525/elementa.2022.00008

Livingstone, C. E., Singh, K. P., & Gray, A. L. (1987). Seasonal and Regional Variations of Active/Passive Microwave Signatures of Sea Ice. *IEEE Transactions on Geoscience and Remote Sensing*, *GE-25*(2), 159–173. https://doi.org/10.1109/TGRS.1987.289815

Mahmud, M. S., Nandan, V., Howell, S. E. L., Geldsetzer, T., & Yackel, J. (2020). Seasonal evolution of L-band SAR backscatter over landfast Arctic sea ice. *Remote Sensing of Environment*, *251*, 112049. https://doi.org/10.1016/j.rse.2020.112049

Martin, J., Tremblay, J., Gagnon, J., Tremblay, G., Lapoussière, A., Jose, C., et al. (2010). Prevalence, structure and properties of subsurface chlorophyll maxima in Canadian Arctic waters. *Marine Ecology Progress Series*, *412*, 69–84. https://doi.org/10.3354/meps08666

Matthes, L. C., Mundy, C. J., L.-Girard, S., Babin, M., Verin, G., & Ehn, J. K. (2020). Spatial Heterogeneity as a Key Variable Influencing Spring-Summer Progression in UVR and PAR Transmission Through Arctic Sea Ice. *Frontiers in Marine Science*, *7*, 183. https://doi.org/10.3389/fmars.2020.00183

Maykut, G. A., & Grenfell, T. C. (1975). The spectral distribution of light beneath first-year sea ice in the Arctic Ocean: Light beneath sea ice. *Limnology and Oceanography*, *20*(4), 554–563. https://doi.org/10.4319/lo.1975.20.4.0554

Meiners, K. M., Arndt, S., Bestley, S., Krumpen, T., Ricker, R., Milnes, M., et al. (2017). Antarctic pack ice algal distribution: Floe-scale spatial variability and predictability from physical parameters. *Geophysical Research Letters*, *44*(14), 7382–7390. https://doi.org/10.1002/2017GL074346

Melbourne-Thomas, J., Meiners, K., Mundy, C., Schallenberg, C., Tattersall, K., & Dieckmann, G. (2015). Algorithms to estimate Antarctic sea ice algal biomass from under-ice irradiance spectra at regional scales. *Marine Ecology Progress Series*, *536*, 107–121. https://doi.org/10.3354/meps11396

Michel, C., Nielsen, T. G., Nozais, C., & Gosselin, M. (2002). Significance of sedimentation and grazing by ice micro- and meiofauna for carbon cycling in annual sea ice (northern Baffin Bay). *Aquatic Microbial Ecology*, *30*(1), 57–68. https://doi.org/10.3354/ame030057

Mieruch, S., Freund, J. A., Feudel, U., Boersma, M., Janisch, S., & Wiltshire, K. H. (2010). A new method of describing phytoplankton blooms: Examples from Helgoland Roads. *Journal of Marine Systems*, *79*(1–2), 36–43. https://doi.org/10.1016/j.jmarsys.2009.06.004

MODIS Science Team. (2017). MYD02HKM MODIS/Aqua Calibrated Radiances 5-Min L1B Swath 500m [Data set]. NASA Level 1 and Atmosphere Archive and Distribution System. https://doi.org/10.5067/MODIS/MYD02HKM.061. Accessed March 19, 2021.

Mioduszewski, J., Vavrus, S., & Wang, M. (2018). Diminishing Arctic Sea Ice Promotes Stronger Surface Winds. *Journal of Climate*, *31*(19), 8101–8119. https://doi.org/10.1175/JCLI-D-18-0109.1

Morel, A. (1978). Available, usable, and stored radiant energy in relation to marine photosynthesis. *Deep Sea Research*, *25*(8), 673–688. https://doi.org/10.1016/0146-6291(78)90623-9

Mundy, C., Gosselin, M., Gratton, Y., Brown, K., Galindo, V., Campbell, K., et al. (2014). Role of environmental factors on phytoplankton bloom initiation under landfast sea ice in Resolute Passage, Canada. *Marine Ecology Progress Series*, *497*, 39–49. https://doi.org/10.3354/meps10587

Mundy, C. J., Ehn, J. K., Barber, D. G., & Michel, C. (2007). Influence of snow cover and algae on the spectral dependence of transmitted irradiance through Arctic landfast first-year sea ice. *Journal of Geophysical Research*, *112*(C3), C03007. https://doi.org/10.1029/2006JC003683

NASA Ocean Biology Processing Group. (2022). Aqua MODIS Level 3 Mapped Chlorophyll Data, Version R2022.0 [Data set]. NASA Ocean Biology DAAC. https://doi.org/10.5067/AQUA/MODIS/L3M/CHL/2022. Accessed December 13, 2022.

Nicolaus, M., & Katlein, C. (2013). Mapping radiation transfer through sea ice using a remotely operated vehicle (ROV). *The Cryosphere*, *7*(3), 763–777. https://doi.org/10.5194/tc-7-763-2013

Nicolaus, M., Petrich, C., Hudson, S. R., & Granskog, M. A. (2013). Variability of light transmission through Arctic land-fast sea ice during spring. *The Cryosphere*, *7*(3), 977–986. https://doi.org/10.5194/tc-7-977-2013

Nielsen, J. M., Pelland, N. A., Bell, S. W., Lomas, M. W., Eisner, L. B., Stabeno, P., et al. (2023). Seasonal dynamics of primary production in the southeastern Bering Sea assessed using continuous temporal and vertical dissolved oxygen and chlorophyll-a measurements. *Journal of Geophysical Research: Oceans*, *n/a*(n/a), e2022JC019076. https://doi.org/10.1029/2022JC019076

Nozais, C., Gosselin, M., Michel, C., & Tita, G. (2001). Abundance, biomass, composition and grazing impact of the sea-ice meiofauna in the North Water, northern Baffin Bay. *Marine Ecology Progress Series*, *217*, 235–250. https://doi.org/10.3354/meps217235

Oziel, L., Massicotte, P., Randelhoff, A., Ferland, J., Vladoiu, A., Lacour, L., et al. (2019). Environmental factors influencing the seasonal dynamics of spring algal blooms in and beneath sea ice in western Baffin Bay. *Elem Sci Anth*, *7*(1), 34. https://doi.org/10.1525/elementa.372

Parsons, T. R., Maita, Y., & Lalli, C. M. (Eds.). (1984). General Notes on Analytical Techniques. In *A Manual of Chemical & Biological Methods for Seawater Analysis* (pp. xiii–xiv). Amsterdam: Pergamon. https://doi.org/10.1016/B978-0-08-030287-4.50009-8

Payne, C. M., Bianucci, L., van Dijken, G. L., & Arrigo, K. R. (2021). Changes in Under-Ice Primary Production in the Chukchi Sea From 1988 to 2018. *Journal of Geophysical Research: Oceans*, *126*(9), e2021JC017483. https://doi.org/10.1029/2021JC017483

Perovich, D. K. (1996). *The optical properties of sea ice*. Hanover, N.H.: US Army Corps of Engineers, Cold Regions Research & Engineering Laboratory ; [Springfield, Va. : Available from National Technical Information Service.

Perovich, D. K. (2007). Light reflection and transmission by a temperate snow cover. *Journal of Glaciology*, *53*(181), 201–210. https://doi.org/10.3189/172756507782202919

Polashenski, C., Perovich, D., & Courville, Z. (2012). The mechanisms of sea ice melt pond formation and evolution. *Journal of Geophysical Research: Oceans*, *117*(C1). https://doi.org/10.1029/2011JC007231

Randelhoff, A., Lacour, L., Marec, C., Leymarie, E., Lagunas, J., Xing, X., et al. (2020). Arctic mid-winter phytoplankton growth revealed by autonomous profilers. *Science Advances*, *6*(39), eabc2678. https://doi.org/10.1126/sciadv.abc2678

Rantanen, M., Karpechko, A. Y., Lipponen, A., Nordling, K., Hyvärinen, O., Ruosteenoja, K., et al. (2022). The Arctic has warmed nearly four times faster than the globe since 1979. *Communications Earth & Environment*, *3*(1), 1–10. https://doi.org/10.1038/s43247-022-00498-3

Rotermund, L. M., Williams, W. J., Klymak, J. M., Wu, Y., Scharien, R. K., & Haas, C. (2021). The Effect of Sea Ice on Tidal Propagation in the Kitikmeot Sea, Canadian Arctic Archipelago. *Journal of Geophysical Research: Oceans*, *126*(5), e2020JC016786. https://doi.org/10.1029/2020JC016786

Selz, V., Saenz, B. T., van Dijken, G. L., & Arrigo, K. R. (2018). Drivers of Ice Algal Bloom Variability Between 1980 and 2015 in the Chukchi Sea. *Journal of Geophysical Research: Oceans*, *123*(10), 7037–7052. https://doi.org/10.1029/2018JC014123

Singh, R. K., Vader, A., Mundy, C. J., Søreide, J. E., Iken, K., Dunton, K. H., et al. (2022). Satellite-Derived Photosynthetically Available Radiation at the Coastal Arctic Seafloor. *Remote Sensing*, *14*(20), 5180. https://doi.org/10.3390/rs14205180

Small, D. (2011). Flattening Gamma: Radiometric Terrain Correction for SAR Imagery. *IEEE Transactions on Geoscience and Remote Sensing*, *49*(8), 3081–3093. https://doi.org/10.1109/TGRS.2011.2120616

Smith, R. E. H., & Herman, A. W. (1991). Productivity of sea ice algae: In situ vs. incubator methods. *Journal of Marine Systems*, *2*(1), 97–110. https://doi.org/10.1016/0924-7963(91)90016-N

Smith, R. E. H., Anning, J., Clement, P., & Cota, G. (1988). Abundance and production of ice algae in Resolute Passage, Canadian Arctic. *Marine Ecology Progress Series*, *48*(3), 251–263.

Søreide, J. E., Leu, E., Berge, J., Graeve, M., & Falk-Petersen, S. (2010). Timing of blooms, algal food quality and Calanus glacialis reproduction and growth in a changing Arctic. *Global Change Biology*, no-no. https://doi.org/10.1111/j.1365-2486.2010.02175.x

Stroeve, J., & Notz, D. (2018). Changing state of Arctic sea ice across all seasons. *Environmental Research Letters*, *13*(10), 103001. https://doi.org/10.1088/1748-9326/aade56

Tremblay, J.-É., Anderson, L. G., Matrai, P., Coupel, P., Bélanger, S., Michel, C., & Reigstad, M. (2015). Global and regional drivers of nutrient supply, primary production and CO2 drawdown in the changing Arctic Ocean. *Progress in Oceanography*, *139*, 171–196. https://doi.org/10.1016/j.pocean.2015.08.009

Vérin, G., Domine, F., Babin, M., Picard, G., & Arnaud, L. (2022). Metamorphism of snow on Arctic sea ice during the melt season: impact on spectral albedo and radiative fluxes through snow. *The Cryosphere*, *16*(9), 3431–3449. https://doi.org/10.5194/tc-16-3431-2022

Veyssière, G., Castellani, G., Wilkinson, J., Karcher, M., Hayward, A., Stroeve, J. C., et al. (2022). Under-Ice Light Field in the Western Arctic Ocean During Late Summer. *Frontiers in Earth Science*, *9*, 643737. https://doi.org/10.3389/feart.2021.643737

Waga, H., & Hirawake, T. (2020). Changing Occurrences of Fall Blooms Associated With Variations in Phytoplankton Size Structure in the Pacific Arctic. *Frontiers in Marine Science*, *7*. Retrieved from https://www.frontiersin.org/articles/10.3389/fmars.2020.00209

Wei, J., & Lee, Z. (2013). Model of the attenuation coefficient of daily photosynthetically available radiation in the upper ocean. *Methods in Oceanography*, *8*, 56–74. https://doi.org/10.1016/j.mio.2013.12.001

Welch, H. E., & Bergmann, M. A. (1989). Seasonal Development of Ice Algae and its Prediction from Environmental Factors near Resolute, N.W.T., Canada. *Canadian Journal of Fisheries and Aquatic Sciences*, *46*(10), 1793–1804. https://doi.org/10.1139/f89-227

Williams, W., Brown, K., Fisheries and Oceans Canada, Institute of Ocean Sciences, Sidney, British Columbia, Canada, Bluhm, B., Carmack, E., Dalman, L., et al. (2019). Stratification in the Canadian Arctic Archipelago's Kitikmeot Sea: Biological and geochemical consequences. *Polar Knowledge: Aqhaliat Report*, *1*(1), 46–52. https://doi.org/10.35298/pkc.2018.06

Williams, W. J., & Carmack, E. C. (2015). The 'interior' shelves of the Arctic Ocean: Physical oceanographic setting, climatology and effects of sea-ice retreat on cross-shelf exchange. *Progress in Oceanography*, *139*, 24–41. https://doi.org/10.1016/j.pocean.2015.07.008

Wongpan, P, Meiners, K. M., Langhorne, P. J., Heil, P., Smith, I. J., Leonard, G. H., et al. (2018). Estimation of Antarctic Land-Fast Sea Ice Algal Biomass and Snow Thickness From Under-Ice Radiance Spectra in Two Contrasting Areas. *Journal of Geophysical Research*, *123*, 1907–1923. https://doi.org/10.1002/2017JC013711

Wongpan, Pat, Nomura, D., Toyota, T., Tanikawa, T., Meiners, K. M., Ishino, T., et al. (2020). Using under-ice hyperspectral transmittance to determine land-fast sea-ice algal biomass in Saroma-ko Lagoon, Hokkaido, Japan. *Annals of Glaciology*, 1–10. https://doi.org/10.1017/aog.2020.69

Yackel, J. J., Barber, D. G., Papakyriakou, T. N., & Breneman, C. (2007). First-year sea ice spring melt transitions in the Canadian Arctic Archipelago from time-series synthetic aperture radar data, 1992–2002. *Hydrological Processes*, *21*(2), 253–265. https://doi.org/10.1002/hyp.6240

Chapter 4 | Conclusions and Recommendations

4.1. Conclusions

This thesis focuses on a study conducted in Dease Strait, which connects Coronation Gulf in the east and Queen Maud Gulf to the west within the Kitikmeot Sea. The Kitikmeot Sea has a unique physical oceanographic setting in the Canadian Arctic, characterized by substantial summer freshwater influx due to terrestrial runoff and sea ice melt, and dense saline Pacific-water inflows across its shallow bounding sills, forming an estuarine-like environment (Williams et al., 2019). These distinct water masses produce a strong seasonal stratification with limited vertical mixing of nutrients, except by reported under-ice currents through narrow straits (Dalman et al., 2019), or wind-driven mixing (Back et al., 2021). With very little dissolved inorganic nitrogen available in the stratified surface waters, ice algal (Campbell et al., 2016; Kim et al., 2020) and phytoplankton (Back et al. 2021) production are strongly nutrient limited in Dease Strait, noted to be among the lowest reported for the Arctic Ocean.

This thesis examined, for the first time, surface bloom phenology from winter-spring (ice-covered) through summer-fall (open water) in a landfast sea ice environment in relation to snow-ice melt state and light availability over two years of a subsurface-taut oceanographic mooring deployment. Satellite SAR products combined with nearby meteorological observations enabled the determination of surface melt states of the snow-/melt pond-covered sea ice. It was noted that

ice algal bloom start times were similar for both years and contingent on snow depth controlling light transmission. The ice algal blooms had similar rates of accumulation and their ends coincided with snow melt onset. However, the 2019 algal bloom lasted 15 days longer than the one observed in 2017, which was linked to a deeper snow cover in 2019. Due to co-limitation of light and nutrients on ice algal growth (Campbell et al. 2016), the deeper snow cover was suggested beneficial to the ice algal community, slowing melt progression and thus, permitting a greater biomass accumulation in the sea ice that likely utilized more of the limited surface nutrient pool. Therefore, as snow accumulation rates decrease over the Arctic Ocean (Webster et al., 2014), a negative impact on ice algal phenology (i.e., earlier bloom termination) can be expected, exacerbating the existing trend towards earlier ice melt (Stroeve & Notz, 2018).

Between snowmelt to ice-free conditions, a 100-fold increase in light transmittance was observed. Of the three melt phases identified, the transition from melt to pond onset encapsulated the most rapid increase in transmitted PAR to the under-ice water column, while the transition from pond onset to open water saw the greatest absolute increase in transmitted irradiance. Interestingly, estimated PUR:PAR ratios revealed that the highest quality of light for photosynthesis occurred in winter just before onset of the ice algal bloom, and gradually diminished throughout the year due to ice algal and phytoplankton accumulation in the upper ocean. During the latter transition was a brief and relatively minor under-ice phytoplankton bloom that occurred close after pond onset, lasting 6-7 days. The carbon net accumulation estimate during the 2019 under-ice bloom (UIB) was lower than that in 2017, surmised to be associated with greater nutrient limitation caused by the extended ice algae bloom.

The UIB ended well before ice break-up, implying that surface nutrients were rapidly exhausted. Ice break-up occurred in early and late July in 2017 and 2019, respectively, causing the

greatest penetration of irradiance into the water column to occur after the summer solstice when insolation was seasonally decreasing. This fact implied that phytoplankton phenology is still limited by light availability with the potential to shift earlier as climate warming causes an earlier melt (Stroeve et al., 2021). In 2019, sustained wind-driven mixing generated a prolonged 31-day late-summer surface phytoplankton bloom that was verified using ocean colour satellite products. It was likely that this bloom was influenced by mixing of a sub-surface chl-*a* maximum (SCM) below our surface observations provided the euphotic zone was estimated to be 39-51 m deep during the period. However, the consistent increase in chl-*a* concentration during the bloom did suggest new nutrients were mixed into the surface layer to support the greater accumulation rates. This conclusion highlights the importance of wind-mixing on phytoplankton production in the system. As the open water period increases with current climate change trends (Barber et al., 2015; Crawford et al., 2021; Stroeve & Notz, 2018), greater atmosphere-ocean coupling can be expected (Liang & Losch, 2018; Mioduszewski et al., 2018; Williams & Carmack, 2015) and thus enhance phytoplankton production in the region.

4.2. Recommendations

The research presented in this thesis builds upon a biological oceanography baseline for Dease Strait first reported by Campbell et al. (2016), and is an important step in developing long-term monitoring capabilities of primary producer responses to physical variables, owing to sensor technological advances. It also has the potential to contribute to monitoring in the region as Cambridge Bay is home to the Canadian High Arctic Research Station (CHARS) and the Kitikmeot Sea Science Study (K_3S) mooring program supported in part by Fisheries and Oceans Canada. The accumulation of long-term Arctic observations is crucial in discerning the effects of climate change on the region. Responses and impacts of primary production blooms extend to

higher trophic levels and subsequently affect northern inhabitants. Given the duration of the study, no larger climate change trends can be elucidated. Yet, this research is indicative of synthesizing remote sensing methods when extended fieldwork is not feasible as the 2019 mooring-derived chl-*a* concentration time series represents a true non-invasive estimation of surface primary producer phenology.

To further explore the capabilities of the method described in this research, several considerations and recommendations are proposed:

1) The main sensors aboard the annual oceanographic mooring used in this research were a surface-facing hyperspectral radiometer and a chl-*a* fluorometer positioned 8.5 m below surface. Lowering the sensors to a deeper location along the mooring line could capture an extended potential phytoplankton bloom; however, as light increasingly attenuates with water depth, the determination of bloom initiation would be impacted, particularly for ice algae. Adding additional hyperspectral sensors at greater depths would solve this problem; however, cost of additional sensors would provide a new limitation. Incorporating other sensors could also provide valuable information about bloom characteristics. For example, an Acoustic Doppler Current Profiler (ADCP) could measure current velocity to assess the influence of tides and winds on surface mixing and subsequent nutrient supply. Variability in water circulation could indicate under-ice phytoplankton movement throughout the bloom and reveal late-summer/fall bloom origins. Additionally, Nelson et al. (2019) observed zooplankton in Dease Strait using ADCP data, suggesting that these data could be used to examine top-down control of grazing on primary production in the region. Another sensor example is a nitrate sensor (Mayot et al., 2020), which would offer insights into nutrient utilization

by primary producers and the impact of ice algal nutrient draw-down on under-ice phytoplankton production rates.

2) Deploying similar moorings in other settings within the region, or multiple deployments, would facilitate further testing and validation. Dease Strait is considered nutrient-deplete due to the effects of seasonal stratification. Placing the mooring outside of the Dolphin Union Strait bounding sill could provide contextual information on how Pacific waters with lower runoff influence affects primary production. Conversely, positioning a mooring in a shallow coastal portion of Coronation Gulf, where the Coppermine, Burnside, and Ellice Rivers flow, would likely see higher levels of terrestrial nutrients mixing with nutrient-dense Pacific waters during in the open water period, potentially lead to higher production estimates. Beyond the Kitikmeot Sea, deploying moorings in landfast ice regions, and buoys in pack-ice (Hill et al., 2018), with hyperspectral sensors across the Arctic Ocean, presents an opportunity to gather a pan-Arctic perspective of long-term primary producer phenology. This suggestion serves as a partial substitute for the BIO-Argo float network in polar waters due to float damage caused by sea ice (André et al., 2020; Klatt et al., 2007).

3) All NDI calibrations to date have been done with ice algae due to easier access with ice cores, control over sampling protocols, and seasonal predictability of collecting samples over an extended duration. Future research should investigate calibrating to phytoplankton for a true measure of phytoplankton bloom magnitude and its impact on the region. Additionally, this research utilized MODIS-derived optical ocean colour products to obtain surface phytoplankton chl-*a* measurements, with a 4-km data product resolution. As the radiometer has a footprint of approximately 15 m, future

work would benefit from utilizing chlorophyll retrieval algorithms developed for the MultiSpectral Instrument (MSI) aboard Sentinel-2 (S2; launched in 2015) with its spatial resolution of 10-20 m. Although much of the chlorophyll data retrieved using S2 have taken place in subarctic regions (Aranha et al., 2022; Cazzaniga et al., 2019; Li et al., 2021), recent research by Asim et al. (2021) was conducted in the Barents Sea. Additionally, the increased spatial resolution would potentially increase the number of cloud-free S2 images for analysis.

4) Another vital recommendation arising from this research is the necessity of funding and establishing a permanent long-term mooring with regular maintenance under the auspices of K_3S. A mooring extending at least 5-10 years is essential for discerning trends in primary production in relation to physical variables. The two years of data in this research have a one-year data gap between them. Real-time monitoring could also offer a viable solution to this issue with continuous assessment of sensor functionality and bloom activity. One possible approach is integrating a hyperspectral radiometer into Ocean Network Canada's observatory platform, which is already equipped with a fluorometer. Alternatively, adopting the methodology employed by the Barrow Strait Real Time Observatory (BSRTO), a cabled underwater ocean observatory operated by Fisheries and Oceans Canada could be beneficial (Richards et al., 2017). Mooring data on this system is acoustically transmitted to a data node, which is then transferred via submarine cable to a station for subsequent data transmission by Iridium satellite for web access.

4.3. References

André, X., Le Traon, P.-Y., Le Reste, S., Dutreuil, V., Leymarie, E., Malardé, D., et al. (2020). Preparing the New Phase of Argo: Technological Developments on Profiling Floats in the NAOS Project. *Frontiers in Marine Science*, *7*. Retrieved from https://www.frontiersin.org/articles/10.3389/fmars.2020.577446

Aranha, T. R. B. T., Martinez, J.-M., Souza, E. P., Barros, M. U. G., & Martins, E. S. P. R. (2022). Remote Analysis of the Chlorophyll-a Concentration Using Sentinel-2 MSI Images in a Semiarid Environment in Northeastern Brazil. *Water*, *14*(3), 451. https://doi.org/10.3390/w14030451

Asim, M., Brekke, C., Mahmood, A., Eltoft, T., & Reigstad, M. (2021). Improving Chlorophyll-A Estimation From Sentinel-2 (MSI) in the Barents Sea Using Machine Learning. *IEEE Journal of Selected Topics in Applied Earth Observations and Remote Sensing*, *14*, 5529–5549. https://doi.org/10.1109/JSTARS.2021.3074975

Back, D.-Y., Ha, S.-Y., Else, B., Hanson, M., Jones, S. F., Shin, K.-H., et al. (2021). On the impact of wastewater effluent on phytoplankton in the Arctic coastal zone: A case study in the Kitikmeot Sea of the Canadian Arctic. *Science of The Total Environment*, *764*, 143861. https://doi.org/10.1016/j.scitotenv.2020.143861

Barber, D. G., Hop, H., Mundy, C. J., Else, B., Dmitrenko, I. A., Tremblay, J.-E., et al. (2015). Selected physical, biological and biogeochemical implications of a rapidly changing Arctic Marginal Ice Zone. *Progress in Oceanography*, *139*, 122–150. https://doi.org/10.1016/j.pocean.2015.09.003

Campbell, K., Mundy, C. J., Landy, J. C., Delaforge, A., Michel, C., & Rysgaard, S. (2016). Community dynamics of bottom-ice algae in Dease Strait of the Canadian Arctic. *Progress in Oceanography*, *149*, 27–39. https://doi.org/10.1016/j.pocean.2016.10.005

Cazzaniga, I., Bresciani, M., Colombo, R., Della Bella, V., Padula, R., & Giardino, C. (2019). A comparison of Sentinel-3-OLCI and Sentinel-2-MSI-derived Chlorophyll- *a* maps for two large Italian lakes. *Remote Sensing Letters*, *10*(10), 978–987. https://doi.org/10.1080/2150704X.2019.1634298

Crawford, A., Stroeve, J., Smith, A., & Jahn, A. (2021). Arctic open-water periods are projected to lengthen dramatically by 2100. *Communications Earth & Environment*, *2*(1), 1–10. https://doi.org/10.1038/s43247-021-00183-x

Dalman, L. A., Else, B. G. T., Barber, D., Carmack, E., Williams, W. J., Campbell, K., et al. (2019). Enhanced bottom-ice algal biomass across a tidal strait in the Kitikmeot Sea of the Canadian Arctic. *Elem Sci Anth*, *7*(1), 22. https://doi.org/10.1525/elementa.361

Hill, V. J., Light, B., Steele, M., & Zimmerman, R. C. (2018). Light Availability and Phytoplankton Growth Beneath Arctic Sea Ice: Integrating Observations and Modeling. *Journal of Geophysical Research: Oceans*, *123*(5), 3651–3667. https://doi.org/10.1029/2017JC013617

Klatt, O., Boebel, O., & Fahrbach, E. (2007). A Profiling Float's Sense of Ice. *Journal of Atmospheric and Oceanic Technology*, *24*(7), 1301–1308. https://doi.org/10.1175/JTECH2026.1

Li, S., Song, K., Wang, S., Liu, G., Wen, Z., Shang, Y., et al. (2021). Quantification of chlorophyll-a in typical lakes across China using Sentinel-2 MSI imagery with machine learning algorithm. *Science of The Total Environment*, *778*, 146271. https://doi.org/10.1016/j.scitotenv.2021.146271

Liang, X., & Losch, M. (2018). On the Effects of Increased Vertical Mixing on the Arctic Ocean and Sea Ice. *Journal of Geophysical Research: Oceans*, *123*(12), 9266–9282. https://doi.org/10.1029/2018JC014303

Mayot, N., Matrai, P. A., Arjona, A., Bélanger, S., Marchese, C., Jaegler, T., et al. (2020). Springtime Export of Arctic Sea Ice Influences Phytoplankton Production in the Greenland Sea. *Journal of Geophysical Research: Oceans*, *125*(3), e2019JC015799. https://doi.org/10.1029/2019JC015799

Mioduszewski, J., Vavrus, S., & Wang, M. (2018). Diminishing Arctic Sea Ice Promotes Stronger Surface Winds. *Journal of Climate*, *31*(19), 8101–8119. https://doi.org/10.1175/JCLI-D-18-0109.1

Nelson, R. J., Young, K. V., & Williams, W. J. (2019). Marine zooplankton of Coronation Gulf and Bathurst Inlet, Nunavut, Canada. *Continental Shelf Research*, *191*, 104003. https://doi.org/10.1016/j.csr.2019.104003

Richards, C., Pittman, M., Phelan, K., Nudds, S., & Hamilton, J. (2017). The Barrow Strait Real Time Observatory: Under-ice Monitoring in the Canadian High Arctic. In *Proceedings of the International Conference on Underwater Networks & Systems* (pp. 1–7). Halifax NS Canada: ACM. https://doi.org/10.1145/3148675.3152195

Stroeve, J., & Notz, D. (2018). Changing state of Arctic sea ice across all seasons. *Environmental Research Letters*, *13*(10), 103001. https://doi.org/10.1088/1748-9326/aade56

Stroeve, J., Vancoppenolle, M., Veyssiere, G., Lebrun, M., Castellani, G., Babin, M., et al. (2021). A Multi-Sensor and Modeling Approach for Mapping Light Under Sea Ice During the Ice-Growth Season. *Frontiers in Marine Science*, *7*. https://doi.org/10.3389/fmars.2020.592337

Webster, M. A., Rigor, I. G., Nghiem, S. V., Kurtz, N. T., Farrell, S. L., Perovich, D. K., & Sturm, M. (2014). Interdecadal changes in snow depth on Arctic sea ice. *Journal of Geophysical Research: Oceans*, *119*(8), 5395–5406. https://doi.org/10.1002/2014JC009985

Williams, W., Brown, K., Fisheries and Oceans Canada, Institute of Ocean Sciences, Sidney, British Columbia, Canada, Bluhm, B., Carmack, E., Dalman, L., et al. (2019). Stratification in the Canadian Arctic Archipelago's Kitikmeot Sea: Biological and geochemical consequences. *Polar Knowledge: Aqhaliat Report*, *1*(1), 46–52. https://doi.org/10.35298/pkc.2018.06

Williams, W. J., & Carmack, E. C. (2015). The 'interior' shelves of the Arctic Ocean: Physical oceanographic setting, climatology and effects of sea-ice retreat on cross-shelf exchange. *Progress in Oceanography*, *139*, 24–41. https://doi.org/10.1016/j.pocean.2015.07.008